

THERMAL DOSIMETRY FROM RADIO-FREQUENCY FIELDS WITHIN A  
HEAD PHANTOM ASSESSED DURING THREE TESLA MAGNETIC  
RESONANCE IMAGING

By

GEORGE HARDER

A DISSERTATION PRESENTED TO THE GRADUATE SCHOOL  
OF THE UNIVERSITY OF FLORIDA IN PARTIAL FULFILLMENT  
OF THE REQUIREMENTS FOR THE DEGREE OF  
DOCTOR OF PHILOSOPHY

UNIVERSITY OF FLORIDA

1998

## ACKNOWLEDGMENTS

My thanks go out to my family and friends for their moral support and encouragement, with special thanks to my sisters Virginia, Angie, Iris and Carol. My appreciation and respect go to my committee for their confidence in my abilities. I want to thank Dr. Jeff Fitzsimmons, Dave Peterson, Michelle Werner, Jim Scott and Dr. Randy Dunsing for their patience in answering my questions. Special thanks to Dr. Emmett Bolch for his moral and financial support during my extended period as a graduate student. I wish to specifically thank Ben Warren for allowing me the time away from work to pursue this degree.

## TABLE OF CONTENTS

ACKNOWLEDGMENTS .....	ii
ABSTRACT .....	v
CHAPTERS	
1 INTRODUCTION .....	1
MRI Fields .....	1
Static Magnetic Fields .....	1
Gradient Magnetic Fields .....	2
Radio-Frequency Fields .....	4
Current Standards .....	6
INIRC-IRPA .....	6
ANSI .....	7
IEC .....	8
FDA .....	10
Contrast .....	12
Specific Absorption Rate .....	13
Loading Factors .....	14
SAR Development with Far-Field Assumptions .....	16
SAR Development Without Far-Field Assumptions .....	21
2 MATERIALS AND METHODS .....	29
Head Phantom .....	29
Thermocouple Measurements .....	30
Fiber Optic Measurements .....	32
Heating Protocol .....	33
Thermal Imaging .....	34
T1 Relaxation Time Imaging .....	34
Diffusion Imaging .....	37
Proton Chemical Shift Imaging .....	40
Phantom Thermal Imaging .....	42

3 RESULTS .....	48
Thermocouple Results .....	48
Fiber Optic Results .....	50
Heating Equation .....	51
Cooling Equations .....	54
Diffusion Imaging .....	55
Procedures .....	55
4 DISCUSSION .....	78
5 CONCLUSION .....	82
Future Work .....	83
APPENDICES	
A INTERNATIONAL ELECTROTECHNICAL COMMISSION (IEC) .....	86
B FOOD AND DRUG ADMINISTRATION (FDA) .....	116
C PHANTOM PROTOCOL - THERMOCOUPLE .....	118
D PHANTOM PROTOCOL - FIBER OPTIC .....	119
E HEAT STRESS INDEX .....	120
F EXPERIMENTAL RESULTS .....	131
G ARTIFACT TUNING .....	140
H DIFFUSION IMAGING .....	142
I DIFFUSION IMAGING PROTOCOL .....	143
J IMAGE TRANSFER .....	144
K DIFFUSION IMAGE CONVERSION PROGRAM .....	146
LIST OF REFERENCES .....	159
LIST OF SUPPLEMENTAL REFERENCES .....	162
BIOGRAPHICAL SKETCH .....	167

Abstract of Dissertation Presented to the Graduate School  
of the University of Florida in Partial Fulfillment of the  
Requirements for the Degree of Doctor of Philosophy

**THERMAL DOSIMETRY FROM RADIO-FREQUENCY FIELDS WITHIN A  
HEAD PHANTOM ASSESSED DURING THREE TESLA MAGNETIC  
RESONANCE IMAGING**

By

George Harder

August 1998

Chairperson: Dr. W. Emmett Bolch

Major Department: Environmental Engineering Sciences

Magnetic Resonance Imaging (MRI) provides radiologists with the tools to better diagnose disease and view internal injuries. As field strengths increase, so does resolution and so do potential health effects. This dissertation focused on tissue heating generated by the radio-frequency (RF) energy. Thermal measurements were first made using thermocouple probes. Experimental results, which were affected by the metallic nature of the thermocouple, were discarded. The experiments were repeated using fiber optic probes. Tests revealed uneven thermal energy deposition throughout the head phantom. Temperatures nearer the outer edge increased sooner. Additionally, there was thermal movement resulting in increased temperatures to the center of the head phantom up to an hour after the RF fields were removed. Finally, a diffusion imaging technique was performed prior to and after a scan. Analysis of the resultant images indicated diffusion imaging may be able to monitor temperatures less than the 1 °C as stated in literature.

## CHAPTER 1 INTRODUCTION

The applied theory of magnetic resonance provided imaging and spectroscopy. Increased field strengths enhanced resolution providing radiologists improved, non-invasive diagnostic tools. Increased field strengths also brought increased potential for health effects. The MRI system utilizes the nuclear spins of isotopes to define the presence of the isotope. At the three Tesla (3T) MRI unit, jointly owned by the Veterans Administration and Shands Teaching Hospital, the isotope of interest during the research of this project was the proton (hydrogen). Since the human body contains a high percentage of water, proton imaging would provide some type of image from every tissue type and every location within the body. MRI produces three fields; the static magnetic field, the gradient magnetic field and the RF field.

### MRI Fields

#### Static Magnetic Fields

According to the Food and Drug Administration (FDA), clinical MRI systems in the United States were permitted to function on a routine clinical basis at static magnetic field strengths of up to 2T. This was recently increased to 4T. Above this level, evidence of safety must be provided by the sponsor or device manufacturer prior to routine clinical use. Static magnetic fields have no effect on skin or body temperature (Budinger, 1992).

Heat was only deposited in tissue when current flowed through the tissue and current was only induced by a changing a magnetic field. In this respect tissue was invisible to static magnetic fields. Patient movement within a static magnetic field was considered a dynamic magnetic field from the tissue's viewpoint. However, this movement was slow and was insufficient in creating a noticeable current.

Problems that have been reported by patients after entering the MRI chamber but before the gradients fields were applied were dizziness and nausea. These effects mimic motion sickness and have a similar root cause. Balance has always been perceived by the circulating inner ear fluids. The calcium carbonate particles, called otoliths, moved against the hair cells in the saccule and utricle sending false signals to the brain that the head was moving. The brain received conflicting signals from the inner ear and the other senses. Increased discomfort compounded the problem. For individuals easily susceptible to motion sickness, very little head movement was required. Since this problem dealt with the motion of the otoliths, this effect was also associated with gradient magnetic fields.

### Gradient Magnetic Fields

Effects have been reported by patients subjected to changing magnetic fields. At switching rates of two Tesla per second (T/s), patients have reported light flashes called magnetophosphenes. Switched magnetic field excited the optic nerve inducing electrical currents. The optic nerve responded as if it received a light pulse from the eye. Since these were random and isolated, the result appeared as flashes of light. This effect was also be achieved in a static magnetic field by rapid movement of the head (Kanal 1990).



At switching rates of 60 T/s patients have experienced neuromuscular excitation. Faraday's Law of Induction stated that a conductor, in the presence of a time-varying magnetic field, would induce a voltage in the conductor that was oriented perpendicular to the rate of change of the magnetic field. When a voltage difference along a nerve approached 6 V/m, neurological impulses trigger a peripheral nerve stimulation. This peripheral nerve stimulation was an uncontrolled, involuntary skeletal muscle contraction and/or twitching (Reilly 1989, Schaefer 1992). One FDA guideline to limit patient exposure to time-varying magnetic fields specifically required demonstration, with "valid scientific evidence," that the rate of change of magnetic field for the system was not sufficient to cause peripheral nerve stimulation. At switching rates of 500 T/s cardiac excitation became possible. A perturbation of an electrocardiogram was identified as a superimposed signal of the gradient pulse (Budinger 1992). No long term effects were demonstrated by the superimposed signal.

While biological tissue was predominantly transparent to dynamic magnetic fields, there were still elements within the tissue that responded to magnetic fields. As magnetic fields increased, these affected elements began causing noticeable effects. Currents, induced by the changing magnetic field, flowed through the resistive body fluids to produce heat. The amount of heat or energy produced was a function of the frequency, intensity and duration of the exposure and the coupling between the RF coil and the subject.



### Radio-Frequency Fields

The predominant effect of RF fields was RF heating. The biological factors of importance were conductivity, specific gravity of the tissue, size of the current loop, circulation and the ability of the body to lose heat. An issue that often arose was not whether localized heating existed but how much and what was its biological impact. The majority of damage to cells and molecules was through ionization caused by heat. RF fields were too high in frequency to stimulate excitable tissues electrically however these fields deposited energy into tissues which raised their temperatures. The normal body temperature remained approximately 37 °C. The highest safe core temperature for individuals was 39.4 °C. The skin pain threshold was 43 °C and proteins denatured at about 45 °C. This small range of temperatures became critical at higher field strengths. The potential for localized heating and subsequent tissue damage increased as RF frequencies increased to the point where the patient's size approached one-half wavelength of the incident excitation frequency (Gordon 1992).

An area of major concern for MRI of the head was the eye. The vitreous body of the eye contained a colorless, jelly mass between the lens and the retina. Heat removal resulted from the formation and circulation of the aqueous humor as well as from the ophthalmic artery. The eye had a reduced capability for heat dissipation as a result of a lack of vascularization. Acute near-field exposures of RF radiation to the eye of laboratory animals created cataracts as a result of the thermal disruption of ocular tissues. The threshold for cataractogenesis had been estimated at 100 W/kg. An investigation revealed no discernible effects on the eyes of rats resulting from MR procedures at

exposures that far exceeded typical levels used in the clinical setting (Shellock 1992).

Patients exposed to SAR levels of 0.5 to 1.3 W/kg had shown significant elevations in temperatures in the cornea. The cornea was anterior to the lens and contained no blood vessels. Heating of the cornea had the potential to lead to keratitis, an inflammation of the cornea while heating of the lens accelerated the onset of cataracts. The cornea was pain-sensitive and a conscious patient would be able to feel this heating before it became severe.

Various underlying health conditions affected an individual's ability to tolerate RF heating. The state of a patient's health, cardiovascular conditioning and obesity were primary factors. Various medications (e.g. diuretics, beta-blockers, calcium blockers, amphetamines, muscle relaxers and sedatives) also altered the thermoregulatory responses to RF heating. The heat loss characteristics of the body were not applicable to head phantom studies so tissue heating characteristics from MRI to the head phantom, therefore, provided a worst-case scenario. Such conditions would exist for a stroke victim with limited thermoregulatory responses in the head.

Static and dynamic magnetic fields produced temporary effects to patients with no long term consequences. The effects from RF fields resulted in increased temperatures to patients which could be dangerous. A head phantom provided a versatile platform for conducting heating tests and defining methods to measure and monitor thermal changes. In order to determine what method to use to measure temperature changes, the range of acceptable temperature changes were derived from standards.

### Current Standards

Radiation falls into one of two categories: ionizing and non-ionizing. Ionizing radiation is defined as having sufficient energy to ionize an atom. MRI falls into the category of non-ionizing radiation since its electromagnetic fields create insufficient energy to ionize molecules, but sufficient energy for thermalization. To quantify this thermal action the energy absorption over a small mass of material is defined as the specific absorption rate (SAR) and is given in units of watts per kilogram. Although the SAR defines the energy absorbed within tissue, it has always been impractical to measure this energy change in live subjects. Instead the surface power density, given in  $\text{W}/\text{cm}^2$ , has been measured. Utilizing the tissue density and tissue attenuation characteristics, the SAR can be inferred. The SAR has been the currently accepted means of indicating RF exposure levels and several organizations have established guidelines for permissible levels of exposure to static and varying magnetic fields and to RF fields.

### INIRC-IRPA

The International Non-Ionizing Radiation Committee of the International Radiation Protection Association (INIRC-IRPA) is an international association providing universal guidance on a variety of non-ionizing radiation standards (INIRC-IRPA 1991). For static magnetic fields, a patient's cardiovascular function should be monitored during exposures above 2T to the head or trunk and above 5T for limbs. For time-varying magnetic fields, a patient's cardiovascular function should be monitored during exposures above 6 T/s. Time-varying magnetic fields should not exceed 20 T/s. For RF fields,

exposures up to one hour should not exceed a total energy deposition of 120 W·min/kg which equates to a SAR of 2 W/kg. To avoid overheating, the following product of time and SAR should not exceed:

- 60 W·min/kg (1 W/kg for 1 hour) averaged over the head,
- 120 W·min/kg (2 W/kg for 1 hour) averaged over the trunk or
- 180 W·min/kg (3 W/kg over 1 hour) averaged over the extremities.

Instantaneous SAR should not exceed:

- 4 W/kg in the head,
- 8 W/kg in the trunk,
- 12 W/kg in the extremities or
- 10 W/kg in 0.01 kg or more than 10 minutes for the eyes.

### ANSI

The National Council on Radiation Protection and Measurements (NCRP) Scientific Committee 39, Report No. 67, is entitled *Radiofrequency Electromagnetic Fields: Properties, Quantities and Units, Biophysical Interaction and Measurements* (NCRP 67). Report No. 67 is a primary source upon which American National Standards Institute (ANSI) C95.1-1982 is based and it concluded there is little possibility of directly measuring the absorption of energy by biological bodies at the cellular level. This becomes important when dealing with hot spot generation which is the concentration of energy into a small volume. Cell death, especially in the brain area, can cause irreversible damage.

The 3T MRI system, for proton imaging, operates at 128 MHz limiting the equivalent power density to one mW/cm<sup>2</sup> (Table 1-1). These guidelines make no provisions for near-field radiation. In far-field radiation, generally one wavelength from the antenna, the electric and magnetic fields become well behaved and remain orthogonal to each other and the direction of propagation. This permits power density calculations using either electric or magnetic field measurements. In the near-field, close to the antenna, the electric field and magnetic fields have not aligned with each other. Additionally, there is a reactive field. This field is the inductive or capacitive storage of energy by the antenna itself. It does not propagate far from the antenna but still can interact with tissue within its influence. ANSI C95.1-1982 provides results from either the electric field or the magnetic field and uses far-field assumptions to calculate SAR. The 3T MRI system operates only in the near field. The equivalent power density must then become a function of both the electric and magnetic fields.

### IEC

The International Electrotechnical Commission (IEC) provides extensive standards for RF exposures. A complete listing of the IEC standards are provided in Appendix A. The following requirements are applicable for room temperatures below 24 °C and where the relative humidity does not exceed 60%. The requirements regarding SAR from RF power further assumes that the SAR averaged over any 10 second period does not exceed 5 times the stated temporal average SAR limit.

- a. Whole-body SAR. Three operating modes with regard to whole-body



SAR are defined, namely Normal Operating Mode, First Level Controlled Operating Mode and Second Level Controlled Operating Mode (Figure 1-1).

- i. The Normal Operating Mode comprises values of whole-body SAR not higher than 1.5 W/kg averaged over any period of 15 minutes.
  - ii. The First Level Controlled Operating Mode comprises values of whole-body SAR not higher than 4 W/kg averaged over any period of 15 minutes.
  - iii. The Second Level Controlled Operating Mode comprises values of whole-body SAR that may exceed 4 W/kg averaged over any period of 15 min.
- b. Head SAR. Two operating modes with regard to head SAR are defined, namely Normal Operating Mode and Second Level Controlled Operating Mode (Figure 1-2).
- i. The Normal Operating Mode comprises values of head SAR not higher than 3 W/kg averaged over any period of 10 minutes.
  - ii. The Second Level Controlled Operating Mode comprises values of head SAR that may exceed 3 W/kg averaged over any period of 10 minutes.
- c. Local Tissue SAR With the Use of Special Coils. Two operating modes with regard to local tissue SAR are defined, namely Normal Operating Mode and Second Level Controlled Operating Mode.

- i. The Normal Operating Mode comprises values of local tissue SAR in any one gram of tissue not exceeding 8 W/kg in the head or torso or 12 W/kg in the extremities averaged over any period of 5 min.
- ii. The Second Level Controlled Operating Mode comprises values of local tissue SAR that may exceed the upper limit for the Normal Operating Mode.

### FDA

The Food and Drug Administration (FDA) provides the approval for MRI systems in the U.S. Currently, static magnetic fields up to 2T are permitted for clinical magnetic resonance systems. Above that level, the system must show evidence of safety before routine clinical use. Therefore the 3T system has not been approved by the FDA for patient use but has been permitted as a research unit. The FDA provided three alternatives for patient exposure to time-varying magnetic fields.

- 1. Demonstrate that the maximum change in magnetic field strength ( $dB/dt$ ) of the system is 6 T/s or less. This is 1/10 the threshold of peripheral nerve stimulation and almost 1/100 the possible threshold for cardiac excitation.
- 2. A. Demonstrate that for axial gradients (Figure 1-3):
  - i.  $dB/dt < 20 \text{ T/s}$  for  $T > 120 \mu\text{s}$ ;
  - ii.  $dB/dt < 2400/(t(\mu\text{s})) \text{ T/s}$  for  $12 \mu\text{s} < T < 120 \mu\text{s}$  or
  - iii.  $dB/dt < 200 \text{ T/s}$  for  $T < 12 \mu\text{s}$ .



- B. Demonstrate that for transverse gradients,  $dB/dt$  is considered to be below the level of concern when less than three times the above limits for axial gradients.
- 3. Demonstrate with “valid scientific evidence” that the rate of change of magnetic fields for the system are not sufficient to cause peripheral nerve stimulation by an adequate margin of safety (which the FDA establishes as at least a factor of three).

Exposure to RF energy, which the FDA considers below the level of concern, is a SAR of

- 1. 0.4 W/kg or less averaged over the body;
- 2. 8.0 W/kg or less spatial peak in any 1 gram of tissue; or
- 3. 3.2 W/kg or less averaged over the head.

The FDA has stated that the exposure to RF energy must not increase the body’s core temperature by 1 °C and that the temperature not exceed 39 °C in the trunk and 40 °C in the extremities. Normal body temperatures range from 35.5 °C to 40 °C with an average of 37 °C.

The FDA issued a document on September 29, 1997 (Appendix B) titled “Guidance for Magnetic Resonance Diagnostic Devices - Criteria for Significant Risk Investigations.” This document was designed to provide guidance only and did not constitute a regulatory change. This guidance allowed exposures to static magnetic fields up to four Tesla. Exposures to RF energy were also modified to SARs of

1. 4 W/kg averaged over the whole body for any 15 minute period;
2. 3 W/kg averaged over the head for any 10 minute period; or
3. 8 W/kg in any gram of tissue in the head or torso or 12 W/kg in any gram of tissue in the extremities for any 5 minute period.

For this research, which dealt with the head, the SAR limits were lowered from 3.2 W/kg to 3 W/kg. The time limits, which were not previously a part of the guidance, limits applications of brief periods of higher energy depositions. Quantitative standards for gradient magnetic fields was removed and replaced with the non-definitive provision that gradient fields should not “produce severe discomfort or painful nerve stimulation.”

### Contrast

The ANSI standards only address SAR in the far-field region where the electric and magnetic fields have become aligned with each other. These standards provide no real guidance for the MRI system. The INIRC-IRPA, FDA and IEC standards address time-varying magnet fields with the predominant reaction of concern being peripheral nerve stimulation which can be most damaging when affecting the heart muscle. Each standard provides a safety factor of 10 with the new FDA guideline removing quantitative values. Most peripheral nerve stimulation was not observed or anticipated until changing magnetic fields exceeded 60 T/s. The 3T MRI can switch magnetic fields at this rate. The IEC standards addressed a uniform method of measuring power deposition. Two methods of SAR measurement are available. One method is designed specifically for whole body

SAR. The other method measures the average power absorbed by an object of known mass to provide a representative indicator of SAR.

Until ratification of the new FDA guidance, the FDA standards must still be met before patient use of the 3T system. There was no guidance on any uniform testing procedure available. It becomes the responsibility of the particular facility to provide proof of compliance. Therefore the results obtained during this research may be used to provide proof of the safety of the 3T MRI system.

### Specific Absorption Rate

Of the three parameters of concern during MRI; static magnetic fields, gradient magnetic fields and RF fields, the RF fields provide effects resulting in possible permanent harm to patients. By definition, the specific absorption rate is “the time derivative of the incremental energy (dW) absorbed by, or dissipated in an incremental mass (dm) contained in a volume element (dV) of a given density.” (NCRP 67). Mathematically this is represented by

$$SAR = \frac{d}{dt} \left( \frac{dW}{dm} \right) = \frac{d}{dt} \left( \frac{dW}{\rho(dV)} \right) \left[ \frac{W}{kg} \right].$$

Realistically the amount of energy deposited within a unit of tissue can not be measured. However, other characteristics can be measured. Power deposition can be inferred if the amount of energy provided to the target tissue were known and certain characteristics of the target tissue were also known. With the power deposition defined

and tissue mass measured, the SAR can be defined over any period of time. This section describes three methods for the development of SAR equations: (1) using loading factors, (2) using Poynting vectors with far-field assumptions and (3) using Poynting vectors without far-field assumptions.

### Loading Factors

Loading factors provided RF deposition measurements by defining the loading factor of an empty coil ( $Q_o$ ) and the loading factor of a coil loaded with the patient ( $Q_1$ ) (Werner 1993). The patient's loading factor,  $Q_T$ , was then calculated.

$$\frac{1}{Q_T} = \frac{1}{Q_1} - \frac{1}{Q_o}$$

The RF power  $P_T$  deposited in tissue in the presence of a linearly polarized  $B_1$  field became

$$P_T = \frac{1}{2} \left( \frac{B_1}{S} \right)^2 \frac{\omega L}{Q_T}$$

where  $\omega = 2\pi f$  was the angular frequency,  $L$  was the coil inductance and  $S$  was a coil constant giving the magnetic field produced per unit current in the coil. The required value of  $B_1$  depended on the desired flip angle  $\alpha$  and the RF pulse length  $\tau$  (Roschmann 1987). If the RF pulses had a rectangular envelope, the required linearly polarized  $B_1$  was to

$$B_1 = 2\alpha/\gamma_i\tau$$

where  $\gamma_i$  was the gyromagnetic ratio of the considered nucleus  $i$  (for protons  $\gamma_i = 42.58$  MHz/T).

The SAR was the result of the scan time and mass of the target.

$$SAR = \frac{P_T T}{m_T}$$

For the phantom this was a valid assumption. For the human head this was not valid but could still be safely assumed at lower field strength MRI system. The amount of tissue heating becomes unique to each part of the brain as a function of its electrical characteristics. Some portions absorb more energy and would display increased temperatures. Overall, temperature increases would remain reasonable for lower field strength MRIs and would not have caused any permanent damage. However, at 3T, power deposition per unit mass encroached on the SAR limits. At the higher energies, the generation of hot spots became an issue. The tissue material with high conductive properties would absorb more RF energy while those with lower conductive properties would absorb less. The total power deposition per unit mass, averaged over the entire head, would meet FDA guidelines but provide no method to determine hot spots. Using loading factors was not an acceptable method for safeguarding patient injuries but may, however, still provide a first step in determining the range of energy deposition.

### SAR Development with Far-Field Assumptions

Another method described for calculating SAR was the Poynting vector. The Poynting vector theorem was developed to find the power in a uniform plane wave made up of an electromagnetic field. An electromagnetic field consists of two parts, the electric field and the magnetic field. The ANSI C95.1-1982 protection guides provide an equivalent power density equation based on one of the measurable fields.

$$SAR = \frac{\sigma}{2\rho} |E_i|^2$$

where  $\sigma$  = tissue conductivity

$\rho$  = tissue density

$E_i$  = electric field

The Poynting vector was defined as the cross product between the electric and magnetic fields and interpreted as an instantaneous power density with units of watts per area ( $W/m^2$ ).

$$P = E \left( \frac{V}{m} \right) \times H \left( \frac{A}{m} \right) = E \times H \left( \frac{W}{m^2} \right)$$

Under the conditions of the SAR equations defined by NCRP Report 67, the target tissue was assumed in the far-field. At the antenna, both the electric field and the magnetic field exist independently. Both begin propagating outward. Since there was no immediate relationship between the two fields, their phase angles were random. In the far field, with

a predictable 90° relationship, an intrinsic impedance,  $\eta$ , was defined as the square root of the ratio of permeability to permittivity.

$$\eta = \sqrt{\frac{\text{permeability}}{\text{permittivity}}} = \sqrt{\frac{\mu}{\epsilon}}$$

Additionally, and simply, in the far-field, the intrinsic impedance, as a perfect dielectric, was defined as the ratio of the electric field to the magnetic field

$$\eta = \frac{E}{H}$$

Using this identity, and averaging the Poynting vector, the magnetic field component of the Poynting vector was removed.

$$P = \frac{1}{2} \frac{E^2}{\eta}$$

The human body can be considered a lossy dielectric in which case the intrinsic impedance became a complex value. The complex value was written in polar form defined by a vector length and a vector angle representing the phase difference of the electric and magnetic fields. As will be demonstrated later, certain assumptions were made to reduce the complex nature of the intrinsic impedance.

$$\eta = \sqrt{\frac{j\omega\mu}{\sigma + j\omega\epsilon}} = \eta_m / \theta_n$$



Additionally, as the electric field progressed into the tissue, it attenuated as a function of the tissue's skin depth,  $e^{-d/\delta}$ , where  $d$  denoted distance into the tissue and  $\delta$  denoted skin depth. The human body, and the head in particular, have different tissue types at different depths and the skin depths of these tissues vary. For the development of the SAR equation for the phantom an assumption of a homogeneous tissue mass was used.

The Poynting vector was modified to

$$P = \frac{1}{2} \frac{(E e^{-d/\delta})^2}{\eta} = \frac{1}{2} \frac{E^2 e^{-2d/\delta}}{\eta_m / \cos \theta_n} = \frac{1}{2} \frac{E^2 e^{-2d/\delta}}{\eta_m} \cos \theta_n$$

The average power from a continuously emitting source applied to a tissue was derived from the total power and the total area of concern.

$$\text{average power} = P \times \text{area} = \frac{1}{2} \frac{E^2 e^{-2d/\delta}}{\eta_m} \cos \theta_n \times A$$

The polar form for average power implied a real and imaginary portion of power. It was only the real portion, that defined the reactive aspect of power, that lead to energy deposition in tissue. The Poynting vector reduced to

$$\text{average power} = \frac{1}{2} \frac{E^2}{\eta_m} e^{-2d/\delta} \cos \theta_n \times A$$

To further simplify the intrinsic impedance, NCRP Report 67 assumed the target tissue met the definition of a good conductor. The larger the ratio of conduction current,

$\sigma$ , to displacement current,  $\omega\epsilon$ , the better the conductor. In a good conductor, the electric and magnetic fields remain close to  $90^\circ$  out of phase which then supports the previous assumption used to remove the magnetic field component from the SAR equation. This was validated by calculating the phase relation when  $\sigma \gg \omega\epsilon$  for a given tissue.

$$\tan^{-1}\left(\frac{\sigma}{\omega\epsilon}\right) \approx 90^\circ$$

Tissue high in water content met this requirement. This included muscles and both white and gray brain matter and the tissue equivalent material used in the head phantom. For adipose laden tissue and bone, with low water content, the tissue conductivity and displacement current are closer. However, for the development of the SAR equation  $\sigma \gg \omega\epsilon$  and the following modification was applied to the intrinsic impedance.

$$\eta = \sqrt{\frac{j\omega\mu}{\sigma + j\omega\epsilon}} = \sqrt{\frac{j\omega\mu}{\sigma}} = \frac{\sqrt{2}j}{\sigma\delta} = \frac{\sqrt{2}}{\sigma\delta} \angle 45^\circ = \frac{\sqrt{2}}{\sigma\delta} \cos(\tan^{-1}(1))$$

$$NOTE: \quad \frac{1}{\delta} = \sqrt{\frac{\omega\mu\sigma}{2}}$$

This was derived from the propagation constant equation

$$\gamma = j\omega\sqrt{\mu\epsilon} \sqrt{1 - j\frac{\sigma}{\omega\epsilon}}$$

For a good conductor,  $\sigma/\omega\epsilon \gg 1$  and

$$\begin{aligned}
 \gamma &= j\omega\sqrt{\mu\epsilon}\sqrt{-j\frac{\sigma}{\omega\mu}} = j\sqrt{-j\omega\mu\sigma} \\
 &= \frac{1}{\sqrt{2}}\sqrt{\omega\mu\sigma} \angle -90^\circ \\
 &= \sqrt{\omega\mu\sigma} \angle 45^\circ \\
 &= \sqrt{\omega\mu\sigma} \cos 45^\circ + j\sqrt{\omega\mu\sigma} \sin 45^\circ \\
 &= \frac{1}{\sqrt{2}}\sqrt{\omega\mu\sigma} + j\frac{1}{\sqrt{2}}\sqrt{\omega\mu\sigma}
 \end{aligned}$$

The real portion of this equation was the attenuation constant which defined the amount of attenuation per distance traveled in the medium. This distance was based on  $1/e$  attenuation which, by definition, also became the foundation of skin depth. The attenuation constant, therefore, was the inverse of the skin depth,  $\delta$ .

$$\delta = \frac{\sqrt{2}}{\sqrt{\omega\mu\sigma}}$$

Using only the real portion of the intrinsic impedance

$$\eta = \frac{\sqrt{2}}{\sigma\delta} \cos(45^\circ) = \frac{1}{\sigma\delta}$$

The simplified intrinsic impedance was applied to the average power equation

$$\text{average power} = \frac{\sigma\delta}{2} E^2 e^{-2d/\delta} \times A$$

The SAR was defined as the average power per mass of the target tissue.

$$SAR = \frac{\text{average power}}{\text{mass}}$$

Substituting the definition of the average power

$$SAR = \frac{\frac{\sigma\delta}{2} E^2 e^{-2d/\delta} \times A}{\rho \times \text{volume}}$$

To simplify the equation, the volume of interest was defined as an area,  $A$ , down to one skin depth,  $\delta$ . Additionally, the power calculation defined the incident power at the skin surface ( $d = 0$ ).

$$SAR = \frac{\sigma}{2\rho} E^2$$

### SAR Development Without Far-Field Assumptions

Two assumptions were made in order to derive the SAR equation. First, that the

target tissue resided in the far-field and second, that the target tissue met the requirement of a good conductor. These assumptions are reviewed in the next two sections.

**Far-Field Assumption.** The far-field region begins at some finite distance from the antenna and stretches to infinity. In the far-field, the electric field strength, magnetic field strength and power density are orthogonal to each other and one parameter can define the others.

$$P = E \times H = \frac{E^2}{120 \pi} = 120 \pi H^2$$

(where P was expressed in W/m<sup>2</sup>, E in V/m and H in A/m)

The area from the antenna to the beginning of the far-field defines the near-field which consists of the radiating field in addition to a reactive (nonradiating) field. This energy can be capacitive or inductive and can affect the electric and magnetic field vectors. The reactive region remains adjacent to the antenna and extends to about one wavelength from the antenna. Like the far-field, the electric and magnetic field intensity decreases with distance but unlike the far-field the radiation still lacks the plane-wave characteristics of the far-field electric and magnetic fields. No relative assumptions are available to characterize one field by the other. Measurement of both fields are required to accurately define the SAR. For a 3T system operating near 128 MHz, one wavelength extends to 2.34 m which placed the target tissue well in the near-field region. Far-field assumptions for SAR were invalid but unfortunately "...recommendations of RF exposure limits are based on the experimental data for the far-field exposures and are usually formulated in

terms of the far-field parameters. Only general guidance regarding the SAR was given for the near-field exposures,” (Stuchley 1985).

**Good Conductor.** The second assumption made in the SAR development was that the material imaged with the MRI was a good conductor. The intrinsic impedance,  $\eta$ , was simplified under the assumption that  $\sigma \gg \omega\epsilon$ , or that the ratio of conduction current to displacement current ( $\sigma/\omega\epsilon$ ) was much greater than unity.

For the human head,  $\sigma/\omega\epsilon$  for bone and fat were 0.47 and 0.52 respectively, which do not approach the definition for a good conductor. Since these were the incident tissues of the head, the good conductor assumption for intrinsic impedance became invalid. Likewise, for the head phantom, the polyethylene casing had a low water content and had a conduction current that was smaller than the displacement current,  $\sigma/\omega\epsilon = 0.0002$ . The electric and magnetic fields, even if they had been orthogonal would have lost cohesion after transcending the bone and fat layers of the head or the polyethylene casing of the head phantom. Brain matter, having a higher water content than fat proved to be a better conductor and fell under the guidelines of a conduction current greater than the displacement current,  $\sigma/\omega\epsilon = 2.71$ . The tissue equivalent material was constructed mainly of water which had a conduction current that was four times the displacement current,  $\sigma/\omega\epsilon = 4$ .

With the good conductor assumption, the skin depth was defined as

$$\frac{1}{\delta} = \sqrt{\frac{\omega\mu\sigma}{2}}$$

or

$$\delta = \frac{\sqrt{2}}{\sqrt{\omega\mu\sigma}}$$

To accurately define the skin depth, regardless of the tissue's conduction property will require recalculation of the propagation constant.

The propagation constant combined an attenuation constant with a phase constant. The attenuation constant defined the loss of signal strength as a wave propagated through a medium. The phase constant defined the angular shift of the wave per distance traveled. The inverse of the attenuation constant yielded the skin depth. Mathematically, the equation for the propagation constant was  $\gamma = \alpha + j\beta$  and the equation for skin depth was  $\delta = 1/\alpha$ .

Differences Between Near-Field and Far-Field Assumptions. Power deposition estimation from a theoretical basis in the near-field, as required by the MRI, is complex. No correlation between the electric and magnetic fields exists allowing only assumptions to be made. The assumptions required to formulate a generalized estimate eliminates the minor imperfections that give rise to individual power deposition values for each individual imaged (Mahony 1995, Bottomley 1985, Bottomley 1981, Boesiger 1992).

The skin depth was used for comparison between near-field and far-field assumptions. Using far-field assumptions,



$$\delta = \frac{\sqrt{2}}{\sqrt{\omega \mu \sigma}}$$

$$\sigma = \frac{\sigma}{\omega \epsilon} \epsilon_R \epsilon_o \omega = 0.00804$$

$$\delta = \frac{\sqrt{2}}{\sqrt{2\pi \times 128 \times 10^6 \times 4\pi \times 10^{-7} \times 8.04 \times 10^{-3}}} = 0.5 \text{ m}$$

Next the propagation constant, which contained no far-field assumptions, was used to calculate skin depth.

$$\gamma = j\omega \sqrt{\mu\epsilon} \sqrt{1 - j\frac{\sigma}{\mu\epsilon}}$$

$$\gamma = 127.5 \angle 89.97^\circ$$

$$\delta = 127.5 \cos(89.97^\circ) = 0.248 \text{ m}$$

The far-field assumption tended to overestimate the skin depth of the polyethylene outer husk by a factor of two. Therefore, using far-field assumptions would cause an under-estimation of power deposition in “poor” conductors. For the head phantom, this would include the out husk. For the human head this would include adipose tissue and bone. Since both of these are near the outer surfaces, the under-estimation of power deposition would be similar, still allowing use of the head phantom in human head power deposition studies.

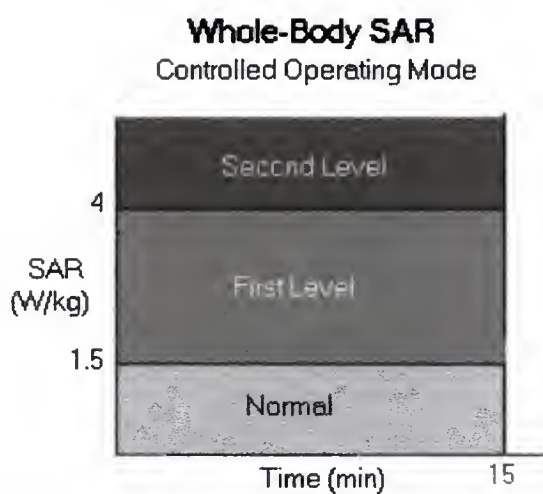


Figure 1-1. IEC Whole-Body SAR Guidelines.

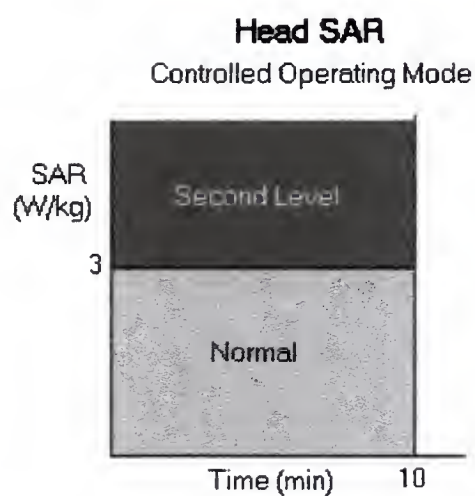


Figure 1-2. IEC Head SAR Guidelines.

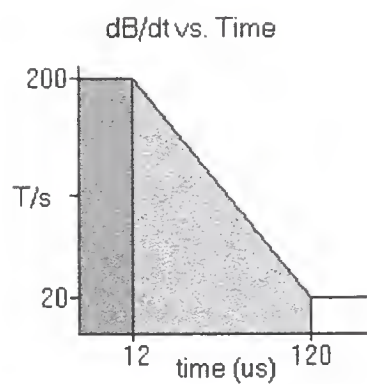


Figure 1-3. FDA Axial Gradient Magnetic Field Guidelines.

Table 1-1. ANSI C95.1-1982 Protection Guide for Radio-Frequency Electromagnetic Radiation.

Frequency range	Equivalent power density <sup>a,b</sup>	(Electrical field) <sup>2</sup>	(Magnetic field) <sup>2</sup>
MHZ	mW/cm <sup>2</sup>	V <sup>2</sup> /m <sup>2</sup>	A <sup>2</sup> /m <sup>2</sup>
0.3 - 3	100	4 X 10 <sup>5</sup>	2.5
3.0 - 30	900/f <sup>2</sup>	4 X 10 <sup>3</sup> (900/f <sup>2</sup> )	0.025 (900/f <sup>2</sup> )
30 - 300	1.0	4 X 10 <sup>3</sup>	0.025
300 - 1500	f/300	4 X 10 <sup>3</sup> (f/300)	0.025 (f/300)
1500 - 100,000	5.0	2 X 10 <sup>4</sup>	0.125

<sup>a</sup> measured 5 cm or greater from any object in the field and averaged for any 0.1 h (6 min.).

<sup>b</sup> (electric field)<sup>2</sup>/1200 $\pi$  or 12 $\pi$ (magnetic field)<sup>2</sup>, whichever is greater.

## CHAPTER 2 MATERIALS AND METHODS

Experiments were performed using invasive and non-invasive temperature measurements at the VA/Shands 3T MRI Unit. Invasive measurements were made using thermocouples and fiber optic cables. A thermocouple system was inexpensive but greatly affected the results. A fiber optic system was expensive but immune to RF fields which provided better results. Temperatures were measured non-invasively using a diffusion MRI technique. All measurements were performed on a head phantom installed in the General Electric (GE) Head Coil.

### Head Phantom

The head phantom used through these experiments was created by Charles Webster and Jim Scott using a plaster cast of a volunteer. A polyethylene covering was form-fitted over the plaster cast which was then broken and removed. The outer husk was constructed of 6.35 mm (1/4") polyethylene which had known electrical properties of permittivity, intrinsic impedance and skin depth (Table 2-1). The polyethylene material contained a low water content and was suspected of being a poor conductor.

The polyethylene mold was filled with tissue equivalent material (Table 2-2). The tissue equivalent material was formulated by Jim Scott to provide similar loading characteristics in the GE Head Coil as the human head (Olsen 1992, Chou 1984).

This material had a density of  $1.01 \text{ g/cm}^3$  and a total volume of 5250 ml.

Equipment was not available to determine the permittivity and conductivity of the tissue equivalent material but certain assumptions allowed useable test results. Tissue, such as brain matter, has a specific heat of  $3.5 \text{ J/cm}^3\text{°C}$ . The tissue equivalent material has a 0.00461 to 1 ratio of NaCl to water. Using this value with known values of specific heat, the tissue equivalent material specific heat was extrapolated (Table 2-3)(Leonard 1984). Therefore, the tissue equivalent material should have thermal characteristics close to that of the brain (Table 2-4).

### Thermocouple Measurements

Temperature measurements in the tissue equivalent material were made using a thermocouple connected to an Atkins Model #39641-T. The T-Type indicated the thermocouple was made of copper-constantan. The junction of the copper and constantan was exposed allowing for fast response times. The Atkins unit provided temperatures to within  $0.1^\circ\text{C}$  or  $0.1^\circ\text{F}$ . Since  $0.1^\circ\text{F}$  was a smaller unit, a slight increase in accuracy was obtained from measurements made in Fahrenheit. Temperature measurements were later converted to Centigrade.

A 6.35 mm ( $1/4"$ ) hole had been drilled into the location of the right eye of the head phantom and used as the insertion point for temperature reading devices. Originally, the thermocouple was inserted into the phantom and left in the phantom during the scan. Interference from the RF signals distorted the readings on the Atkins unit so a low-pass filter was installed. The calibration of the Atkins unit was invalidated with the addition of

the low-pass filter. The unit was then disconnected from the thermocouple during the scan. A pre-existing phantom protocol had been programmed into the Advanced NMR (ANMR) console. This protocol was modified to provide a higher range of output power. The modified protocol is listed in Appendix C.

A 48 minute scan at 18 watts average power (as indicated on the Omega process indicator) exhibited a 3.9 °C rise in temperature using the Atkins thermocouple. The temperature immediately dropped an average of 1.1 °C within two minutes of the end of the scan. Further testing revealed that the temperature of the tissue equivalent material was raised by the presence of the thermocouple cable during the scan. This invalidated results.

The experimental method was adjusted. Prior to the scan the thermocouple was inserted to one of three depths: the top surface, middle of the tissue equivalent material or the back of the head phantom (Figure 2-1). The temperature was read for approximately two minutes or until the reading on the Atkins unit stabilized. After the initial temperature was determined the thermocouple was removed and the head phantom scanned for a predetermined time using the modified Phantom Protocol. At the conclusion of the scan, the phantom was removed from the MRI unit and the thermocouple reinserted. Temperature measurements were generally obtained within 30 seconds of termination of the scan and were subsequently recorded at 0.1 °F intervals at one minute intervals. To improve results, fiber optic cables with ten meter extensions were purchased.



### Fiber Optic Measurements

Three fiber optic probes were purchased to replace the thermocouple cables. The Fluoroptic® Thermometer used a patented fiberoptic probe manufactured by Luxtron. The tips of the fiber optic cables use the fluorescence of phosphors to sense temperatures. The probes are immune to electromagnetic interference and can operate with the -200 °C to 450 °C range. Since the fiber optic probes were immune to RF effects, the probes remained in the phantom during the scan. The probes were linearly positioned approximately four centimeters from each other. The exact location of the probes was determined for each experiment through imaging the head phantom. Using the landmark as a common reference. The hole at the right eye was plotted sagittally and axially. The tip of each probe was then plotted. To account for any rotation of the head phantom between testing dates, the outer periphery was plotted.

Using the drill hole location and the outer bounds of the head phantom, the distance from the surface to the probe head was calculated. This distance was defined in millimeters and represented the “concentric ring” (Figure 2-2).

Once the locations of the probes were determined, the temperature measurements were recorded. Some experiments were performed on weekends allowing the head phantom twenty-four hours to come into thermal equilibrium with the room which ranged from 17.2 to 17.8 °C. Even allowing forty-eight hours for the head phantom to come into equilibrium, the head phantom would still have differing internal temperatures. On the average, the temperature varied 0.2 °C between points within the head phantom. To compensate for variations between probes and starting temperatures, each probe was

evaluated independently. Equations were derived using absolute temperature variations only.

### Heating Protocol

A head phantom imaging protocol had been previously programmed into the ANMR console. Appendix D lists the program's parameters. The output power was adjusted by increasing or decreasing the Transmission Repetition (TR) value. The TR was the length of time between subsequent starts of a pulse sequence. The phantom protocol used a spin echo which had a  $90^\circ$  pulse followed by a  $180^\circ$  pulse (Figure 2-3). The TR was the length of time between subsequent  $90^\circ$  pulses.

By decreasing the TR value, the pulses cycled in faster succession which increased the average power being transmitted. The majority of experiments were conducted at an average power of 18 watts as indicated on the Omega. The head phantom was placed into the GE Head Coil in the same orientation as a patient. The "landmark" of the imager was set on the bridge of the nose of the head phantom. This represented the iso-center of the head phantom and represented the spatial location of  $x=0$ ,  $y=0$  and  $z=0$  of the imaging chamber. The patient carriage containing the GE Head Coil and head phantom was then sent into the imaging chamber. The Phantom Protocol was selected on the ANMR console and the TR adjusted to obtain a desired average power deposition. A 8 mm camcorder was positioned to record the fiber optic probe results, the average power as indicated on the Omega and the current time. The camcorder images were used in post imaging analysis to enter time, average power and temperature into a database program.

### Thermal Imaging

MRI affects tissue by depositing thermal energy. This thermal energy can alter some parameters measurable by MRI. Temperature resolution using MRI was first applied to imaging hypothermia patients. For hypothermia patients, MRI had the dual benefit of providing heat directly to the body core and imaging the temperature changes within the body. Unwanted heat deposition was also the problem for general imaging. The MRI system can be self-regulating by monitoring heat deposition during a scan. Imaging relies on the detection and quantification of signals from the tissue. Thermal imaging described in literature required a reference thermal image (Delannoy 1991, Hall 1990, Schwarzbauer 1995). The temperature was then defined for this reference image. This method required extensive calibration within each tissue type. Establishing a reference temperature had an inherent accuracy problem which propagated into a larger error during subsequent imaging. To reduce this error, the first diffusion image only defined the baseline. Regardless of the starting temperature, any differences in subsequent images would provide a difference in temperature from the reference image. Quantifying temperature changes in this method should reduce errors and increase accuracies. There were at least three characteristics of protons that lent themselves to measuring changes in temperature: T1 relaxation time, diffusion and proton chemical shift.

### T1 Relaxation Time Imaging

The T1 relaxation time, also known as the Spin Lattice or Longitudinal Relaxation Time, was defined as the characteristic time constant for the return of the proton's

longitudinal axis to alignment with  $B_0$ , the main magnetic field. A T1 map of the target tissue can be generated by an RF pulse of sufficient frequency and strength, acting in a direction  $90^\circ$  from  $B_0$  (Figure 2-4). Shutting off the transmitter and using the transmit antenna as a receiver, the signal strength was a function of the quantity of the nuclear spins realigning with  $B_0$  and provided the T1 map. After absorption of the RF energy, the absorbed energy dissipated into the surrounding molecules at an exponential rate. After one T1 period, 63% of the protons are realigned with  $B_0$ , also known as their rest value. After two T1 periods, 86% have realigned and after three T1 periods, 95% have realigned (Figure 2-5). As temperature increased, the relaxation time decreased (Nelson 1987). Normally the T1 for protons in water was two seconds.

For thermal imaging, a reference image would be taken at a known temperature. After tissue heating, another T1 image was taken and the images compared. The difference in T1 times defined the temperature change. One aspect of thermal imaging was no change in temperature of the cerebral spinal fluid and blood from short, localized heating tests. The fluids present during a slice selective RF pulse would have moved to another physical location by the time a second image was taken. The replacing fluids, not having absorbed any RF energy, would already be at their rest value. The temperature would appear to remain constant. Early in the development of T1 mapping a sensitivity of about  $2^\circ\text{C}$  was obtained (Parker 1983). Since the FDA standards that the MRI system must abide by restricted temperature increases to only  $1^\circ\text{C}$ , this method would prove unuseable. The sensitivity was directly related to the scan time which lasted five minutes. During this scan period, the entire tissue continued to absorb RF energy which in turn



continued to increase the temperature. The solution to making T1 imaging a viable thermal indicator was to shorten the scan time.

Using an inversion-recovery Snapshot FLASH MRI technique reduced acquisition times to approximately two seconds (Deichmann 1992, Nekolla 1992). An inversion recovery technique began with a  $180^\circ$  pulse which inverted the magnetization and flipped the proton axial spin opposite to  $B_0$ . After a time period,  $\tau$ , a  $90^\circ$  pulse would be applied (Figure 2-6). Transverse magnetization would be detected (Figure 2-7). The inversion-recovery Snapshot FLASH MRI technique took images within milliseconds of the RF pulse by using smaller flip angles. Since smaller flip angles require less RF energy, temperature increases were minimal. One sacrifice for this rapid measurement was a reduction of signal-to-noise. This can be compensated for by averaging several images in quick succession. The precision of the T1 measurement had improved to better than three percent with this method (Schwarzbauer 1995). A three percent precision at a normal body temperature of  $37^\circ\text{C}$  was  $1.1^\circ\text{C}$ . This method would still not satisfy FDA requirements since a reading of  $0^\circ\text{C}$  change could in reality exceed the  $1^\circ\text{C}$  limit.

In addition, temperature changes were not the only factors affecting the T1 relaxation times. The presence of free radicals and water concentration also affected T1 (Knüttel 1986). These factors became a concern when their concentrations changed from the time the reference set of images were taken until the time the final T1 images were taken. A larger quantity of protons in the second T1 image would increase the apparent percentage of realignment of nuclear spins with  $B_0$ . This increased quantity, and subsequent apparent increased realignment would promote a misconceived perception of

increased tissue temperature. The MRI system only generates non-ionizing radiation, so it was unlikely the generator of it created additional free radicals during the imaging process. Since the free radicals do possess a polarity which was subject to magnetic fields, only if the free radicals were uniformly distributed, whereby the movement of radicals out of a particular location matched the movement of radicals into the particular location, could the effects of free radicals be ignored.

Two additional factors that affected the T1 relaxation times were perfusion and diffusion. Perfusion was the pseudo-random flow at low velocities of blood moving along finely divided structures of the capillaries. Diffusion was the Brownian motion of individual molecules moving with large random thermal velocities. Brownian motion was the constant erratic movement of particles being struck by other particles. Temperature changes affected the rate of Brownian motion by affecting the viscosity and diffusion of water in tissue.

### Diffusion Imaging

In biological tissue, a fraction of the water movement in capillaries was affected by diffusion (LeBihan 1988). Water flowing down a linear path has an overall direction down the path, but upon closer attention, the water molecules collide and deflect off each other creating a random motion. This interaction was calculated by differentiating the Stokes-Einstein relation between viscosity and diffusion.

$$\frac{dD}{D} = \left( \frac{E_a}{kT} \right) \frac{dT}{T}$$



where  $k$  = Boltzmann constant,

$E_a$  = the activation energy for translational molecular diffusion,

$D$  = the translational molecular diffusion and

$T$  = temperature.

A temperature change map can be derived from two diffusion images (LeBihan 1989).

$$T - T_0 = \frac{kT_0^2}{E_a} \left( \frac{D - D_0}{D_0} \right)$$

An initial reference diffusion image,  $D_0$ , was required as well as the initial temperature.

Using  $E_a = 0.21$  eV, and applying a 1 °C increase in temperature, the diffusion coefficient increased by 2.4%. This value was dependent on an accurate  $E_a$ . For water the activation energy remained relatively constant at 0.21 eV. For tissue, this value may be different and should be determined for each tissue type present in the image. If this activation energy varied as a function of either T1 and/or T2, an image weighted in favor of one or the other would be required. The intensity of the resultant image would suffice to assign  $E_a$  values to each tissue type. Then a pre- and post-exam diffusion image sequence would map the temperature changes.

Both perfusion and diffusion images can be obtained using the Intravoxel Incoherent Motion (IVIM) method. The velocities of molecules in a particular tissue type were directly related to the kinetic energy of the molecules. This kinetic energy, in the

form of thermal energy can be imaged using a spin-echo sequence followed by a second sequence with increased gradient pulses. The increased gradient pulses increase the effects of the perfusion and diffusion. Since the pulse sequences are identical, except for the gradient pulses, T1 and T2 effects were negated. This leaves only an apparent diffusion coefficient (ADC) which was a combination of both perfusion and diffusion. A third sequence with an even stronger gradient pulse greatly reduced perfusion while only moderately reducing diffusion effects. A comparison between the second and third sequences defined a diffusion image. A comparison of the diffusion image with the ADC image from the first two sequences produced a perfusion image. Temperature changes do not greatly affect perfusion. Perfusion, the blood flow through capillaries, may increase from increased cardiac action caused by the deposition of heat elsewhere in the body. The body's response to thermal changes through a long imaging session were possible but would only reflect an overall temperature increase throughout the body. Appendix E, "Heat Stress Index", described this effect in greater detail. Localized heating, which was a consideration for imaging at 3T, would not be accurately represented by perfusion imaging.

The IVIM method was sensitive to motion artifacts. For head imaging, cardiac gating would reduce artifacts from blood flow, and to a lesser degree, cerebral spinal fluid (CSF) flow. Eye movement artifacts would be reduced by preplanning the direction of the phase-encoding gradient pulses. Increased IVIM images using faster techniques would also reduce motion artifacts. The brain was a non-moving organ and thermal imaging resolution would be possible as long as patient movement was reduced. The eye, as a

result of its limited vascularization, was the tissue most susceptible to thermal damage and the most difficult to image using the IVIM method. An alternative would be to use echo-planar imaging.

Echo-planar imaging used a gradient echo technique consisting of a rapid sequence of phase steps between each repeated pulse sequence. The echo-planar imaging provides rapid images, from 15 to 30 images a second. This produced virtually real-time images for functional studies of the brain. During brain activity there is a rapid, momentary increase in the blood flow to the active area of the brain. Therefore, echo-planar imaging allows mapping of brain activity. Echo-planar imaging also becomes a benefit to limit motion artifacts by imaging in a fraction of a second. Since the echo-planar imaging gradients follow in rapid succession, the signal-to-noise decreased. However, the large quantity of data points from the multiple sequences improved the estimation of the perfusion and diffusion (Turner 1990). With decreased imaging times, diffusion imaging without regard for perfusion artifacts may also become possible.

### Proton Chemical Shift Imaging

A third method of non-invasive temperature measurements used chemical shift imaging. Fat protons and water protons have differing chemical shifts when imaged in a MRI. Generally, chemical shift imaging was used as fat suppression imaging. The pure water proton chemical shift was proportional to a change in temperature by approximately  $-0.01 \text{ ppm}/^{\circ}\text{C}$  (Ishihara 1995). This temperature dependence resulted from the stretching, rupturing and/or bending of the hydrogen bonds. Temperature changes were difficult to

detect using the chemical shift because of the small shift. An accuracy of 1 °C was usually expected which was at the FDA allowable threshold of 1 °C change in tissue temperature. This meant that a reading of 1 °C from the chemical shift could actually be from 0 °C to 2 °C. The chemical shift was detected by measuring the time between the 90° pulse and 180° pulse and comparing this to the difference in time between the 180° pulse and the spin echo (Figure 2-3). The time difference between sets of images was the result of temperature.

Chemical shift imaging used the echo planar imaging technique to help reduce motion artifacts from diffusion-weighted techniques. However, the echo planar imaging had a strong sensitivity to magnetic susceptibility. Even though human tissue was mostly not affected by the magnetic field, at 3T even small differences in the electrical properties of tissue caused a dephasing of spins and frequency shifts. This made the chemical shift of a particular tissue weighted by the concentration of KCl and NaCl in the tissue. To use an absolute temperature difference between the same tissue over a heating period, the concentration of electrolytes would have to be assumed constant over a temperature range. The chemical shift of protons was also affected by the pH of the tissue. Since the MRI was non-ionizing, hydrogen ions were not created, but since they are polarized they may be moved from a region of high density to a region of low density. Again, for absolute temperature measurements between two time frames, the pH should not change rapidly and the reference set of images, if taken just prior to the exam, would still provide a good baseline for comparison of post-exam chemical shift images.

### Phantom Thermal Imaging

Of the three thermal imaging techniques described above, diffusion imaging using echo planar imaging, appeared the best alternative. Neither T1 nor chemical shift imaging was solely affected by temperature and both were affected by diffusion. This would require techniques to eliminate diffusion effects. The best method to do that was from two sets of diffusion weighted images to remove the diffusion affects. This, in effect, relied on running diffusion techniques in addition to other techniques to image T1 or the chemical shift as a function of temperature. Since diffusion changes from one image to another was solely affected by temperature, using just diffusion techniques reduced imaging time thereby decreasing the effect from RF deposition in tissue.

The benefit of using diffusion imaging was three-fold. First, with less techniques, less RF energy deposition took place during temperature measurements. Second, with shorter imaging techniques, results would be easier to post process. Third, while not applicable to phantom studies, with shorter imaging techniques the effects of patient motion would be reduced.

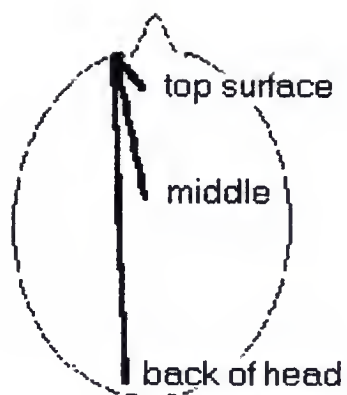


Figure 2-1. Thermocouple Probe Locations.

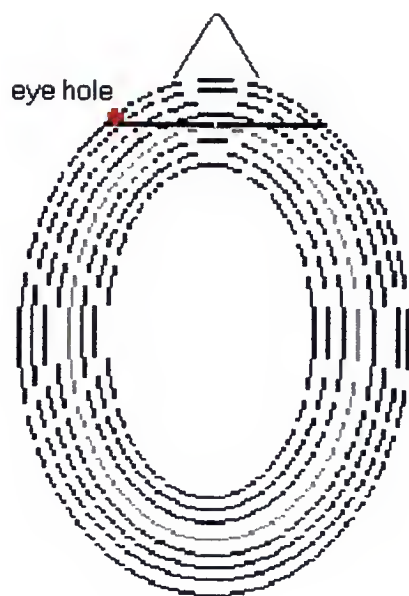


Figure 2-2. Concentric Rings Used to Define Location in Head Phantom.

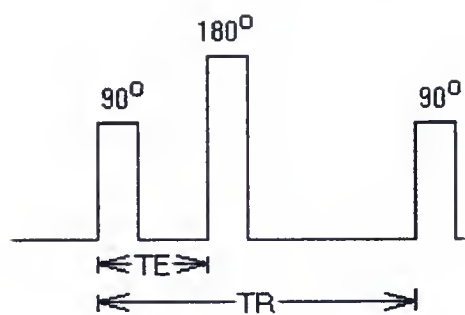


Figure 2-3. Spin Echo Sequence.

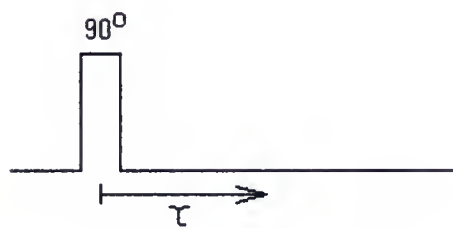


Figure 2-4.  $90^\circ$  RF Pulse.



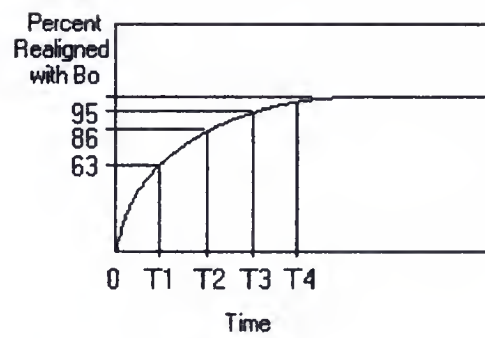


Figure 2-5. T<sub>1</sub> Recovery Time.

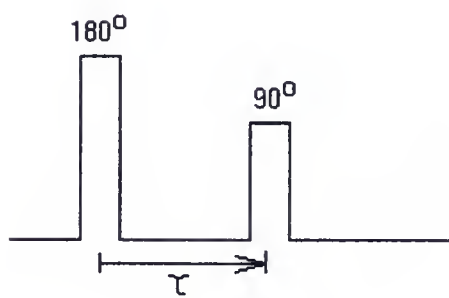


Figure 2-6. Inversion Recovery Pulse.

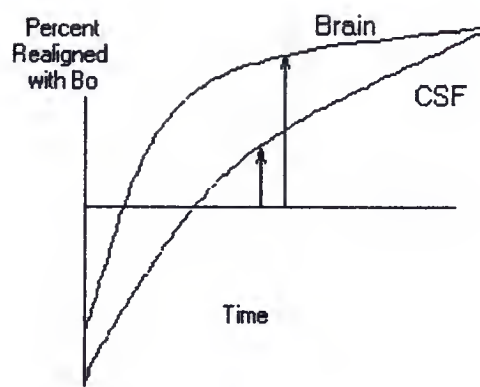


Figure 2-7. Water and Fat Discrimination Using T1.

Table 2-1. Electrical Properties For Polyethylene Husk of Head Phantom.

Loss Tangent	Permittivity	Intrinsic Impedance	Skin Depth
$\frac{\sigma}{\omega\epsilon} \left( \frac{V \cdot s}{F} \right)$	$\epsilon_R \left( \frac{F}{V} \right)$	$\eta (\Omega)$	$\delta (m)$
0.0005	2.26	27.9 / <u>0.2</u>	0.248

Table 2-2. Ingredients to Create Tissue Equivalent Material.

7.5% TX-51	290g/gal. Water
0.45% NaCl	17.44g/gal. Water
0.07 mole Gadopentetate Dimiglumine	0.544 ml/gal. Water

Table 2-3. Thermal Properties of Tissue Equivalent Material in Head Phantom.

NaCl Ratio	Thermal Conductivity (W/m <sup>2</sup> K)	Specific Heat (J/cm <sup>3</sup> °K)
0.000765	0.674 ± 0.025	3.52
0.00306	0.646 ± 0.097	3.53
0.00461	0.629	3.54

Table 2-4. Electrical Properties of Tissue Equivalent Material in Head Phantom.

Loss Tangent	Permittivity	Intrinsic Impedance	Skin Depth
$\frac{\sigma}{\omega\epsilon} \left( \frac{V \cdot s}{F} \right)$	$\epsilon_R \left( \frac{F}{V} \right)$	$\eta (\Omega)$	$\delta (m)$
2.71	61	34.3 / <u>32.6</u>	0.06

## CHAPTER 3

### RESULTS

Three sets of results were obtained from this project. The first set was thermocouple results. These results were recorded just prior to heating with the MRI system and then immediately after the scan. The thermocouple wire generated interference and increased temperatures when left in the head phantom during the scan. The second set of results were from the fiber optic cables which were immune to RF fields and provided information during the heating of the head phantom. The third set of data was from a diffusion imaging technique. Previous thermal data from invasive temperature measurements determined the diffusion technique could provide accurate temperature results.

#### Thermocouple Results

All plots from experiments with thermocouple probes displayed a combination of two curves (Figure 3-1). The predominant curve during the first minutes resulted from the creation of a “depletion zone.” After insertion the thermocouple wire became a heat sink for the surrounding tissue equivalent material and accelerated the heat loss for the first two to four minutes. Using the plots from the first four minutes, an equation was derived of this initial cooling. Since the first recorded temperature was approximately thirty seconds after the scan ended and a few seconds after the thermocouple was inserted, the

initial temperature was calculated from the assumption that the cooling followed an exponentially decaying function over time with the following general format.

$$F_{t_1} = F_o e^{-\lambda t_1}$$

$F_o$  is the unknown initial temperature,  $F_{t_1}$  is the known temperature approximately thirty seconds after the scan,  $t_1$  is the thirty seconds of thermal decay time and  $\lambda$  is the unknown thermal decay constant.

From data gathered after the initial four minutes, a second exponential curve was derived which defined the expected cooling curve of the phantom. This cooling curve was then adjusted to compensate for the initial heat loss provided by the thermocouple wire. This method depended on the validity of the thermocouple cable acting as a heat sink.

Temperature measurements were made just below the top surface of the phantom's husk and through the tissue equivalent material to the back of the head phantom. There was more fluctuation in temperature measurements at the top surface of the phantom which was exposed to the air. The back of the head phantom was placed on a cushion which provided insulation from heat loss. Temperature measurements from this region provided stable results (Table 3-1). The heating of the phantom from RF transmissions were compiled and a heating equation, as a function of the average power read off the Omega process indicator and the scan duration, was derived.

$$\text{Temp. Inc. (}^{\circ}\text{C)} = ((4\text{E-4} \times \text{Power}^2 - (1/9)\text{E-4} \times \text{Power}^3) \times \text{Scan Time})(5/9)$$

This equation provided close approximations to actual thermocouple results up to thirty watts average power. Complications were found when measuring temperatures in the middle of the head phantom. After the scan was complete and the thermocouple installed, temperatures continued to rise. This indicated that thermal movement would become an issue of concern when mapping temperatures. By suggestion this also indicated the RF energy did not penetrate the entire phantom during a scan. If it had, then core temperatures would have matched the outer surfaces. This demonstrated the phenomenon of “skin effect.” At high frequencies, a current carrying conductor maintains a flux on the outer edges only. This theory is used by the power industry which allows them to use high tensile strength, but low current carrying potential, material to string long power lines. Only the outer sheath requires current conductor properties. This same effect was demonstrated during thermal testing of the head phantom. With this complication and relying on the subjective interpretation of the heat sink properties of the thermocouples, accurate results with thermocouples were suspect.

### Fiber Optic Results

Three fiber optic probes were simultaneously inserted into the head phantom. The fiber optic probes provided temperature measurements during the scan to better characterize the heating of the head phantom. Appendix F contains the raw data and graphs derived from phantom testing using the fiber optic probes. The average power measurements were obtained from the Omega at one minute intervals. The shaded portions of the graphs represent the period the imaging was performed.

### Heating Equation

An exponential function was assumed for the heating of the tissue.

$$T = T_{\max} \left( 1 - e^{\frac{-\ln(2)t}{t_{1/2}}} \right)$$

Two assumptions were used in determining this function. First, the tissue equivalent material, similar to human tissue, would not have an unlimited capability to absorb thermal energy. At some point the tissue would stop increasing in temperature as energy was applied. This implied some upper threshold,  $T_{\max}$ . Since both the tissue equivalent material and human brain contain mostly water, this upper threshold would be similar and would also be far above the pain threshold of an individual. Therefore, the determination of this threshold was not significant to this research. Only the assumption that this threshold was above the current operating temperatures was required. Second, temperature increases as a function of power would not be linear as they approached the threshold. As the temperature increases there would be a constant decrease in the amount and rate that additional energy could increase temperatures. This implies an exponential function. Since the function changes exponentially, it was assumed that there would be a thermal half-life,  $t_{1/2}$ . Experimental data would be used to define these parameters.

The thermal data results were measured using three fiber optic probes and the location of each probe tip was determined using the scanned image. Table 3-2, 3-3 and 3-4 list the locations of the probe tips in relation to the outer edge of the head phantom and



to the eye hole drilled into the head phantom. There was no probe #1 cable used during the testing. Appendix F lists the results of the temperature readings for the first thirty minutes of the experiment. For the majority of the experimental scans, the thirty minute period included the entire scanning time of twenty-two minutes and several minutes afterward.

There were four effects apparent in the data. Three of the effects dealt with a delay time which was the time, in minutes, since the beginning of the scan until there was a noticeable increase in temperature.

1. The delay time was a function of distance from the outer surface. This was intuitive once the other effects were defined and validates some of the thermocouple results. The electric field attenuated as it passed through the tissue equivalent material. This attenuation deposited energy in the outer layer thereby heating it first. The remaining energy, deposited farther into the tissue, heated the tissue equivalent material at a lower rate.
2. The temperature gradient within the head phantom caused a delay by “passing” thermal energy to the lower temperature tissue equivalent material. Temperatures varied 0.5 °C within one centimeter of the probes at the start of Test #3. The plots showed a slower increase in temperature where the tissue was warmer. This demonstrated an increased thermal conductivity of the warmer tissue equivalent material. The results from Test #9 also demonstrated this pattern. There the temperature gradient between probes was 0.8 °C over two centimeters. The higher

temperature zone increased in temperature at a slower rate than the inner core even though it was closer to the skin and should have heated first.

3. The lower the starting temperature of the head phantom the sooner a temperature increase was registered. If the head phantom had sufficient time to remove thermal energy then the delay time in seeing a response from a scan of 18 watts average power was one minute per centimeter depth. The higher the starting temperature, the delay time increased by twenty-five percent for every one degree centigrade. A comparison of the experimental results from Test #2, which had a higher starting temperature, to that of Test #1, where the temperatures were stable, demonstrated this point. With just under a one degree centigrade change in starting temperatures, delay times in registering a temperature rise increased from ten minutes to twelve minutes at a depth of 74 mm.
4. After the completion of the scan, temperatures at the inner core continued to rise. Test #1 showed a continued increase in temperatures after completion of the scan at 62 mm and 73 mm depths. The temperature rise at the 41 mm depth continued to rise for approximately 5 minutes before stabilizing. This reinforced the concept that the electric field was not uniformly distributed throughout the head phantom and that the majority of the thermal energy was deposited along the outer edges.

Several experiments were run at lower average power. These scans generated less thermal energy and, as expected, the rate of temperature increase was less. Since the temperature increase appeared as an exponential function, a “thermal half-life” of temperature increase was derived. From test results, this value appeared as a function of

the average power (Table 3-5). These values are subjective and derived only from the appearance of the curve. A plot of the natural logs of the half-life against the average power allowed a slight modification of the numbers to create an exponential function relating average power to half-life (Figure 3-2).

$$t_{1/2} = e^{6.375 - 0.134 * (\text{avg power})}$$

Using this relationship between thermal half-life and average power reading, as displayed on the Omega, a heating equation was defined.

$$T = T_0 \left( 1 - e^{\left( \frac{-0.693 \times t}{e^{(6.375 - 0.134 \times \text{power})}} \right)} \right)$$

### Cooling Equations

Cooling equations would provide additional information on the thermal characteristics of the head phantom tissue equivalent material. Ideally the tissue equivalent material would begin cooling at the end of the scan. This, however, did not take into account the thermal movement within the tissue. Thermal measurements taken with fiber optic cables (Figure 3-3 through 3-8) show temperatures taken after the scan was complete and no further energy was deposited into the head phantom. The tissue equivalent material closer to the outer edge of the head phantom began reducing temperatures. The tissue equivalent material closer to the core continued to increase in temperature.

The increased temperatures made creating a cooling curve impossible. Some useful information was still obtained from these results. Thermal energy traveled in the direction of cooler tissue equivalent material. This direction was towards the center of the head phantom. This implied that the polyethylene outer husk of the phantom provided insulation to the tissue equivalent material and minimal heat transfer to the atmosphere. This was also demonstrated when temperatures had not stabilized within the head phantom after twenty-four hours of sitting at room temperature.

### Diffusion Imaging

Diffusion imaging was preferred over other imaging techniques since the only parameter that affected it was temperature. Other imaging techniques, such as T2-weighted and perfusion, also required a diffusion image technique to remove the diffusion effects from the image. The diffusion technique was run on the head phantom prior to heating. After the diffusion technique was run and images captured, an imaging technique was performed on the head phantom that generated approximately 18 watts, as indicated on the Omega, for approximately twenty-two minutes. Immediately after the head phantom was heated, another diffusion technique was performed. A comparison of the two spatially different diffusion techniques would indicate changes as a result of temperature alone.

### Procedures

To capture the diffusion images required the InstaScan computer system connected to the ANMR unit. Figure 3-9 displays the connections between the InstaScan

computer, the ANMR Console, the uf3T Sun Workstation and the Windows-based computer. Also listed are the program names used to transfer and manipulate images. Prior to diffusion imaging, “ghosts” needed to be tuned from the system. Ghosts were unwanted artifacts of the original image. Appendix G lists the steps performed on the InstaScan computer and the ANMR console for ghost tuning.

**Diffusion Imaging.** Once the ghost images were attenuated, the diffusion technique was run. Appendix H lists the steps performed on the InstaScan computer and the ANMR console for diffusion imaging. Appendix I lists the parameters for diffusion imaging on the ANMR console. The diffusion technique provided seven images. The first image was a T2-weighted image. The next three images were diffusion images, at the slice location, for the three vectors X, Y and Z. The final three images were another set of diffusion images with increased gradients. For phantom studies the second set of images were not required. The diffusion technique actually provides both perfusion and diffusion which was described earlier as the ADC. Perfusion is blood flow through small capillaries and a second diffusion image with increased gradients reduces the perfusion effects more than the diffusion effects. Since the phantom did not have capillaries, there were no effects from perfusion. However, for this diffusion technique to be effective on humans, a second diffusion technique will be required. If desired, the second set of images can be subtracted from the first set of images to provide images that predominately contain perfusion effects and a small portion of diffusion effects.



**Image Conversion.** The diffusion images were physically located on the InstaScan computer. In order to manipulate them, they were first moved back to the ANMR console by selecting the images from the database on the InstaScan computer and selecting TRANSFER. From this location they were retrieved from the uf3T Sun Workstation. Appendix J lists the steps to transfer the images from the ANMR console to the Sun Workstation. Once on the Sun Workstation the files were converted to another format that was transferred to a Microsoft® Windows-based computer for further processing.

**Image Manipulation.** Appendix K lists the program written by the author for this research. The program was written for a Windows® 95 platform and was designed to take a bitmap image and digitize each pixel into a long integer indicating its color. The location of the pixel, given in X and Y coordinates, and the number associated with its color, was saved in a Microsoft® Access database. Once the images were saved into the database, the program would take the images from the first diffusion run and subtract the images from the second diffusion run. The result represented the change in the two images. Since a change in diffusion images was only affected by temperature, the values from the program characterized temperature changes.

Figure 3-10 is a display of the entire set of images. The first row shows the seven images from the diffusion imaging performed prior to heating the head phantom. The second row shows the seven images from the diffusion imaging performed after a twenty-two minute spin echo sequence generating approximately 18 watts as indicated on the Omega. The third row shows the comparison of the two images. Since the image transfer

process involved several steps, some noise was expected from signal degradation in the final images. As a check for undesired degradation of the images, the second row of images was saved twice from the InstaScan computer. This was accomplished by transferring the same set of images twice back over to the ANMR system. Each set was saved as the next sequential series number. At that point the second, duplicate set of diffusion images were processed identically as the original. The images were transferred to bitmaps and digitized. The two sets of identical images were then subtracted from each other and displayed in the fourth row.

**Image Analysis.** The images in the first row of Figure 3-10 were provided by the diffusion technique taken prior to heating the head phantom (Figure 3-11). The same heating technique that had been used for fiber optic tests was applied to the head phantom to increase its temperature. This technique applied eighteen watts average for twenty-two minutes. The diffusion technique was run for a second time and the results displayed in row two of Figure 3-10. The first diffusion image (the second image in the series) is displayed in Figure 3-12. The two images were digitized and a number was assigned to the color of each pixel. The color values derived for each pixel of each image were subtracted to provide a method to quantify the change in diffusion. This was validated by test results beginning with the Atkins thermocouple unit and later with the fiber optic system. The fiber optic probes indicated that the temperature increased along the outer rim of the head phantom before temperatures would increase deeper in the head phantom. This would translate into an initially greater change in diffusion along the outer portions of



the head phantom but that by the end of the scan temperatures would be similar and the overall diffusion image would be more uniform.

The numerical value which defines each pixel in the image is a long integer representation of its color. The numerical format consisted of six hex digits representing the colors red, green and blue with each color having a magnitude of 0 to FF (hex). For instance, a pure red color would have the hex number 0000FF, a pure green color would have the hex number 00FF00 and a pure blue color would have the hex number FF0000. Since the images were displayed on a gray scale, the values for red, green and blue were identical (i.e. white equals 000000, light gray equals 111111, dark gray equals AAAAAA and black equals FFFFFFFF). This simplified numerical interpretation by allowing subtraction of only one color which had a range of 0 to 255. Changes in these numbers would indicate the magnitude of change in diffusion, and thereby, change in temperature.

Figures 3-13 through 3-15 represent T2-weighted images that accompanied the diffusion image technique. The images had noise attached to the images as they were processed. This noise transferred as darker pixels when converted to mathematical values. The noise was later reduced by programming a filter to remove numerical values below 50 (on a scale of 0 to 255). Relevant portions of the scan had image values above 50. The filter value was derived experimentally through trial and error. Also present on the image was a horizontal line. The line represented the location of the displayed histogram.

The top histogram (Image 002 window) was taken from the pre-heating diffusion image and the middle histogram (Image 004 window) was taken from the post-heating diffusion image. The scale of the window was from 0 to 255. These two images appeared

similar so a composite image was created. The histogram from the post-heating diffusion image was subtracted from the pre-heating diffusion image.

The third histogram is the Composite window which was scaled vertically from 100 to -100. Image composites where the post-heating images were less intense than the pre-heating images would have the histogram generated upwards. The downward generated histogram indicated that the intensity of the pixel increased in intensity, which translated into an increased numerical value when digitized by the computer, as temperatures increased. Three slices, as indicated by the horizontal line on the right side image of Figures 3-13 through 3-24, were taken from each axis of the diffusion image. Slices were taken from the top, which represented the eye and nose area of the head phantom, the middle and the lower or back portion of the head phantom.

The Composite images from all subtracted diffusion results displayed histograms in the negative direction. This indicated the intensity of the images increased with increased temperature. Had the Composite histogram been random, where equal numbers of points would have been positive and negative, then this diffusion imaging technique to measure temperature changes could be considered non-effective. The histograms demonstrated diffusion imaging does provide a means of measure temperature changes.

The diffusion images represent diffusion changes in three orthogonal vectors. To quantify one numerical results for each pixel, a vector sum of the three diffusion images was obtained. For this research, the average intensity of all the pixels was calculated for each vector. The average was obtained from adding the intensity differences of the three slices taken from each axis. The sum of the Composite images from Figure 3-16 through

3-18 provided the average intensity change for the X-axis. The sum of the Composite images from Figure 3-19 through 3-21 provided the average intensity change for the Y-axis. The sum of the Composite images from Figures 3-22 through 3-24 provided the average intensity change for the Z-axis. These averages were summed using the following equation.

$$\text{Pixel Intensity} = \sqrt{X^2 + Y^2 + Z^2}$$

The average change in intensity of the composite images displayed in Figures 3-16 through 3-24 was 40.7 on a scale of 0 to 255. The imaging technique used for heating the head phantom generated sufficient thermal energy to increase temperatures by approximately 0.5 °C. These results indicated temperature changes less than 1 °C can be measured.

## Phantom Cooling Curve

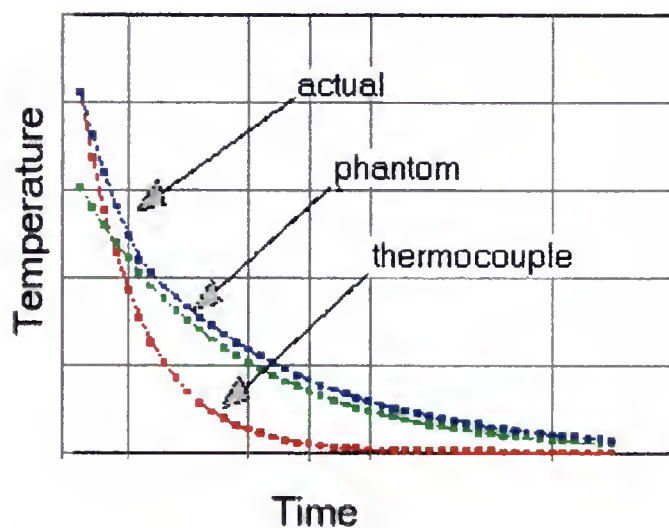


Figure 3-1. Cooling Curve Using Thermocouple Probes.

## Thermal Half-life

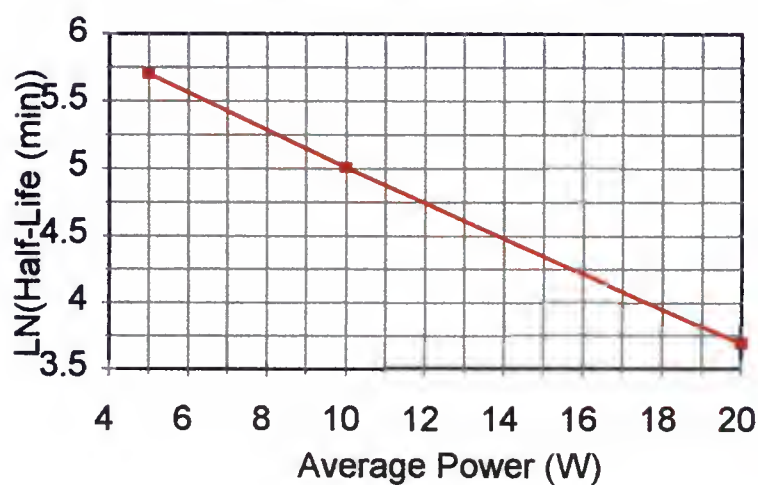


Figure 3-2. Natural Log of Thermal Half-Life.

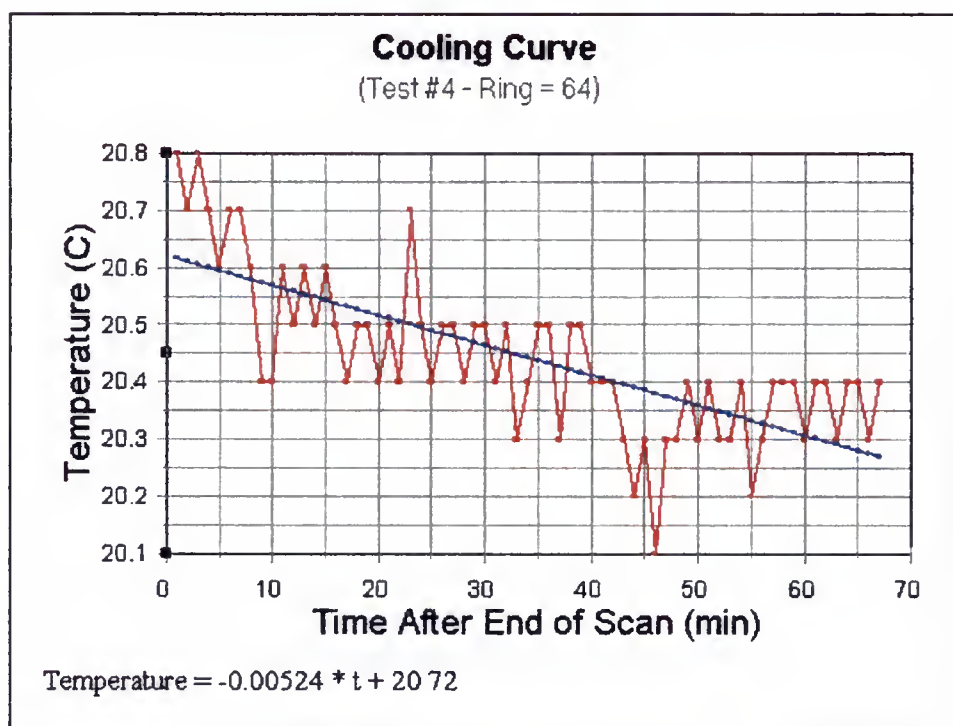


Figure 3-3. Test #4 Post Scan Temperature Measurements.

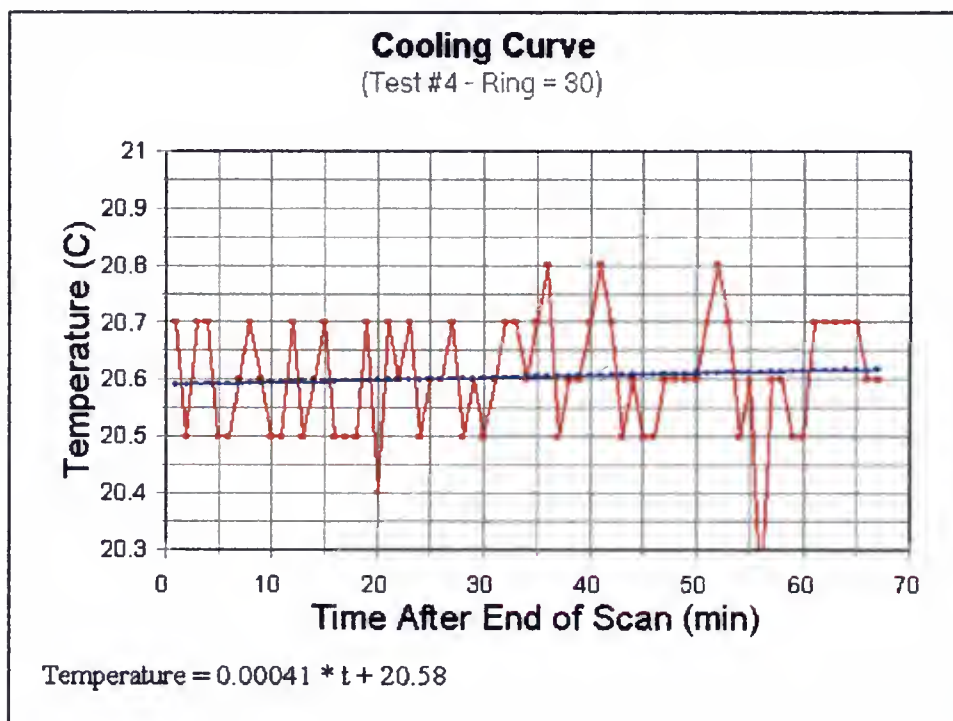


Figure 3-4. Test #4 Post Scan Temperature Measurements.

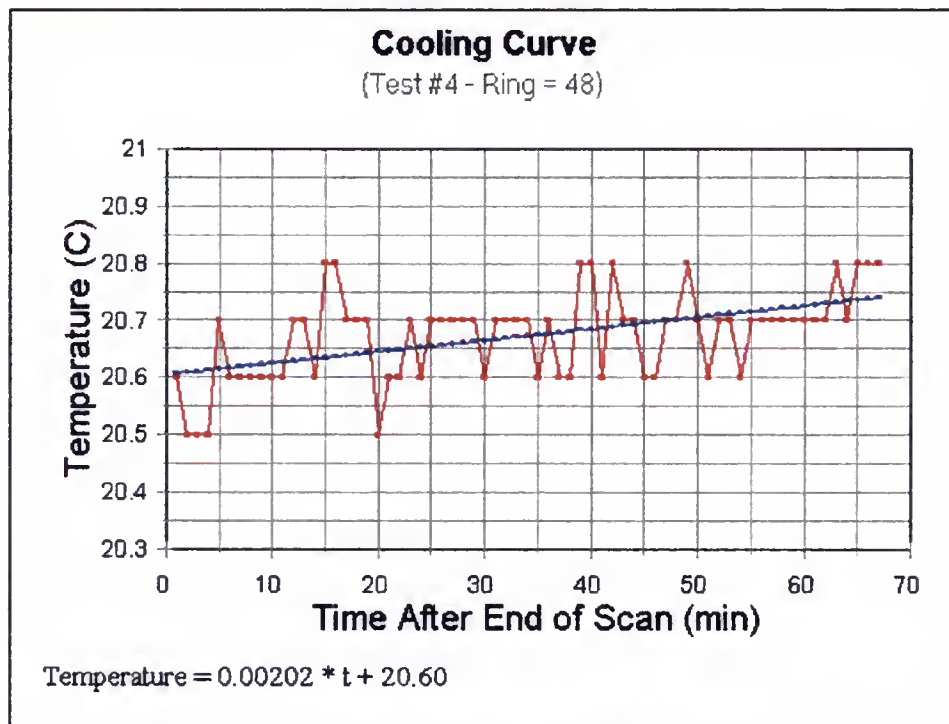


Figure 3-5. Test #4 Post Scan Temperature Measurements.

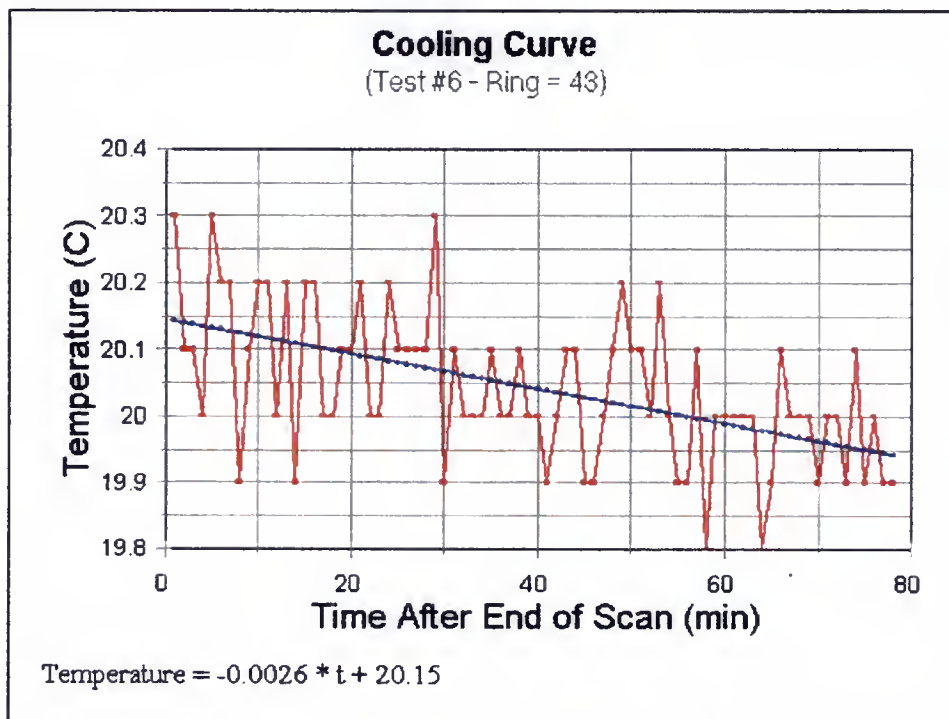


Figure 3-6. Test #6 Post Scan Temperature Measurements.



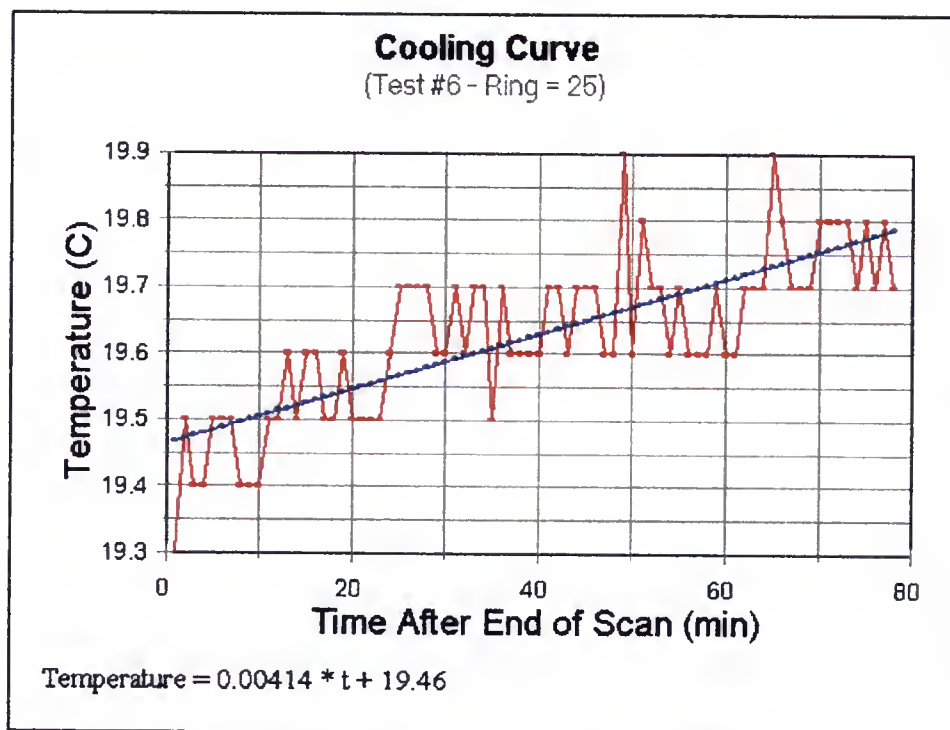


Figure 3-7. Test #6 Post Scan Temperature Measurements.

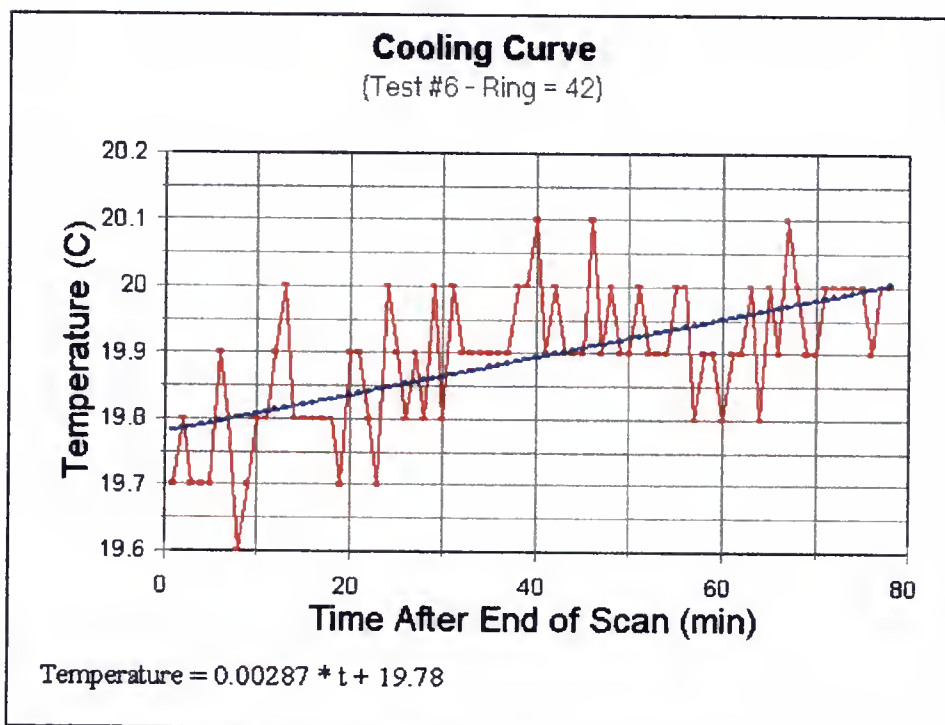


Figure 3-8. Test #6 Post Scan Temperature Measurements.

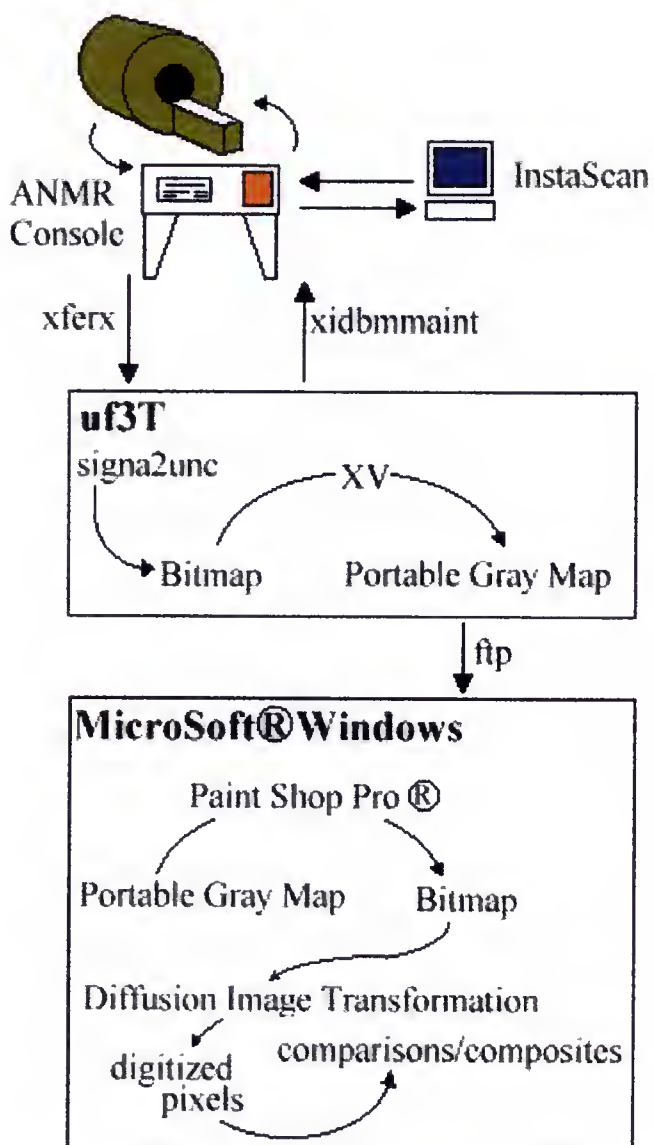


Figure 3-9. Diffusion Imaging Equipment and Software Flowchart.

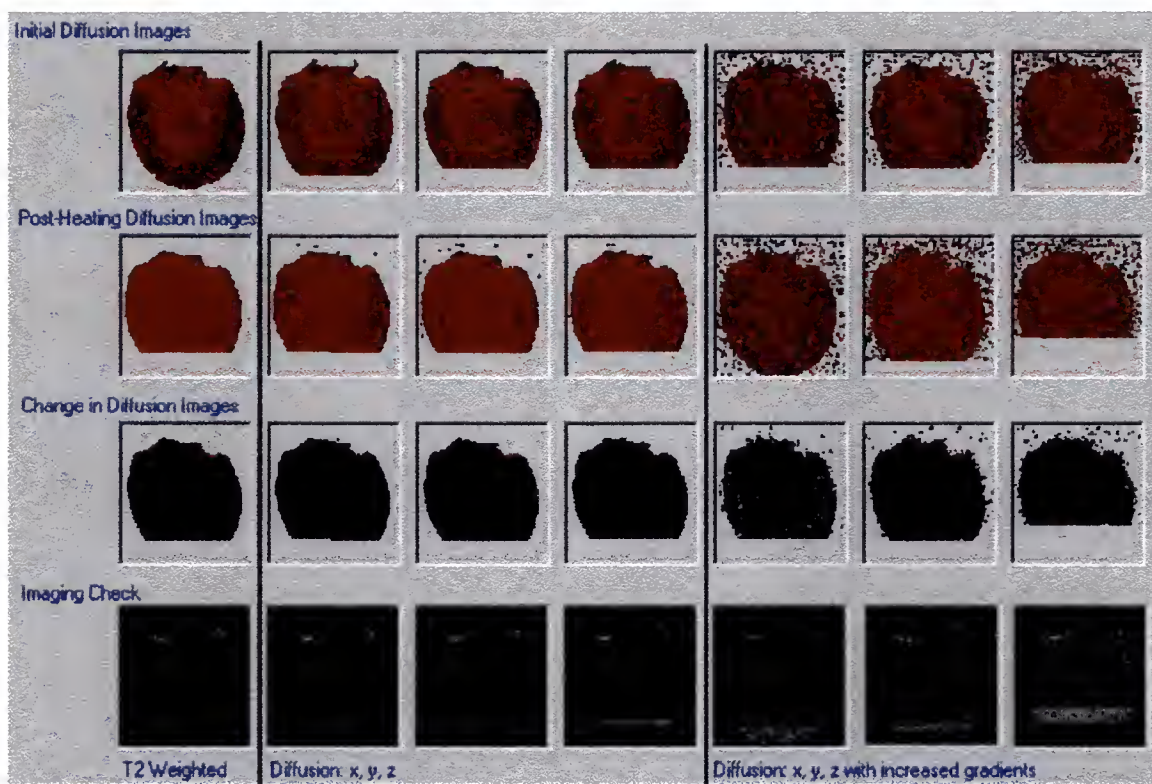


Figure 3-10. Diffusion Technique Images and Changes in Images.

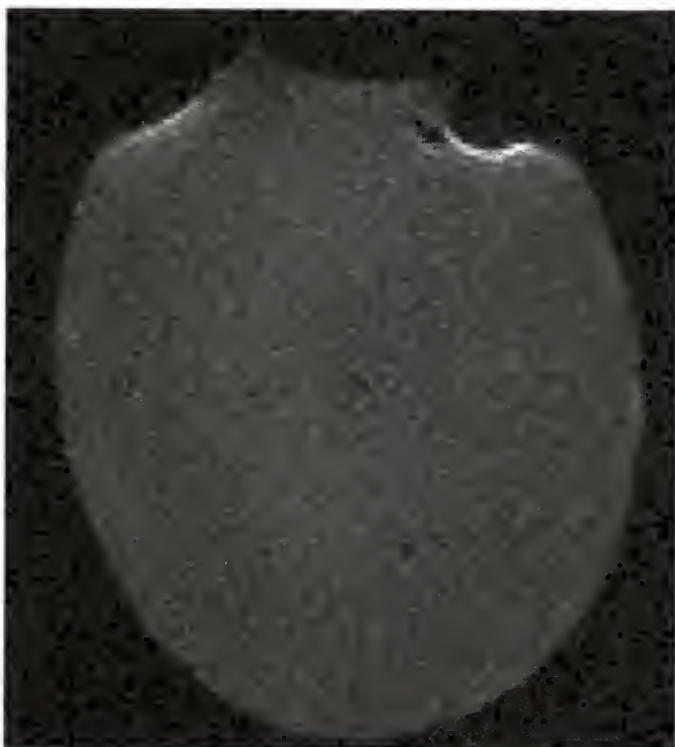


Figure 3-11. Diffusion Image Prior to Heating Head Phantom.

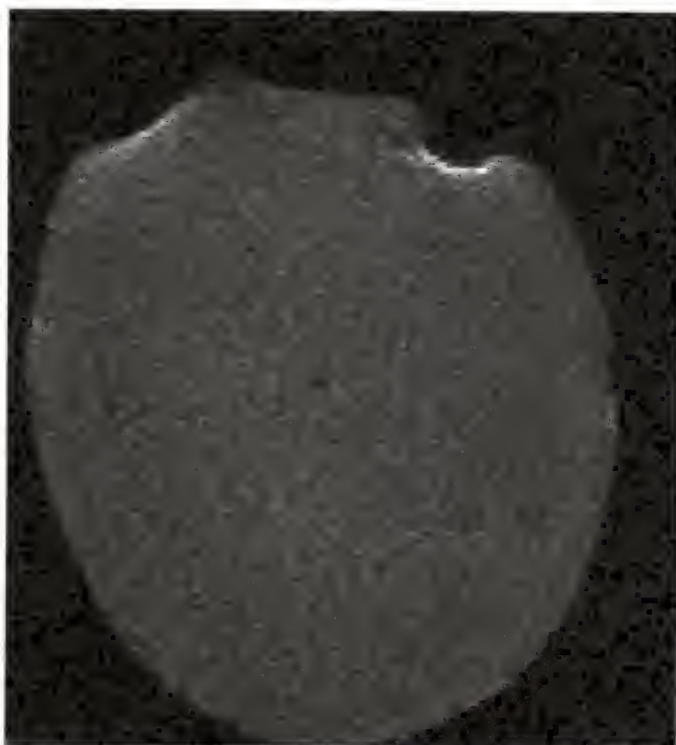


Figure 3-12. Diffusion Image After Heating Head Phantom.



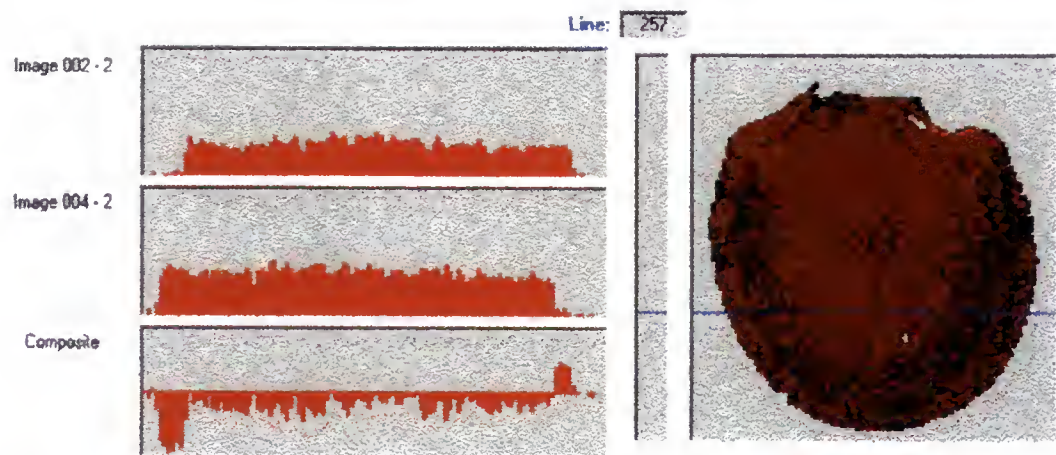


Figure 3-13. Histogram From Slice of T2-Weighted Image.

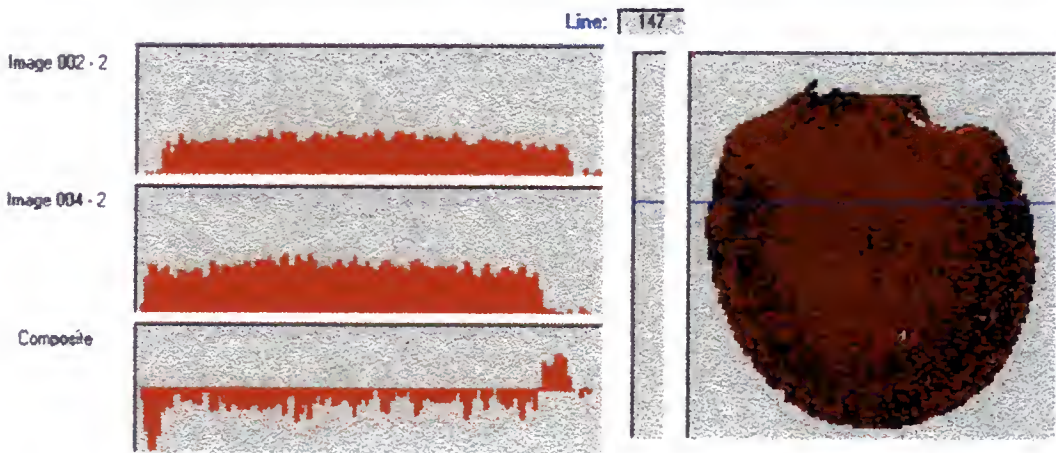


Figure 3-14. Histogram From Slice of T2-Weighted Image.

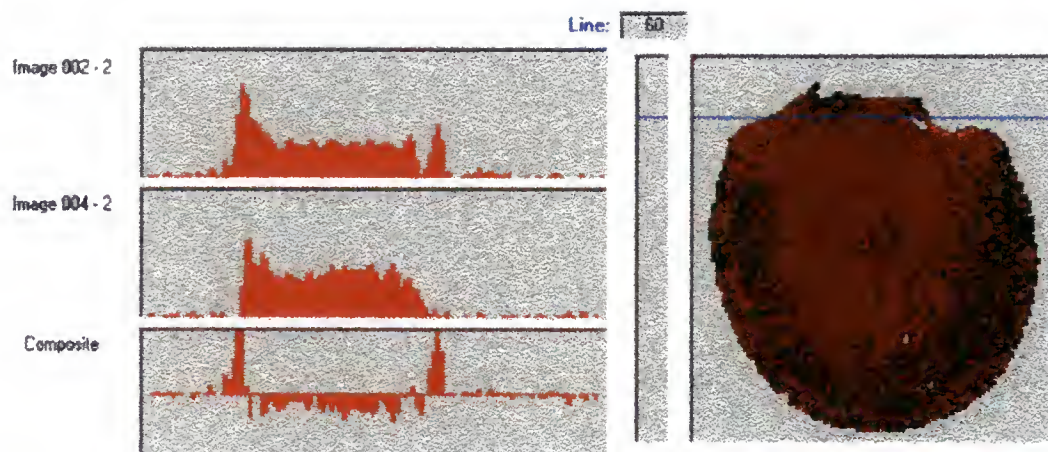


Figure 3-15. Histogram From Slice of T2-Weighted Image.

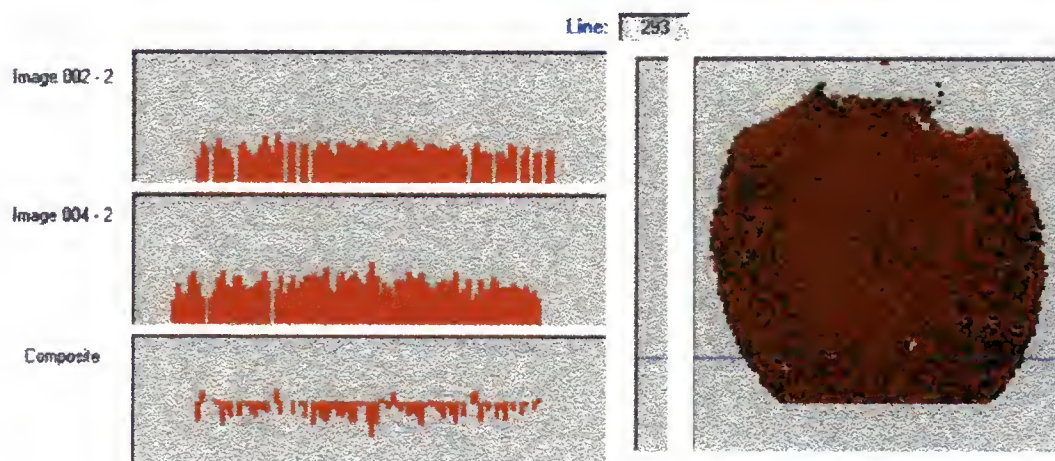


Figure 3-16. Histogram From Slice of Diffusion Image X-Axis.



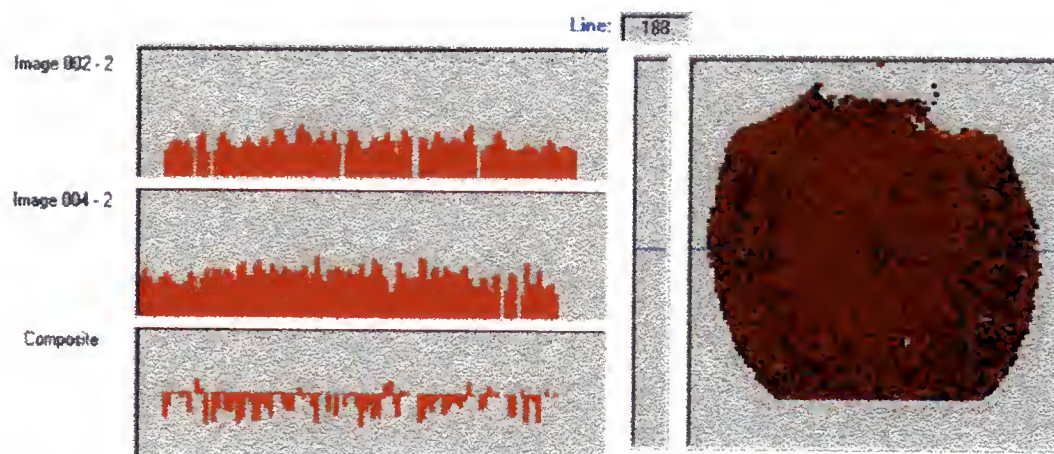


Figure 3-17. Histogram From Slice of Diffusion Image X-Axis.

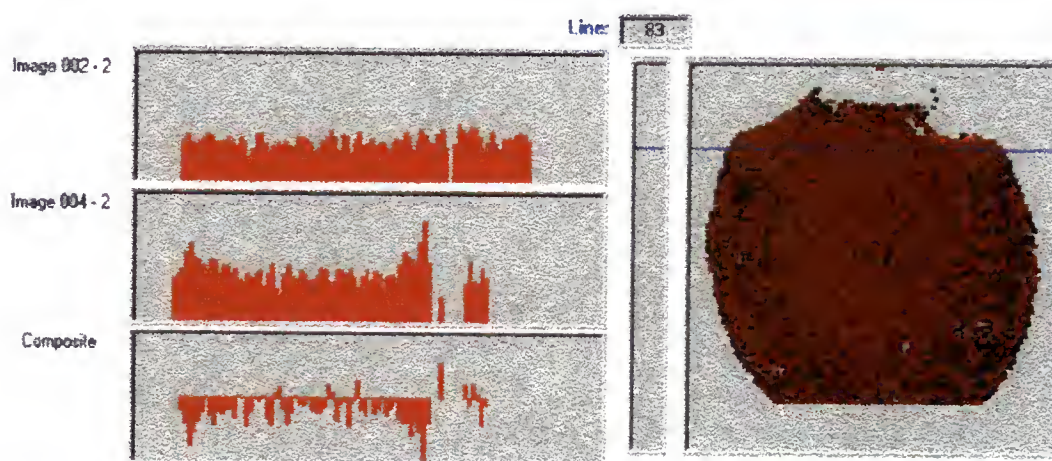


Figure 3-18. Histogram From Slice of Diffusion Image X-Axis.

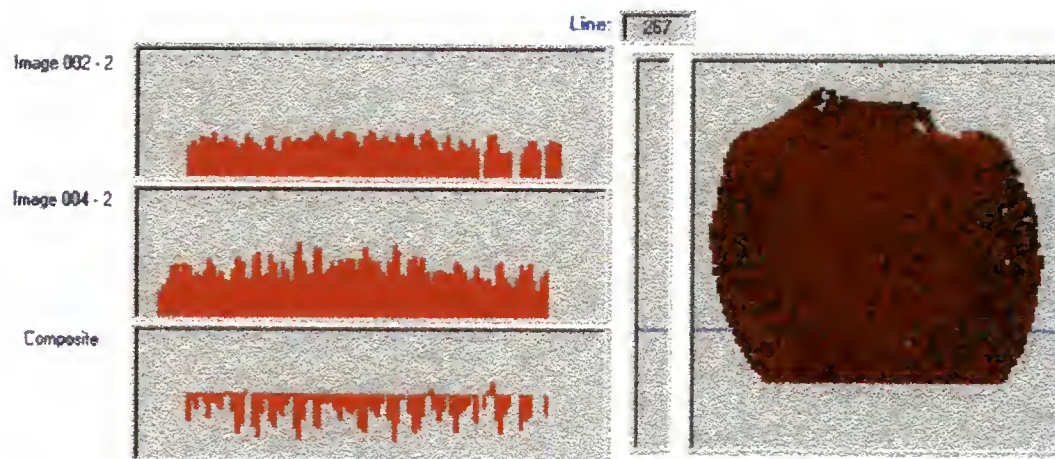


Figure 3-19. Histogram From Slice of Diffusion Image Y-Axis.

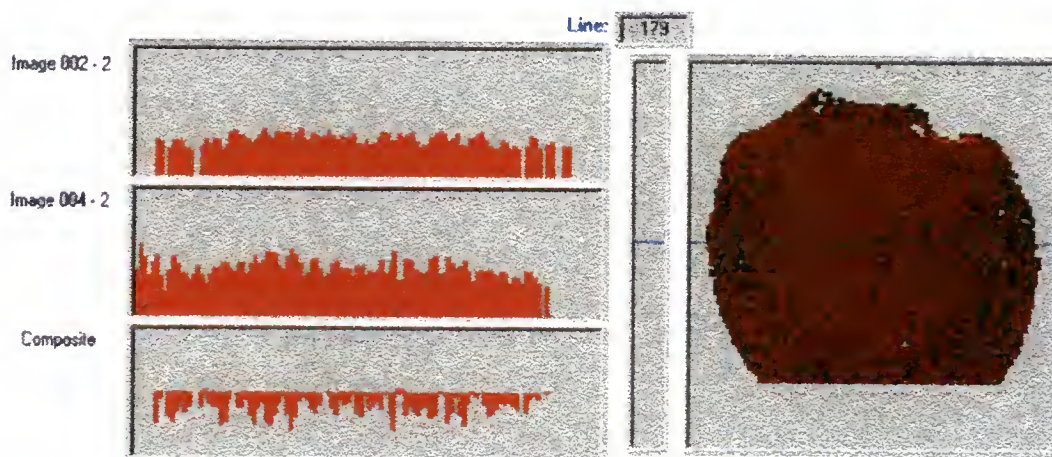


Figure 3-20. Histogram From Slice of Diffusion Image Y-Axis.



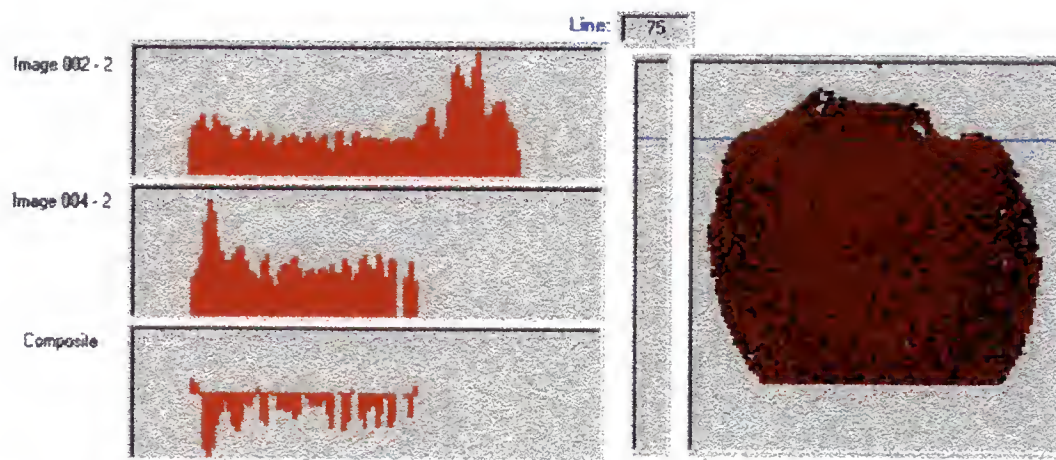


Figure 3-21. Histogram From Slice of Diffusion Image Y-Axis.

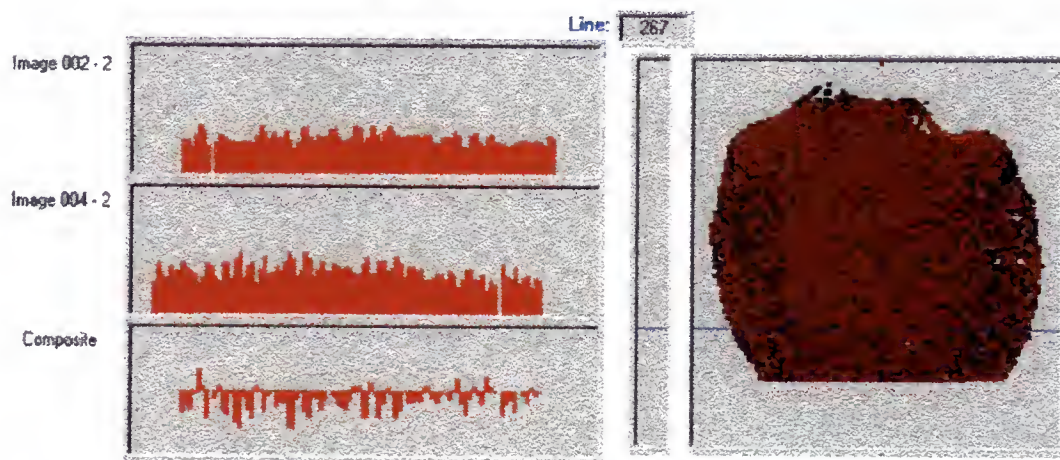


Figure 3-22. Histogram From Slice of Diffusion Image Z-Axis.

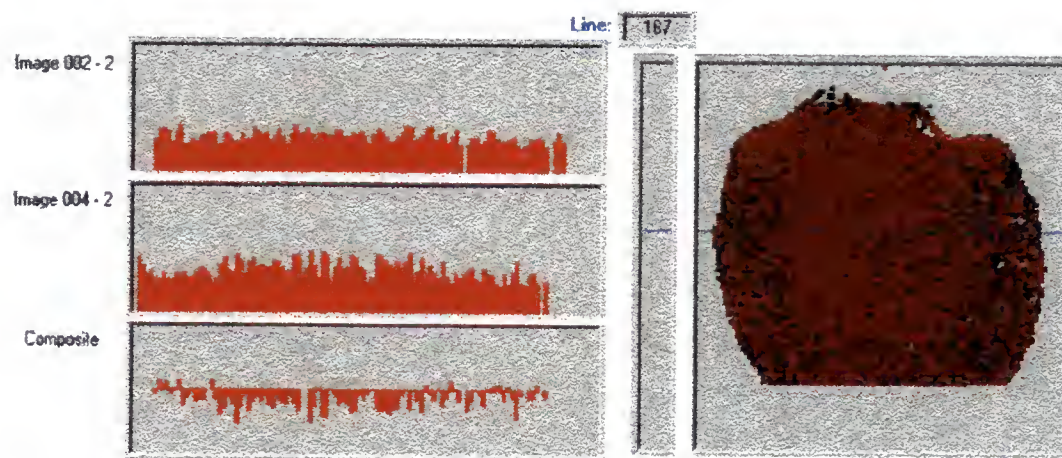


Figure 3-23. Histogram From Slice of Diffusion Image Z-Axis.

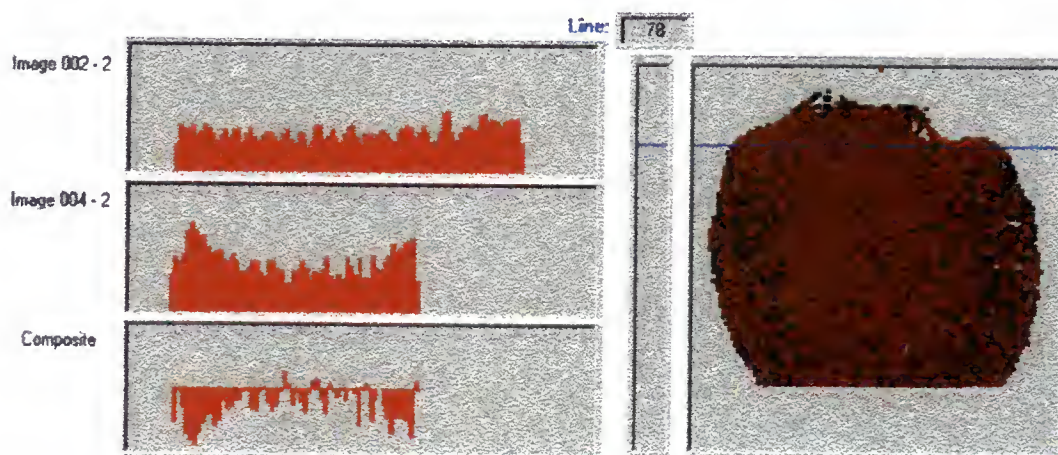


Figure 3-24. Histogram From Slice of Diffusion Image Z-Axis.

Table 3-1. Temperature Measurements Using Thermocouples.

Date	Power (W)	Location	Start Temp (F)	Stop Temp (F)	Scan Time (min)
11/13/96	30	back	70.6	73.5	48.22
11/13/96	30	back	73.1	76.2	48.22
11/20/96	31	front	69.5	70.1	10.02
11/20/96	31	front	68.7	70.7	10.02
11/20/96	31	back	69.8	71.5	10.02
11/20/96	31	back	71.1	71.8	10.02
11/25/96	30	front	70.5	73.8	48.42
12/16/96	17	back	68.8	70.4	32.07
12/16/96	17	back	70.2	72.3	32.07
12/28/96	14	back	67.7	70.0	42.73
12/28/96	14	back	69.4	72.3	42.73
12/28/96	14	back	70.9	73.0	42.73
12/29/96	14	front	68.1	71.5	42.73
12/29/96	14	front	70.9	73.4	42.73
12/29/96	14	front	72.5	74.7	42.73
1/4/97	9	back	67.2	68.7	42.73
1/4/97	9	back	68.3	69.4	42.73
1/5/97	37	back	69.7	74.5	42.45
1/5/97	37	back	74.0	78.6	42.45
1/5/97	37	back	77.9	81.9	42.45



Table 3-2. Head Phantom Probe #2 Location.

Test	Location on Drawing				Concentric Ring No.
	Dx	Dy	x	y	
#1	12.2	26.3	70	52	41
#2	14.1	25.4	72	51	40
#3	0	22.5	58	49	38
#4	0.9	15	59	41	30
#5	1.9	13.1	60	39	28
#6	3.7	10.3	62	36	25
#7	-8.1	29.2	50	55	30
#8	6.5	10.3	65	36	25
#9	-2.8	19.6	55	46	35

Table 3-3. Head Phantom Probe #3 Location.

Test	Location on Drawing				Concentric Ring No.
	Dx	Dy	x	y	
#1	24.4	84.4	82	110	62
#2	35.7	65.7	94	92	74
#3	9.4	57.2	67	83	47
#4	36.5	30.99	94	57	46
#5	13.1	62.8	71	89	51
#6	4.7	88.1	63	114	43
#7	-14.1	59.1	44	85	24
#8	28.1	50.8	86	77	66
#9	1.9	62.8	60	89	40

Table 3-4. Head Phantom Probe #4 Location.

Test	Location on Drawing				Concentric Ring No.
	Dx	Dy	x	y	
#1	34.7	121.9	93	148	73
#2	52.8	95.3	111	121	91
#3	18.8	86.3	77	112	57
#4	26.2	67.5	84	94	64
#5	15.0	101.2	73	127	53
#6	3.7	95.6	62	122	42
#7	-30.0	94.7	28	121	8
#8	42.2	80.6	100	107	80
#9	16.0	99.3	74	125	54



Table 3-5. Thermal Half-Life Using Fiber Optic Cables.

Average Power	Half-Life
5	300
10	150
20	40

## CHAPTER 4 DISCUSSION

In the first series of thermal test, thermocouples were considered a cost effective method of testing. Analysis of data revealed three major problems. First, the thermocouple wires, being metallic, interfered with the imaging of the head phantom by creating artifacts. For use with diffusion imaging the exact locations of the thermocouples are required. With artifacts on the images it was difficult to plot the exact location of the thermocouple tip. Additionally, the artifacts would also affect the diffusion image. This would not provide an accurate indication of the change in diffusion as a function of temperature, especially near the thermocouple probes which were the temperature indicators.

Second, the wires conducted the RF fields and increased the temperatures in the tissue equivalent materials surrounding the wires. This created a false indication that more energy was being deposited into the tissue resulting in greater temperature increases. The equation of average power as indicated on the Omega and length of the scan indicated a greater increase in temperatures over a shorter time interval. A comparison of this equation with the one derived from fiber optic system results, revealed an increase in temperature increases in the tissue equivalent material as a function of average power and scan time. From the standpoint of safety, the thermocouple results had an inherent safety

margin by over estimating temperature increases. This margin, however, limited the capabilities of 3T MRI.

Third, after the thermocouples were removed from the head phantom during a scan and later reinstalled, the wire acted as a heat sink. The wires, being at room temperature, were slightly cooler than the tissue equivalent material of the head phantom. Once installed into the head phantom, the cooler wire acted as an excellent thermal conductor and rapidly lower temperatures. Readings of 1 °C drop in temperature within two to four minutes were common. One method to reduce this would be to shield the thermocouple end in plastic. This would insulate the wire from the tissue equivalent material but would also slow down the response time of the thermocouple. Since the cooling of the head phantom is slow this may be possible, however, the thermocouple wire would still conduct heat faster until it reached equilibrium with the tissue equivalent material.

Fiber optic cables were immune to magnetic and RF fields. Three fiber optic probes were simultaneously installed in the head phantom. Measurements of temperatures were possible and revealed characteristics that would never have been seen with thermocouple wires. Since the RF output power was constant during a long scan, it was assumed that temperatures would increase linearly. The majority of temperature increases were exponential. This exponential curve started earlier in the scan the closer the probe was to the outer edge of the head phantom. This demonstrated that RF deposition, and subsequently temperature increases, were greater on the outer edge. Thermal energy did move inward and at the end of a scan the entire head phantom had increased in

temperature. Additionally, test results from Test #9 showed a slower rate of temperature increase along the outer edge in comparison to an inner core probe. This validates the assumption that the capability of the tissue equivalent material to increase temperatures from a given power deposition decreases as the tissue equivalent material increases in temperature. The amount of energy deposited in the tissue equivalent material nearer the core was less than the energy deposited near the outer edge, but since the inner tissue equivalent material was lower in temperature the deposited energy increased the temperature more. These mechanisms were not detectable with the thermocouple system. Fiber optic cables, remaining installed during a scan, will be instrumental in testing diffusion images at different stages of a scan.

Deriving cooling curves would better quantify thermal energy deposition. The temperature of any volume of tissue can be mathematically defined as simultaneously receiving energy and dissipating energy during a scan.

$$T_{Volume} = \int (E_{IN} - E_{OUT})$$

After a scan, with no source of energy, the temperature of a volume of tissue is a function of energy loss only.

$$T_{Volume} = \int E_{OUT}$$

Defining the energy deposition properties of the 3T system would be a matter of subtracting the cooling equation from the heating equation. However, during these tests, there was constant thermal movement up to an hour after the scan.

These results would prove useful in better characterizing the tissue equivalent material. Unless the same process is performed on human tissue, there would be no correlation and the information would not be useful. Additionally, the human head has a thermal regulatory mechanism which is not available to the head phantom. A better characterization of the tissue equivalent material would not improve test results.

Diffusion imaging, being only affected by temperature, can provide non-invasive measurement of temperature increases. The FDA's guideline limiting temperature increases to any 1 gram of tissue to 1 °C can only be met through imaging. Any other method requires invasive techniques that would not be comfortable to patients. Diffusion is the only technique developed so far that is only affected by temperature. All other imaging techniques are affected by some other parameter besides temperature. Until another technique is developed or the other parameters can be mitigated, further testing using diffusion imaging is warranted.

## CHAPTER 5 CONCLUSION

For the results obtained during this research to be valid for the human head, the head phantom must be a good representative of the human head. Physically the head phantom is an identical shape of a human head. Its electrical loading characteristics were defined through an average loading of volunteers from 3T MRI. Using an established recipe and retesting in the 3T imager, a tissue equivalent material to simulate the human head was determined (Olsen 1992, Chou 1984). The primary component in the recipe was water which is also the primary component in brain tissue. This suggests the thermal characteristics of the head phantom and human head would also be similar. The outer husk of the head phantom was an insulator similar to the skull and skin of the human head. Both contain low water content and should have similar thermal characteristics. Fortunately, with the use of diffusion imaging, exact duplication of test results between the head phantom and human head may not be required.

Diffusion imaging had proved effective in determining the change in temperatures in-vivo (LeBihan 1989, Stehling 1991, DePoorter 1994, McCain 1995, Mischler 1995). Results mentioned in literature indicated an accuracy of 1.0 °C. Temperatures during the diffusion imaging for this research used a heating technique that raised temperatures by 0.5 °C which was easily noticeable in test results.



This research has demonstrated that a diffusion imaging technique, already available on MRIs, can be used to measure and monitor temperature increases in the human head with resolution better than 1 °C. An on-line program, similar to the one written for this research would provide real time analysis of thermal changes by utilizing a quick, initial diffusion image and then subsequent images throughout the session to compare the change in diffusion. Further testing is required to better characterize the temperature increase relationship to RF fields.

### Future Work

Accuracy in determining temperature changes through diffusion imaging would entail using the fiber optic probes in conjunction with the diffusion imaging technique. The result would be a description of the change in pixel intensity with change in temperature. Temperature gradients existed in the head phantom and would be a cause for increased errors in temperature comparisons between the diffusion image results and the fiber optic results. To minimize this effect, the diffusion image should be run on the slice containing the fiber optic probe tips.

A variety of heating techniques resulting in a variety of different temperature increases from 0.1 °C to 2 °C should be performed. The representative diffusion images would then be transferred, digitized and analyzed using software similar to that used during this research. Since noise was added each time an image was processed, an analysis program should be written for the InstaScan unit or the Sun workstation. This would eliminate the need to transpose the images from a Unix bitmap to a portable gray

map to a Windows® bitmap and finally digitized. A program written for the InstaScan would also reduce the time required to analyze images.

The next step in applying this technique to humans would be to run the diffusion imaging technique on a cadaver head. The cadaver head, like the head phantom, should start at room temperature. Artificially warming the cadaver to normal body temperature would present a problem of maintaining that temperature. Once removed from the warming mechanism, the head would begin to cool. The change in temperature would skew the temperature changes as a function of MRI and also skew diffusion results. Temperature increases by the RF fields would be negated by the cooling of the head. The amount of temperature increase as a function of the length and strength of the RF fields would have to be assumed as similar for tissue at normal body temperatures (37 °C) and at room temperature (18 °C).

Fiber optic probes would be inserted into the various brain and optic tissues. A diffusion image would be acquired in the location of the fiber optic probe tips. A heating technique would then be applied to the cadaver head. Post-heating diffusion images would then be compared in the same manner as the head phantom diffusion images. Only a handful of images, providing different temperature changes, would generate a relationship between tissue type and pixel intensity as a function of temperature. This pixel intensity verses temperature change would provide a conversion factor for each tissue type. Most brain tissue (white matter and gray matter) have a high water content. Temperature changes as a function of the RF fields would most likely be similar. As long as the thermal characteristics of the brain tissues remain similar between room temperature

and normal body temperature, the conversion factor would be valid for living tissue at normal body temperature.

APPENDIX A  
INTERNATIONAL ELECTROTECHNICAL COMMISSION (IEC)

## Operating Mode Ranges for dB/dt

### Normal Operating Mode

$\text{dB/dt} < 20$	T/s for $120 \mu\text{s} < T$
$\text{dB/dt} < 2400/T$	T/s for $2.5 \mu\text{s} < T \leq 120 \mu\text{s}$
$\text{dB/dt} < 960$	T/s for $T \leq 2.5 \mu\text{s}$

Where the pulse width,  $T$ , is defined as the duration of the change of magnetic flux density expressed in microseconds ( $\mu\text{s}$ ). For sinusoidally or other continuously varying periodic magnetic fields the duration of change shall be considered to be the half period the magnetic flux waveform.

For values of  $T$  not exceeding  $2.5 \mu\text{s}$ , the limit on peak dB/dt is based on heating, assuming a sinusoidal waveform. Therefore, the limit on peak dB/dt of 960 T/s may be exceeded for non-sinusoidal waveforms, provided that the r.m.s. value of dB/dt is less than 960 T/s and the peak dB/dt is less than  $2400/T$  T/s.

### First Level Controlled Operating Mode

$\text{dB/dt} < 20$	T/s for $3000 \mu\text{s} < T$
$\text{dB/dt} < 60000/T$	T/s for $45 \mu\text{s} < T \leq 3000 \mu\text{s}$
$\text{dB/dt} < 1330$	T/s for $T \leq 45 \mu\text{s}$

For values of  $T$  not exceeding  $45 \mu\text{s}$ , the limit on peak dB/dt is based on heating, assuming a sinusoidal waveform. Therefore, the limit on peak dB/dt of 1330 T/s may be exceeded for non-sinusoidal waveforms, provided that the r.m.s. values of dB/dt is less than 1330 T/s and the peak dB/dt is less than  $60,000/T$  T/s.

### Second Level Controlled Operating Mode

Comprises values of dB/dt which exceed the upper limit for range of the First Level Controlled Operating Mode.

## Operating Modes

### First Level Controlled Operating Mode

Magnetic Resonance equipment that is capable of values of dB/dt and/or SAR above the upper limits of the Normal Operating Mode, shall comply with the following:

- a) Before the start of each scan, an indication of the operating mode defined by the maximum dB/dt value for the scan and a prediction of the value of SAR that will actually be used during the scan shall be displayed at the Operators console.
- b) If the value of dB/dt or SAR is such as to enter the First Level Controlled Operating Mode, the attention of the Operator shall be drawn to this condition by a clear indication on the Operators console and provision shall be made so that a deliberate action of the Operator shall be necessary to start the scan. A record of these values shall be inseparable from the image data.
- c) A means of control shall be provided to ensure that values of dB/dt and SAR do not exceed the upper limits for the First Level Controlled Operating Mode. This control shall be independent of Operator input as the patient size, weight or position.

### Second Level Controlled Operating Mode

Magnetic Resonance equipment which allows values of dB/dt or SAR within the Second Level Controlled Operating Mode shall comply with the requirements above and in addition:

- a) Shall include specific security measures that allow entry in the Second Level Controlled Operating Mode. These measure shall include an indication to the Operator that the operating conditions are potentially hazardous and that these conditions should be not applied for normal clinical use.
- b) The specific security measures shall be so constructed that it can be made accessible only under the authorization of the medically responsible person.
- c) The specific security measures shall be effective for each scan for which the predicted values of dB/dt or SAR are above the limits for the First Level Controlled Operating Mode.
- d) The specific security measures shall involve a key-lock, a combination local, a software password or other protective devices.



## Checking Compliance

The accuracy of the predicted SAR with the specification shall be checked by measurement at the maximum SAR of which the Magnetic Resonance equipment is capable or at a SAR of 3W/kg, whichever is lower.

The upper limit of the First Level Controlled Operating Mode shall be measured to check that it complies with the maximum SAR of which the Magnetic Resonance equipment is capable or at a SAR of 4 W/kg, whichever is lower.

The requirement to prevent exceeding the upper limit of the First Level Controlled Operating Mode for dB/dt shall be demonstrated by measurement using the maximum gradient rate.

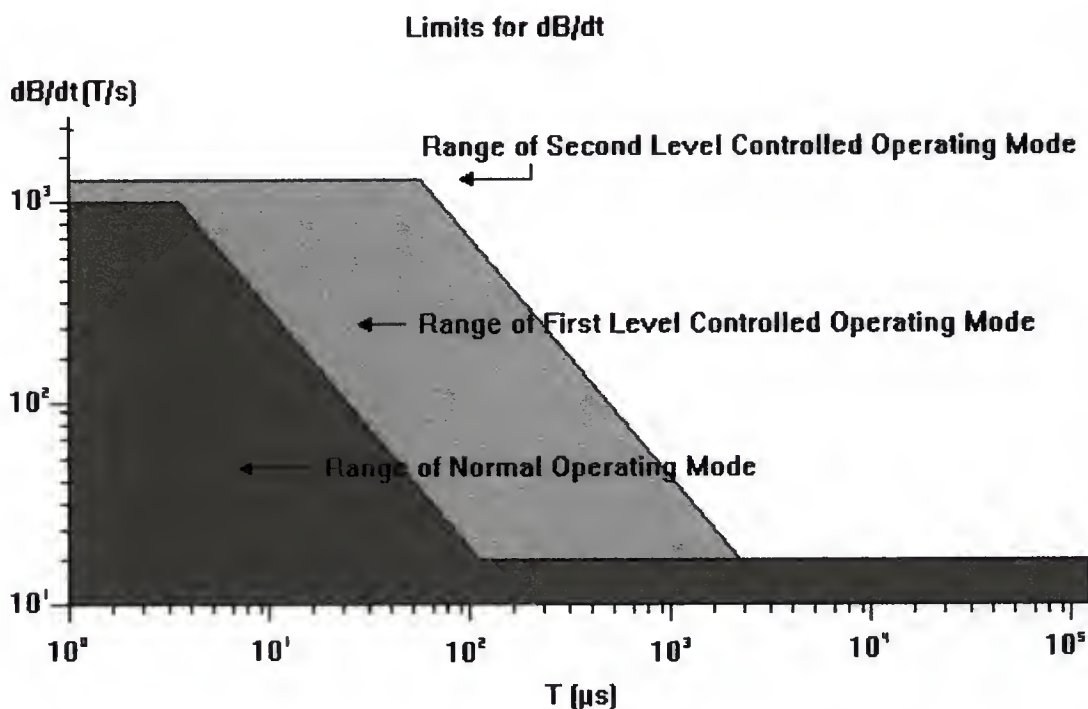


**Figure 103 - Limits for dB/dt.**

Compliance is checked by measurement of the maximum trapezoidal dB/dt or the maximum sinusoidal dB/dt component, that the system is capable of generating under any conditions allowed for clinical use in the First Level Controlled Operating Mode.

Method of measurement of dB/dt to demonstrate compliance with the given requirements:

Method of measurement of maximum trapezoidal dB/dt:



## a) Auxiliary definitions:

- search coil a small diameter coil used to measure gradient field rates of change.
- magnet isocentre normally defined by magnet geometry, in this document it is defined as the zero crossing for all three gradients.
- Patient space radius the distance from magnet isocentre to the patient support (without pads) along the lines  $y = \pm x$  (see **figure 103**).
- dB/dt pulse width, T: the Full Width at Half Maximum of a single dB/dt pulse or the half period of a sinusoidal dB/dt waveform (see **figure 104**)

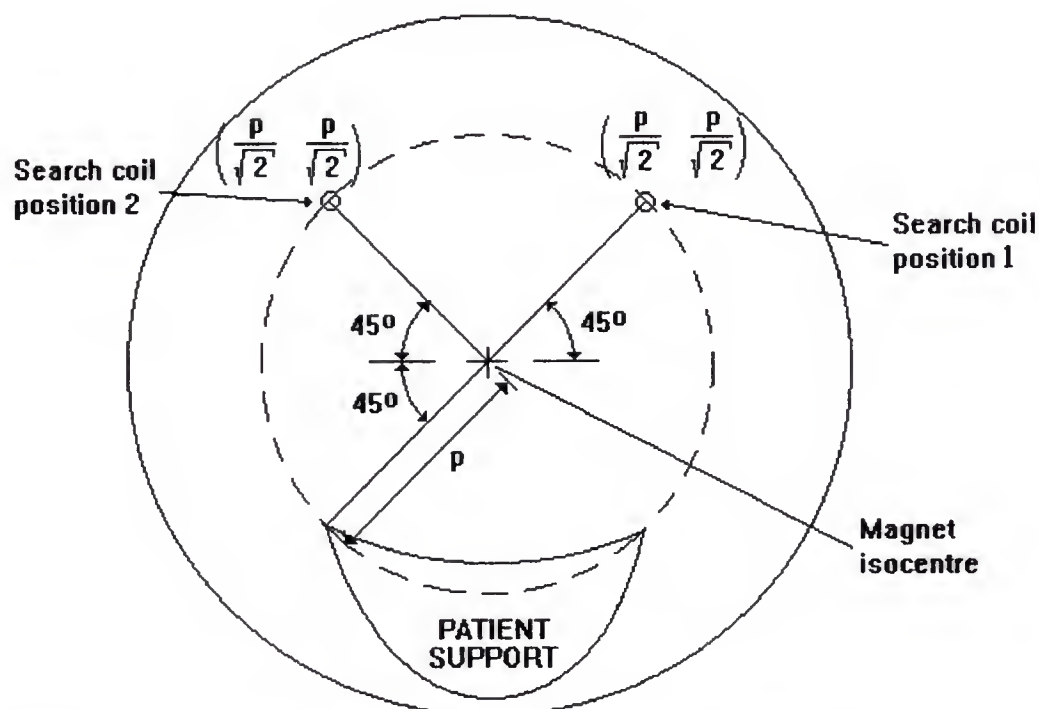


**Figure 103 - Search coil placement for measurement of dB/dt.**

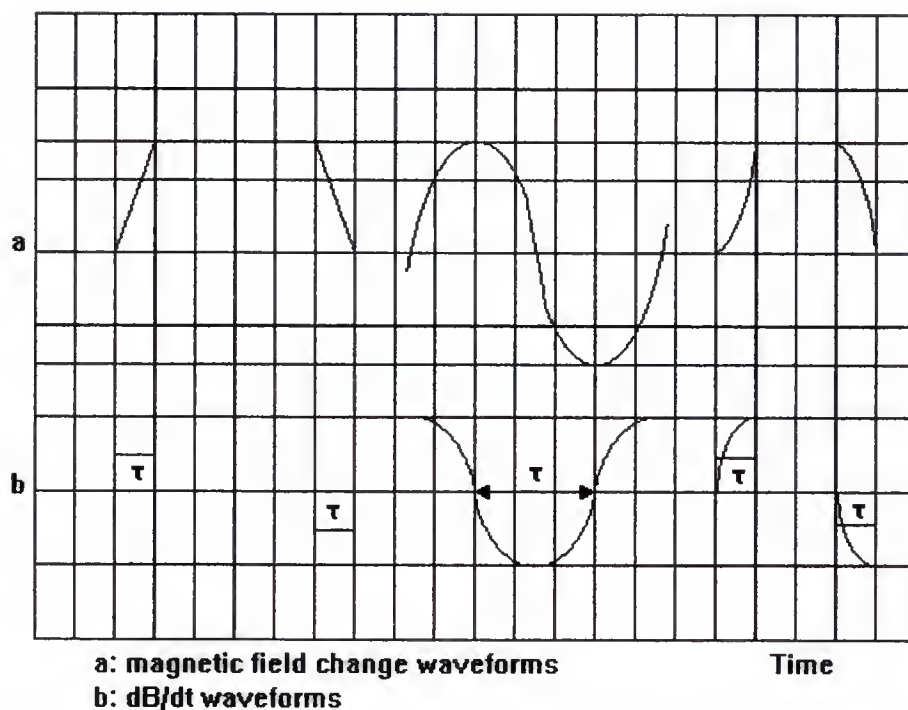


**Figure 104 - Magnetic field change waveforms and dB/dt waveforms.**

b) Test hardware:

1) Search coil

The search coil shall be circular and shall be small with respect to the gradient coils under test to ensure accuracy. The search coil consists of  $n$  turns of wire with a radius of  $r$  meters. The axial length of the coil shall be less than 20% of its diameter.

The search coil shall be no more than 50 mm in diameter. The response of the search coil shall be determined by calculation. The instantaneous magnitude of the component of  $dB/dt$  coaxial with the search coil shall be determined from the peak voltage,  $V$ , induced in the coil by the time varying magnetic flux:

$$\left| \frac{dB}{dt} \right| = \left| \frac{V}{nr^2} \right|$$

For example a typical coil would consist of 15 turns of copper wire of 0.8 mm diameter on a form of 50 mm diameter ( $r = 25$  mm) resulting in a circular coil approximately 12 mm long. An induced voltage of 200 mV would then result in a  $dB/dt = 6.79$  T/s coaxial with the search coil.

## 2) Voltage measurement device

The device used to measure voltage induced in the search coil shall have a high input impedance and sufficient bandwidth to prevent signal attenuation, e.g. a storage oscilloscope.

The voltage measuring device (storage oscilloscope) shall be placed at a location where it is accurate and not affected by magnetic fields.

The search coil shall be connected to the voltage measurement device by means of a low inductance cable, e.g. a twisted pair to avoid ringing on the waveform that may be experienced with coaxial cables.

## 3) Positing device

A means shall be provided for positioning and aligning the search coil in the magnet in a stable and reproducible manner. The device shall permit positioning of the search coil throughout the region normally occupied by the patient while maintaining the search coil coaxial with the static magnetic field.

## c) Maximum gradient rate measurement for trapezoidal gradients:

Turn off or maximally attenuate the radio frequency (RF) transmitter to prevent interference.

Position the search coil in the Magnetic Resonance equipment using the positioning device so that the search coil axis is aligned with that of the static magnetic field, regardless of patient orientation.

The amplitudes,  $A_{+max}$  and  $A_{-max}$  are defined as the maximum gradient strength that can be generated by the systems under normal scan conditions. The transition time  $t_1$ ,  $t_2$ ,  $t_3$  and  $t_4$  shall be the minimum that the system can generate using the standard pulse sequence generation software and hardware used by the manufacturer. Begin simultaneous pulsing of all three gradients (x, y and z) using the maximum amplitude bipolar gradient waveform.

Move the search coil to locate the position of the maximum induced voltage that can be found within the region of the Magnetic Resonance equipment normally occupied by a

patient. Once this position is established, the coil shall be immobilized to prevent movement-induced voltage from interfering with the measurement.

The following procedure locates the approximate position of maximum  $dB_z/dt$  in the patient space of the Magnetic Resonance equipment with an axial field magnet and whole-body gradient coils. Consider a cartesian coordinate system with the Z-axis pointing in the direction of the static field and the Y-axis pointing vertically (e.g. as in figure 103). For the maximum gradient rate measurement for trapezoidal gradients procedure, the points of maximum  $dB/dt$  will occur where each of the gradients is near maximum and all the gradient fields add. Typically, this is near the maximum winding density for the z-coil and near the wall of the bore for X- and Y-gradients.

Assume that the distance,  $p$ , from the magnet isocentre to the patient support along the lines  $y = \pm x$  is the same as the maximum distance the patient may extend above the magnet isocentre along the lines  $y = \pm x$ , then the maximum  $dB/dt$  value is located at the points:

$$\left( \pm \frac{p}{\sqrt{2}}, \frac{p}{\sqrt{2}}, Z_m \right)$$

Where  $Z_m$  is the Z coordinate of maximum  $dB/dt$ .

Assuming all three gradients are applied simultaneously and with equal amplitudes, the highest induced voltages will be found near the walls of the magnet shroud near the ends of the gradient coils along the lines  $y = \pm x$  (see figure 103).

Search coil position 1 in figure 103 shall be located at:

$$Y = X = \frac{p}{\sqrt{2}}$$

Similarly, search coil position 2 shall be located at:

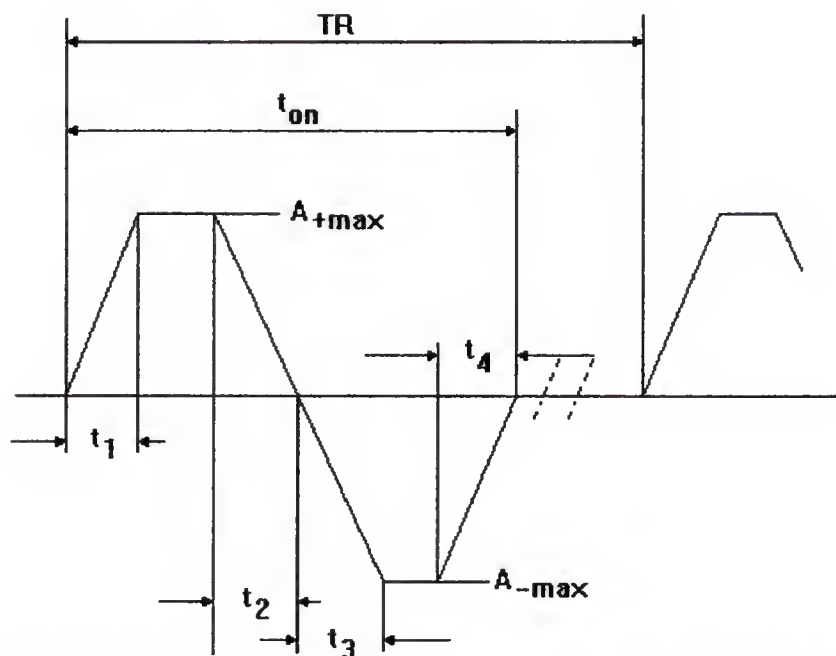
$$Y = -X = \frac{p}{\sqrt{2}}$$

Place the search coil coaxial with the static magnetic field at position 1 and constrain the search coil so it may move only in the Z direction. Move the coil in the Z direction to the position where the maximum voltage is induced in the search coil. Repeat this procedure

for position 2. The results from the position which yields the greatest search coil voltage shall be recorded.

Measure the peak voltages which correspond to the maximum  $\text{dB}/\text{dt}$  for transitions  $t_1$ ,  $t_2$ ,  $t_3$  and  $t_4$  (see figure 101).

Record the pulse width,  $T$ , of the  $\text{dB}/\text{dt}$  waveform corresponding to the  $t_1$ ,  $t_2$ ,  $t_3$  and  $t_4$  (see figure 101).



**Maximum amplitude bipolar gradient amplifier input waveform  
(without pre-emphasis)**

**Figure 101 - Waveform for performing measurements of acoustic noise and dB/dt.**

d) Maximum sinusoidal dB/dt:

**Step 1:** turn off or maximally attenuate the radio frequency (RF) transmitter to prevent interference.

**Step 2:** position the search coil in the Magnetic Resonance scanner using the positioning device so that the search coil axis is aligned with that of the static magnetic field.



Step 3: turn off all gradients other than the sinusoidal gradient of interest. Apply the maximum amplitude and frequency waveform that the system can generate using the standard pulse sequence generation software and hardware used by the manufacturer.

Step 4: move the search coil to locate the position of the maximum induced voltage that can be found within the region of the machine normally occupied by the patient. Once the position is established, the coil shall be immobilized to prevent movement-induced voltage from interfering with the measurement.

Step 5: for most coils a suitable search procedure is as follows:

for x gradients, fix the coil along  $X = p$ ,  $Y = 0$

for y gradients, fix the coil along  $X = 0$ ,  $Y = p$

for z gradients, fix the coil along  $X = 0$ ,  $Y = p$

Step 6: then search along Z to locate the position of the maximum induced voltage that can be found within the region of the Magnetic Resonance equipment normally occupied by the patient.

Step 7: measure the peak voltage which corresponds to the maximum dB/dt.

Record the pulse width, T, of the dB/dt waveform.

Repeat the above procedure for any other sinusoidally driven gradient.

a) Report of results:

The following data shall be recorded for the maximum gradient rate measurement for trapezoidal gradients:

Parameter	Dimension
- maximum gradient pulse amplitude	mT/m
- patient space radius, p	M
- $t_1$	$\mu s$
- $t_2$	$\mu s$
- $t_3$	$\mu s$
- $t_4$	$\mu s$
- measured voltage	voltage indicating T/s

The following data shall be recorded for the maximum sinusoidal dB/dt method:



Parameter	Dimension
- maximum gradient pulse amplitude	mT/m
- patient space radius, p	M
- pulse width, T	$\mu$ s
- measured voltage	voltage indicating T/s

## Protection against high Radio Frequency energy

NOTE: The requirements regarding SAR from RF power assumes that the manufacturers recommendations regarding the control of temperature, humidity and other environmental conditions are met.

### SAR Limits

The following requirements on whole-body SAR should be used only where the environmental temperature does not exceed 24°C and the relative humidity does not exceed 60%. For temperatures above 24°C or relative humidity above 60%, the limits in the definitions of the operating modes for whole-body SAR shall be reduced as described in the rationale, possibility changing the operating mode for a given value of SAR.

NOTE: The requirements regarding SAR from RF power further assume that the SAR averaged over any 10 s period does not exceed 5 times the stated temporal average SAR limit.

#### a) Whole-body SAR

Whole-body SAR is the value of the SAR averaged over the entire body of the patient.

Three operating modes with regard to whole-body SAR are defined, namely Normal Operating Mode, First Level Controlled Operating Mode and Second Level Controlled Operating Mode:

- 1) the Normal Operating Mode comprises values of whole-body SAR not higher than 1.5 W/kg averaged over any period of 15 min:
- 2) the First Level Controlled Operating Mode comprises values of whole-body SAR not higher than 4 W/kg averaged over any period of 15 min:
- 3) the Second Level Controlled Operating Mode comprises values of whole-body SAR than may exceed 4 W/kg averaged over any period of 15 min.

#### b) Head SAR

Head SAR is the value of the SAR averaged over the head of the patient.

Two operating modes with regard to head SAR are defined, namely Normal Operating Mode and Second Level Controlled Operating Mode:

1) the Normal Operating Mode comprises values of head SAR not higher than 3 W/kg averaged over any period of 10 min:

2) the Second Level Controlled Operating Mode comprises values of head SAR that may exceed 3 W/kg averaged over any period of 10 min.

c) Local tissue SAR using e.g. transmitting special coils

Local tissue SAR is the value of the SAR averaged over any localized mass of tissue.

Two operating modes with regard to local tissue SAR are defined, namely Normal Operating Mode and Second Level Controlled Operating Mode:

1) the Normal Operating Mode comprises values of local tissue SAR in any gram of tissue not exceeding 8 W/kg in the head or torso of 12 W/kg in the extremities averaged over any period of 5 min;

2) the Second Level Controlled Operating Mode comprises values of local tissue SAR that may exceed the upper limit for the Normal Operating Mode.

## Control of SAR

a) Transmission of body coil:

- when the body coil is used to image the torso, the system shall control the whole-body SAR;

- when the body coil is used to image the head, the system shall control either the head SAR or the SAR averaged over the part of the body that is being irradiated. In the latter case the limits that apply are numerically equal to those for the whole-body SAR;

- when the body coil is used to image extremities, the system shall control either the local tissue SAR or the SAR averaged over the part of the body that is being irradiated. In the latter case the limits that apply are numerically equal to those for the whole-body SAR.

b) Transmission by head coil:

- when the head coil is used to image the head, the system shall control the head SAR;

- when the head coil is used to image extremities, the system shall control either the local tissue SAR or the SAR averaged over the part of the body that is being irradiated. In the latter case the limits that apply are numerically equal to those for the head SAR.

c) Other combinations of coil and body areas:

- regardless of the coil used for RF excitation, the system shall control whole body SAR, and local tissue SAR appropriately.

## Display of SAR

The value of the SAR that is displayed shall be the value that is controlled by the system.

Compliance shall be tested by measurement of the SAR according to one of the methods specified below.

Method of measurement of SAR to demonstrate compliance.

The methods employed may be known as “pulse energy method” and “calorimetric method”.

a) Auxiliary definitions:

tip angle:	Angle through which macroscopic magnetization vector is moved by a radio frequency pulse
landmark:	Region of the body to be placed in the center of the RF body coil
$P_{\text{forward } 2}$ :	Forward peak RF power going into the terminals of the RF coil when loaded with test object 2
$P_{\text{reflected } 2}$ :	Peak RF power reflected from the terminals of the RF coil when loaded with test object 2
$P_{\text{other } 2}$ :	Peak RF power absorbed or dissipated elsewhere in the system when the coil is loaded with test object 2. For example, in a quadrature system fed by a four-port splitter, this is the peak RF power delivered to the dummy load.
$P_{\text{object}}$ :	Net peak RF power delivered to test object 2
$P_{\text{coil}}$ :	Net peak RF power absorbed by the RF transmit coil for the tip angle specified
$P_{\text{forward } 1}$ :	Forward peak RF power going into the terminals of the RF coil when loaded with test object 1

$P_{\text{reflected } 1}$ :	Peak radio RF reflected from the terminals of the RF coil when loaded with test object 1
$P_{\text{other } 1}$ :	Peak RF power absorbed or dissipated elsewhere in the system when the RF coil is nearly unloaded. For example, in a quadrature system fed by a four-port splitter, this is the peak power delivered to the dummy load when the radio frequency coil is loaded with test object 1
$B_1$ :	Magnetic induction of the RF magnetic field used in Magnetic Resonance imaging and spectroscopy

## b) Test hardware

### Test object 1

Test object 1 shall be a physically small object used during the calibration of tip angles and during the determination of radio frequency coil losses with the pulse-energy method. Test object 1 shall be filled with a material which can be imaged by the Magnetic Resonance equipment, but whose conductivity shall be less than 0.003 S/m. This ensures that the radio frequency losses of the object are negligible, thus permitting the measurement of coil losses while contributing little to system losses. Test object 1 shall be physically small and compact in shape. The test object volume shall be less than 250 ml. The longest dimension of the test object shall be not more than three times the shortest dimension.

### Test object 2

Test object 2 shall be the test object whose SAR shall be determined using the pulse-energy method. This test object should have coil loading characteristics similar to patient loading. These loading characteristics will differ for the case of whole-body SAR, head SAR and local tissue SAR.

## c) Test arrangements

Peak radio frequency power measurements shall be made either with the use of an oscilloscope whose bandwidth exceeds the desired frequency by a factor of 5 or more and dual directional couplers whose directivity exceeds 30 dB, or with attenuators.

Connect the directional coupler, oscilloscope and other power measurement equipment with 50  $\Omega$  coaxial transmission lines as shown in figure 105 or figure 106. Ensure that the oscilloscope input is terminated in a 50  $\Omega$  impedance. The oscilloscope shall be placed at a location where it is accurate and not affected by magnetic fields.

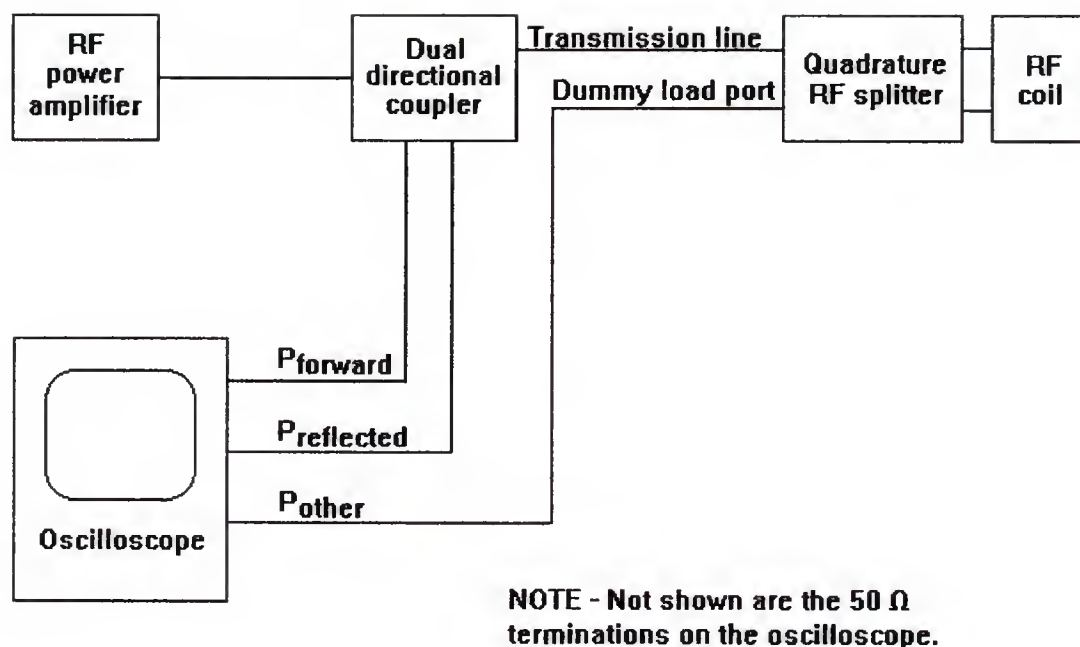


**Figure 105 - Hardware setup for pulse-energy method for the measurement of SAR with a quadrature coil.**



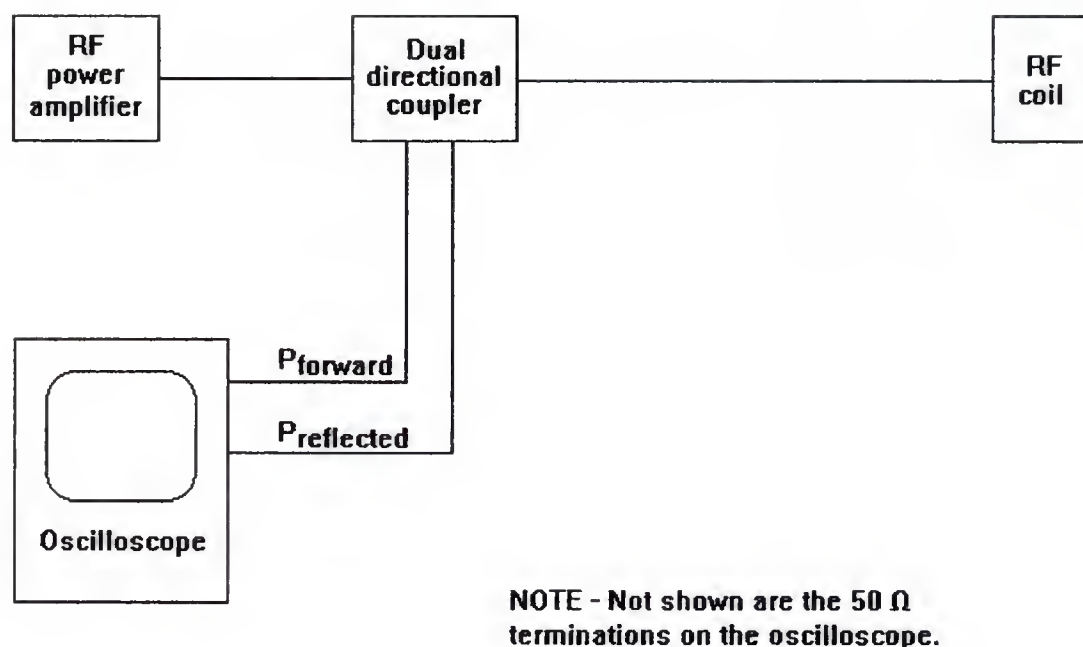


**Figure 106 - Hardware setup for pulse-energy method for the measurement of SAR with a linear coil.**

d) SAR measurement procedure, pulse-energy method

Step 1: position test object 1 in the scanner at isocentre.

Step 2: calibrate the tip angle. The standard method (hardware and/or software) employed by each manufacturer shall be used to set the tip angle to the desired value for the type of scan selected. The same tip angle shall be used for test object 1 and test object 2 power measurements.

Step 3: start the scan sequence chosen for the SAR measurement. Ensure that the scan time is long enough to allow the completion of the desired measurements, or set the scanner to repeat the pulse sequence indefinitely.

Step 4: measure the peak-to-peak radio frequency envelope voltages (forward, reflected and other) for each radio frequency pulse in the sequence, or use other means to measure the instantaneous, radio frequency peak power levels (forward, reflected and other if applicable).

Step 5: measure the power attenuation of the transmission line between the body-coil and the coupler and the transmission line between the dummy load port and the oscilloscope.

Step 6: convert the peak-to-peak voltage measurements into peak measurements. The peak power measured at the oscilloscope is:

$$\frac{V_{pp}^2}{8 Z_o}$$

where

$V_{pp}$  is the measured peak-to-peak voltage;  
 $Z_o$  is the characteristic impedance of the transmission line (and also the input impedance of the oscilloscope).

The calculated peak power at the oscilloscope shall be converted into peak power referenced to the input terminals of the radio frequency coil by considering transmission line attenuation and directional coupler coupling constants.

For a quadrature radio frequency coil:

$$\begin{aligned} P_{\text{forward}} &= P_{\text{fm}} \times \alpha_1 \\ P_{\text{reflected}} &= P_{\text{rm}} / \alpha_1 \\ P_{\text{other}} &= P_{\text{om}} / \alpha_2 \end{aligned}$$

where

$P_{\text{fm}}$  is the forward power measured at the terminals of the oscilloscope coupler;  
 $P_{\text{rm}}$  is the reflected power measured at the terminals of the oscilloscope;  
 $P_{\text{om}}$  is the “other” power measured at the terminals of the oscilloscope;  
 $\alpha_1$  is the fractional power attenuation (not in dB) of the transmission line between the body coil and the coupler; and  
 $\alpha_2$  is the attenuation between the dummy load part and the oscilloscope.

Note that for unmatched linear coils, transmission line attenuation increases with the mismatch:

$$\alpha = \alpha_o \times (R^2 + 1) / (2 \times R)$$

where

- $\alpha$  is the resultant attenuation;
- $\alpha_o$  is the attenuation under matched conditions;
- $R$  is the standing wave ratio.

Calculate the peak power absorbed by the unloaded coil,  $P_{coil}$ .

$$P_{coil} = P_{forward\ 1} - P_{reflected\ 1} - P_{other\ 1}$$

Note that  $P_{forward\ 1}$ ,  $P_{reflected\ 1}$  and  $P_{other\ 1}$  are from the experiment using test object 1.

After initial measurements are made on test object 1, they are repeated using test object 2.

Remove test object 1 from the coil, place test object 2 in the scanner at isocentre and repeat steps 4 and 6. The same tip angle shall be used for test object 2 as was used for test object 1.

Calculate the peak power absorbed in test object 2,  $P_{object}$ .

$$P_{object} = P_{forward\ 2} - P_{reflected\ 2} - P_{other\ 2} - P_{coil}$$

Note that  $P_{forward\ 2}$ ,  $P_{reflected\ 2}$  and  $P_{other\ 2}$  are all obtained from the measurements on test object 2, while  $P_{coil}$  is obtained from calculations using test object 1.

Calculate the energy per pulse absorbed by the object: integrate each of the radio frequency waveforms in the pulse sequence and find the pulse durations of equivalent (in energy) rectangular pulses which have the same peak power levels as the pulse sequence being evaluated. This step shall be repeated for each type of radio frequency pulse in the pulse sequence (e.g. 90° pulses as well as 180° pulses). The equivalent rectangular pulses shall result in both the same peak power and in the same energy deposition as the pulse being evaluated. The pulse duration,  $W_{rectangle}$  shall be calculated from the radio frequency pulse waveform,  $B1(t)$  normalized to its peak value  $B1_{peak}$  as follows:

$$W_{rectangle} = \int B1(t)^2 \frac{dt}{(B1^2_{peak})}$$

For example, a sinc (or  $\sin\theta/\theta$ ) pulse is approximately equivalent in energy to a rectangular pulse with the same peak power and half the width of the main lobe of the sinc pulse.

Calculate the energy per pulse,  $E_i$ , as:

$$E_i = P_{object} \times W_{rectangle}$$

Calculate the total average power,  $P_{ave}$ , absorbed by the object. The total average power for sequences with well-defined pulse repetition times (TR) is the sum of all the energies in all the pulses per repetition divided by TR:

$$P_{ave} = \sum \left( \frac{E_i}{TR} \right)$$

For sequences where TR is undefined (such as single-shot sequences), the total average power shall be calculated from the sum of all energies in all pulses used in the scan divided by the total scan time, S:

$$P_{ave} = \sum \left( \frac{E_i}{S} \right)$$

Calculate the SAR for test object 2, whose mass is M:

$$TAS = \frac{P_{ave}}{M}$$

e) Report of results, pulse energy method

The following data shall be recorded:

Measured values of SAR for each object and pulse sequence used

Parameter	
Dimension	
- Peak forward power	
W	
- Peak reflected power	W
- Peak coil loss power	W
- Other peak power lost	W
- Radio frequency waveform	
---	
- Pulse parameters	
---	
o Tip angle(s)	
- Accuracy of power measurement equipment	%

- Equivalent rectangular pulse duration ( $W_{\text{rectangle}}$ )  $\mu\text{s}$
- TR or S ms
- Mass of test object 2 kg
- Any other parameters required to ensure repeatability
- 

f) Test hardware, calorimetry method (whole-body SAR only)

Test object 1

Test object 1 shall be a physically small object used during the calibration of tip angles and during the determination of radio frequency coil losses with the pulse-energy method.

Test object 1 shall be filled with a material which can be imaged by the Magnetic Resonance equipment, but whole conductivity shall be less than 0.003 S/m. This ensures that the radio frequency losses of the object are negligible, thus permitting the measurement of coil losses while contributing little to system losses. Test object 1 shall be physically small and compact in shape. The test object volume shall be less than 250 ml. The longest dimension of the test object shall be not more than three times the shortest dimension.

Test object 3

Test object 3 shall be an annular test object designed to provide radio frequency coil loading equivalent to that of a human. It shall be filled with an aqueous sodium chloride solution whose concentration is adjusted to yield a conductivity which produces the loading specified below. The filling solution shall also contain a doping material such as manganese chloride to shorten the relaxation properties of the solution to render it invisible in Magnetic Resonance images. The total volume of the test object shall be less than 25 L. The test object shall be designed to load the same as a 50 kg to 90 kg human, positioned for a scan with the stated tolerances:

Coil 3 dB bandwidth	$\pm 15\%$
Coil impedance:	$\pm 20\%$ phase
Coil center frequency shift:	$\pm 1\%$ of centre frequency

Annular test object thermal properties shall be sufficient to maintain a 2 °C temperature rise over ambient temperature (in the filler material) to within 5% for 1 h.

Temperature measurement

A temperature measurement system accurate to within 0.1 °C over the range of 15 °C to 45 °C shall be provided. The system will be used to make initial and final measurements of



temperature. It is not necessary for the system to be immune to radio frequency interference from a Magnetic Resonance equipment nor to temperature artifacts induced by the static magnetic field. Acceptable examples are fiber-optic temperature sensors, thermister-based temperature sensors and the thermocouple temperature sensors.

g) Test arrangement, calorimetry method

Place the temperature measurement hardware in a convenient location remote from the magnet to permit measurement of test object filler temperature quickly before and after scanning. This will prevent inaccuracies due to the static magnetic field.

Position test object 3 at isocentre in the radio frequency body coil before the scan.

The number of acquisitions for the scan shall be adjusted to yield a scan sufficiently long to create a temperature rise at least 20 times greater than the error of the temperature measurement system. For an aqueous solution, an exposure of one hour to an SAR of 1 W/kg will result in an average temperature rise of 0.86 °C (0.0143 °C/min), assuming no thermal losses. Higher temperature rises may be measured to more significant places than small temperature rises. However, higher temperatures rises may increase heat loss errors.

h) SAR measurement procedure, calorimetry method

Step 1: equilibrium test object 3 in the magnet bore with air flow turned off.

Step 2: measure the initial temperature of the bore of the Magnetic Resonance equipment and the initial temperature of the scan room.

Step 3: remove the test object from the bore and invert three times to stir the filler material.

Step 4: measure the initial temperature,  $T_i$ , of the test object by inserting a temperature sensor into the filler material. The initial bore temperature should not differ from  $T_i$  by more than 1 °C.

Step 5: quickly replace the test object 3 in the Magnetic Resonance scanner at isocentre and place test object 1 centrally within it.

Step 6: calibrate the tip angle. The standard methods (hardware and/or software) employed by each manufacturer shall be used to set the tip angle to the desired value for the type of scan selected.

Step 7: scan with enough acquisitions to ensure the desired measurement (see item g above).



Remove the test object from the bore and measure the final temperature,  $T_f$ , of the filler solution of test object 3 after inverting the test object three times.

If  $T_f - T_i \leq 2\text{ }^{\circ}\text{C}$ , the experiment can be continued by replacing the test object in the bore and restarting the scan. The measurement delay time shall be subtracted from the total time to assure accuracy.

Measurement the final bore and the final scan room temperatures. If the scan room temperatures of bore temperature changes by more than  $0.5\text{ }^{\circ}\text{C/h}$  then the experiment should be repeated under more stable conditions.

Calculate the energy,  $E$  (in J), absorbed by the test object 3 in terms of the mass,  $M$ , of the filler (in kg) and of the specific heat,  $c$ , of the filler fluid (in  $\text{J/kg }^{\circ}\text{C}$ ):

$$E = M \times c \times (T_f - T_i)$$

Calculate the average power  $P$  (in W) during the scan time  $T$  (in s):

$$P = E/\tau$$

Calculate the SAR of the test object filler material from:

$$\text{SAR} = P/M$$

Calculate the apparent SAR,  $\text{SAR}_{\text{app}}$  using:

$$\text{SAR}_{\text{app}} = P/M_{\text{bod}}$$

where  $M_{\text{od}}$  is the mass of a body which test object 3 simulates (assuming that the validity of the simulation has been independently verified).

Report of results, calorimetry method

Parameter	Dimension
- Initial test object 3 temperature	$^{\circ}\text{C}$
- Final test object 3 temperature	$^{\circ}\text{C}$
- Initial bore temperature	$^{\circ}\text{C}$
- Final bore temperature	$^{\circ}\text{C}$
- Initial scan room temperature	$^{\circ}\text{C}$
- Final scan room temperature	$^{\circ}\text{C}$
- Test object 3 mass	kg
- Test object 3 simulated mass ( $M_{\text{bod}}$ )	kg

- Test object 3 volume l
- Test object 3 dimensions m
- Radio frequency waveform description ---
- Repetition time (TR) ms
- Echo time (TE) ms
- Number of slices ---
- Number of echoes ---
- Total scan time s
- Magnetic Resonance tip angle employed in study degree
- Any other parameters required to ensure repeatability
- The accuracy, type of location (during the measurement)  
of the temperature measurement

## Definitions:

**Scan Duration** - This term is often referred to as acquisition time and is a variable needed in algorithms that predict the energy exposure to radio frequency power. Scan duration for acquisition gated to period functions of the patient may be difficult to assess accurately. A conservative calculation of scan duration in such cases can be assumed to be based on the shortest period that can be realized under the circumstances.

**Magnetic Resonance Examination** - A magnetic resonance examination usually is comprised of more than one acquisition of data, each with a predictable scan duration during one session.

**Magnetic Resonance** - The phenomenon of magnetic resonance occurs when the frequency of electro-magnetic radiation equals the Larmor precession frequency of the nuclear or electron magnetic moments.

**Specific Absorption Rate (SAR)** - The SAR is a function of the frequency (increasing approximately as the square of the frequency), the type and number of radio frequency pulses, the duration and repetition rate of pulses and the type of coil used for transmission. The important biological factors are: conductivity of tissue, specific gravity of the tissue, anatomical region examined, tissue type (e.g. the degree of perfusion) and mass of the patient.

**Time Rate of Change of Magnetic Field (dB/dt)** - The rate of change of the magnetic flux density with time is a potential concern for safety limits, since changing magnetic fields induce eddy currents within the patient.

**Quench** - a quench is due to excessive heating of the wires of the magnet immersed in liquid helium.

Superconducting magnet can vent up to several hundred liters of cryogenic gases per hour during normal operation. During the quench, approximately  $1^{04}$  L to  $1^{05}$  L of gas at atmospheric pressure can be vented within a few minutes.

Usually, a quench occurs when the quantity of liquid helium becomes insufficient to cool the superconducting coil. Due to the increase in the temperature of the coil, the superconducting wire exhibits normal conductivity and an excessive boil-off starts.

If proper venting is not used, three effects can occur during rapid boil-off at a quench:

- excessively cooled gases will freeze water molecules in the area adjacent to the magnet causing a dense white fog;

- oxygen in the room will be displaced by helium making it difficult, if not impossible, to breathe;
- the helium gas that escapes during a quench will freeze any object it contacts.

### **Electromagnetic compatibility**

Within the controlled access area the magnetic resonance system will generally not comply with the current requirements for radio frequency emission. These requirements are primarily intended to protect radio communication and are laid down in International Standards such as CISPR 11. Permissible limits for radio frequency emission are in the range of  $30 \text{ dB}\mu\text{V/m}$  to  $50 \text{ dB}\mu\text{V/m}$ . It is proposed that in coming standards emission levels of magnetic resonance, computed tomography and large x-ray systems are to be measured at the boundaries of the room or of the building.

IEC standards on EMC are in preparation that deal with the immunity for radio frequency fields of medical equipment. It is expected that immunity will be required for the general case of fields up to  $1 \text{ V/m}$  or  $3 \text{ V/m}$  and for special cases, such as life sustaining and some patient monitoring equipment, at fields up to  $10 \text{ V/m}$  or  $100 \text{ V/m}$ .

Actually, within the controlled access area around the magnetic resonance equipment, radio frequency field strengths may easily exceed these limits and can have values in excess of  $100 \text{ V/m}$ . It is clear, that peripheral equipment used in the controlled access area might be disturbed by this field.

### **Protection against high $\text{dB/dt}$ associated with gradient coils**

Time-varying magnetic fields induce electrical potentials and eddy currents in accord with Faraday's law. In the simple case of a circular loop intersected by a uniform time-varying magnetic field, the magnitude of the average induced electric field depends directly on the radius of the loop and the magnitude of  $\text{dB/dt}$ . The larger the radius and  $\text{dB/dt}$ , the larger is the induced current.

The  $\text{dB/dt}$  waveform may be pulsed or sinusoidal. The pulse width,  $T$ , is defined as the full width at half maximum of a single pulse of  $\text{dB/dt}$ . It should be noted, that "pulse" and "waveform" refer to the time function of  $\text{dB/dt}$  and not to the current pulse in the gradient coil. When the waveform is sinusoidal rather than pulsed,  $T$  is the half period of the sinusoid.

When a time-varying magnetic field impinges on the human body, currents are induced in the body in planes perpendicular to the magnetic field. These induced currents can affect excitable tissue with thresholds that are frequency dependent. At higher frequencies, higher currents are required for an effect. Although induced currents will also cause heating according to Ohm's law, heating effects become the limiting consideration only for



frequencies above 200 kHz, or pulse widths shorter than 2.5  $\mu$ s. Heating effects are covered in the sections on radio frequency energy.

The primary concerns regarding dB/dt are cardiac fibrillation and the stimulation of cardiac and peripheral nerve and muscle (twitching), fibrillation being most serious in nature and induced by a larger dB/dt value and peripheral muscle stimulation being of least concern and induced by a smaller dB/dt value. Protection against peripheral nerve stimulation should serve to protect also against cardiac stimulation.

Most empirical data on thresholds for cardiac and neuromuscular responses are based on animal studies or a limited number of observations on humans during application of 50 Hz or 60 Hz sinusoidal currents using electrodes. It has been reported that in animal studies time-varying magnetic fields induce skeletal muscle contractions at dB/dt values at which no disturbances in cardiac function occur.

Reports describe peripheral nerve and phrenic nerve stimulation at dB/dt values and frequencies that are similar to those predicted are described below. A more recent report describes the threshold dB/dt for localized excitation of the brachial plexus in human subjects using a train of trapezoidal pulsed magnetic fields for read-out gradient pulses of “echo-planar” imaging systems. These later results are also consistent with the predications outlined.

Cardiac fibrillation thresholds from animal experiments where electrodes were placed directly on the heart show a log-normal distribution with the one-percentile value at about half the medium value. Combining this relationship with human data which showed an average fibrillation threshold of about 5 A/m<sup>2</sup>, the one-percentile level for fibrillation would be about 2.5 A/m<sup>2</sup>. At 60 Hz the cardiac excitation thresholds for humans are about 40% of the 60 Hz fibrillation values, and this would indicate a threshold for excitation of about 1 A/m<sup>2</sup>.

A model study compared the expected thresholds for cardiac and peripheral nerve stimulation as a function of  $\tau$ . For  $\tau$  shorter than 0.4 ms (frequency greater than 1200 Hz), the threshold for peripheral nerve stimulation is at least 10 times lower than for cardiac stimulation. For  $\tau$  longer than 5 ms (frequency below 100 Hz), however, the modeled threshold for peripheral nerve stimulation (about 60 T/s for the main magnetic field parallel to the body) is only about 15% below that for cardiac stimulation (about 70 T/s).

“Echo-planar” imaging techniques use sinusoidal excitation at about 1200 Hz to 1500 Hz on one or more of the gradient coils. For frequencies above 1200 Hz, peripheral nerve stimulation should have a 10 times lower value than that for cardiac stimulation threshold and supra-threshold peripheral stimulation should provide an early warning for cardiac



stimulation with an adequate margin of safety. Cardiac fibrillation has a threshold 5 to 10 times higher than cardiac stimulation at these frequencies.

Extensive calculations suggest that peripheral nerve and muscle (including cardiac muscle) stimulation will be avoided if induced current density is restricted to less than  $400 \text{ mA/m}^2$  at any body location for induced current pulse widths exceeding  $120 \text{ }\mu\text{s}$ . For shorter current pulse widths, the induced current density should be restricted according to the relationship  $J \times t < 48 \times 10^3$ , where  $J$  is the value of the induced current density expressed in  $\text{mA/m}^2$  and  $t$  is the duration of the induced current pulse in  $\mu\text{s}$ . When only cardiac stimulation is to be avoided, i.e. when the risk of peripheral nerve stimulation is not taken into account, relaxation of this restriction is allowed for periods of magnetic field change of less than 3 ms according to the relationship  $J \times t < 1.2 \times 10^6$ .

Making certain assumptions, limits expressed in  $\text{dB/dt}$  can be derived from these restrictions on induced current density. It can be calculated that peripheral nerve and cardiac stimulation will be avoided by an adequate margin of safety if the time-varying magnetic field does not exceed  $20 \text{ T/s}$  peak value for  $\tau$  greater than  $120 \text{ }\mu\text{s}$ . As the value of  $\tau$  decreases between  $120 \text{ }\mu\text{s}$  and  $2.5 \text{ }\mu\text{s}$ , the safe level increases linearly to a value of  $960 \text{ T/s}$ , above which heating from eddy currents will dominate (greater than  $1 \text{ W/kg}$ ), and the radio frequency SAR limits are more appropriate limiting factors than  $\text{dB/dt}$ .

Recent reports cite peripheral and cardiac nerve stimulation at  $\text{dB/dt}$  values and frequencies which are remarkably similar to those predicted and lend further credence to the  $\text{dB/dt}$  limits stated in 51.102.

The values suggested in 51.102 are intended to avoid cardiac stimulation by an adequate margin of safety. Operation of the system beyond those levels entails the users and/or operators direct responsibility.

For  $\tau$  greater than 5 ms (frequency less than 100 Hz), cardiac stimulation thresholds are only slightly higher than peripheral nerve stimulation thresholds. In this range peripheral nerve stimulation thresholds. In this range peripheral nerve stimulation should not be used as a surrogate or “early warning” for cardiac stimulation. However it is not expected that Magnetic Resonance equipment will operate with such frequencies or pulse widths.

The derived restrictions on  $\text{dB/dt}$  can be exceeded if it can be shown that the basic restriction on induced current density is not exceeded.

### **Protection against high radio frequency energy**

Heating is a major consequence of exposure to the RF frequencies used in Magnetic Resonance (usually greater than 1 MHz). Many of the biological effects of acute exposure to RF are consistent with responses to induced heating resulting from rises in tissue or

body temperature of about 1°C or more, or with responses for minimizing the total heat load.

The RF induced heat load can be directly related to the SAE or to the SAR. Other important factors which influence patient response to a given heat load include the air temperature, relative humidity, air flow rate and the degree of patient insulation.

Localized regions of heating or “hot spots” may cause local temperature rises. In practice, the local tissue SAE is always higher than the average whole-body value: only part of the body is exposed to RF, power absorption increases in proportion to the square of the radial distance from the center of the body and the electrical inhomogeneity of the body alters current flow and local energy absorption. Studies using spherical models predict that worst case “hot spots” would be produced by a sphere of low conductivity (bone or fat) located on the outer edge of a large conductive sphere (e.g. muscle); a “hot spot” can occur with an SAR of up to 2.5 times the local average value. Recent calculations based on a heterogeneous mathematical model of the human body suggest that localized tissue SAR within the body could be up to 10 or even 70 times greater over small volumes compared to the whole body average value. However, these relative increases are reduced to a factor of about 2 to 4 when averaged over complete individual body organs. The probability of high localized tissue SAR is reduced by quadrature excitation and its effects are moderated by thermal diffusion and blood flow.

Thermal effects arise because of the temperature sensitivity of most biological processes. The primary concerns regarding RF exposure are to avoid excessive physiological responses to a marked rise in body temperature and to avoid raising tissue temperature to a level which incur some degree of harm.

The most sensitive responses of humans to acute whole-body heating by radio frequency are probably those concerned with thermoregulation and include increased cardiac output and skin blood flow coupled with a slight drop in arterial blood pressure. These responses become maximal, even in subjects lying passively in ambient temperatures, as body temperatures rise by more than about 2°C. Adverse health effects are not expected in people with unimpaired thermoregulatory and cardiovascular functions if the increase in body temperature does not exceed 1°C; some specific exceptions are given below.

The health of some patients might be comprised under these conditions. Physiological and physical correlates which are associated with a decreased ability to adapt to an increased heat load include old age, obesity and hypertension. Various drugs such as diuretics, tranquillizers and sedatives, vasodilators and others decrease heat tolerance. In addition, the thermoregulatory ability of infants is not well developed; pregnant women may also be comprised in their ability to dissipate heat. In this context, it is worth noting that heat loss from the embryo and fetus across the placental barrier may be less efficient than heat dissipation in other well vascularized tissue. Raised body temperature is known to be



teratogenic to a number of mammalian species including primates, and has been implicated in central nervous system and facial defects in children whose mothers developed prolonged severe hyperthermia ( $> 39^{\circ}\text{C}$ ), especially during the first trimester of pregnancy. In these cases it is desirable to limit rises in body temperature to less than  $0.5^{\circ}\text{C}$  (IRPA/INIRC, 1991)

The whole-body thermoregulatory response of humans exposed to Magnetic Resonance imaging has been mathematically modeled. The body temperature of a lightly clothed patient whose thermoregulatory ability was unimpaired would rise by up to  $0.6^{\circ}\text{C}$ , depending on environmental conditions, during exposure at whole-body SARs of up to  $4\text{ W/kg}$ . The results of these calculations are in reasonable agreement with studies of volunteers exposed to up to  $4\text{ W/kg}$  for 20 min to 30 min. In addition, there have been no reports of adverse health effects from excessive local or systematic heating in patients exposed at whole-body SARs of up to about  $1.5\text{ W/kg}$ .

Limits on whole-body SAR are presented in 51.103. A limit of  $1.5\text{ W/kg}$  for the Normal Operating Mode is recommended as the highest whole-body SAR which all persons, regardless of health status, should be able to tolerate. People with unimpaired thermoregulatory and cardiovascular system should tolerate higher whole-body SARs; an upper limit of  $4\text{ W/kg}$  for the First Level Controlled Operating Mode is recommended. Individual tolerance to raised body temperature is highly variable, however, even in healthy people (NIOSH, 1986); therefore, medical supervision is required.

The limits described above were developed assuming temperatures in the Magnetic Resonance equipment examination room of less than  $24^{\circ}\text{C}$ , a relative humidity of less than 60%, and minimal air flow; in addition, the patient is assumed to be lightly clothed. Calculations can be used to derive correction factors for environments which restrict heat loss. It can be estimated that, for each  $^{\circ}\text{C}$  of ambient temperature above  $24^{\circ}\text{C}$ , First Level Controlled Operating Mode restrictions on whole-body SAR should be lowered by  $0.25\text{ W/kg}$ . Similarly, for each 10% of excess relative humidity, the limits would be lowered by  $0.1\text{ W/kg}$ . For the Normal Operating Mode, reductions in the SAR restrictions should be half these amounts, except that it is not necessary to reduce the limit below  $1\text{ W/kg}$  for ambient temperatures less than  $30^{\circ}\text{C}$ . Individual responses will, however, be variable; increased attention at the appropriate level of supervision should be observed when using these correction factors.

Some regions of the body, such as the head, may be particularly vulnerable to raised temperature. The developing embryo or fetus should be regarded as particularly sensitive to raised temperatures; however, tissues in the trunk and limbs are considered less sensitive. It has been suggested that localized temperatures of about  $38^{\circ}\text{C}$  in the head,  $39^{\circ}\text{C}$  in the trunk and  $40^{\circ}\text{C}$  in the extremities are unlikely to produce adverse effects. Simple calculation relating localized heating in the eye to SAR in the head suggests that exposure resulting in  $3\text{ W/kg}$  to the head is unlikely to raise the temperature of the eye by

more than 1.6 °C; brain temperatures are unlikely to rise by more than 1 °C under these conditions. It seems probable that higher SARs are acceptable for the trunk (except during pregnancy) and limbs providing that whole-body heat loads are not exceeded. However, restrictions on local tissue SAR which will appropriately limit the temperature rise in these tissues are not well-defined; there is, in addition, little information available at present to justify a First Level Controlled Operating Mode standards.

The rise in temperature in any object that occurs in response to the intermittent absorption of radio frequency energy from, e.g. a pulsed radio frequency source can be equated with the SAR value averaged over the 50% thermal equilibrium time, the time taken for the temperature increase at the center of a heated region to rise by 50% of the maximum value after the application of a heat source. The thermal equilibrium time for the body is not known accurately, but can be estimated as around 15 min to 30 min, whereas smaller masses of tissues, such as the eye, have a thermal equilibrium time of about 5 min.

The control of whole-body SAR alone in the case of body-coil imaging, as prescribed by requirement 51.103 d) 1) offers a simplification of the provisions for control of the SAR in Magnetic Resonance systems. The simplification enables the safe use of a relatively large amount of radio frequency power for this type of operation. The restriction of this simplified operation to cases where the transmit coil is of sufficient size and homogeneity (as can be assumed to be the case for body coils) is chosen in order to limit the ratio between whole-body average SAR on the one hand and head SAR or local tissue SAR on the other. A similar line of argument has been used in requirement 51.103 d) 2), where the control of the system of the head SAR alone is permitted in cases where a head coil is used as the transmit coil.

## APPENDIX B FDA GUIDANCE

### Guidance For Magnetic Resonance Diagnostic Devices - Criteria For Significant Risk Investigations

This document is intended to provide guidance in the preparation of a regulatory submission. It does not bind the FDA or the regulated industry in any manner.

Computed Imaging Devices Branch  
Division of Reproductive, Abdominal,  
Ear, Nose, Throat and Radiological Devices  
Office of Device Evaluation

Document Issued on September 29, 1997

While this guidance document represents a final document, comments and suggestions may be submitted at any time for Agency consideration by writing Robert A. Phillips, Ph.D., Chief, Computed Imaging Devices Branch, Center for Devices and Radiological Health, HFZ-470, 9200 Corporate Blvd., Rockville, MD 20850. For questions regarding the use or interpretation of this guidance, contact Loren A. Zaremba, Ph.D., at 301-594-1212.

U.S. Department of Health and Human Services  
Food and Drug Administration  
Center for Devices and Radiological Health

---

### Magnetic Resonance Diagnostic Devices

### Criteria for Significant Risk Investigations

Patient studies utilizing magnetic resonance diagnostic devices which are conducted under any one of the following operating conditions are considered significant risk investigations, and require approval of an



investigational device exemption (IDE) by the Food and Drug Administration (FDA) Center for Devices and Radiological Health (CDRH):

1. Main static magnetic field greater than 4 tesla;
2. Specific absorption rate (SAR) greater than
  - a. 4 W/kg averaged over the whole body for any period of 15 minutes;  
or
  - b. 3 W/kg averaged over the head for any period of 10 minutes; or
  - c. 8 W/kg in any gram of tissue in the head or torso, or 12 W/kg in any gram of tissue in the extremities, for any period of 5 minutes;
3. Time rate of change of gradient fields (dB/dt) sufficient to produce severe discomfort or painful nerve stimulation; or
4. Peak unweighted sound pressure level greater than 140 dB or A-weighted r.m.s. sound pressure level greater than 99 dBA with hearing protection in place.

These criteria apply only to device operating conditions. Other aspects of the study may involve significant risks and the study may therefore require IDE approval.

## APPENDIX C

### PHANTOM PROTOCOL - THERMOCOUPLE

Protocol: PHANTOM

#### PATIENT POSITION

Patient Entry: Head First  
 Patient Position: Supine  
 Axial/Sag Landmark:  
 Coil Type: Head  
 Scan Plane: Axial

#### IMAGING PARAMETERS

Image Mode: 2D  
 Pulse Sequence: Spin Echo  
 Imaging Option: None  
 Enter PSD Filename:

#### SCAN TIMING

Number of Echoes: 1  
 TE: 17  
 TE2: 153  
 Rep Time (TR): 500

#### SCAN SET-UP

Prescan Options:  
     Autoshim  
 Auto CF: Water  
 Receive bandwidth (+/-) 16.00  
     kHz

#### SCANNING RANGE

Field of View: 24 cm  
 Scan Thickness: 5.0 mm  
 Interscan Spacing: 1.5 mm  
 Start Location: (I/S) I35  
 End Location: (I/S) S36.5  
 No. Of Scan Locations: 12  
 FOV Center:  
     (L/R): 0  
     (P/A): 0

#### ACQUISITION TIME

Acq Matrix: freq 256  
 Ac1 Matrix: phase 128  
 Frequency Direction: A/P  
 Phase FOV: 24 cm  
 Imaging Time: 30 NEX  
     48:25  
 Contrast: No

## APPENDIX D

### PHANTOM PROTOCOL - FIBER OPTIC

Protocol 45: GEORGE HARDER TEST

2. Series: Head,Axial,2D,Spin Echo,None

Scan 1: HEAD,Axial,2D,Spin Echo, memp,None

#### PATIENT POSITION

Patient Entry: Head First  
 Patient Position: Supine  
 Axial/Sag Landmark:  
 Coil Type: Head  
 Scan Plane: Axial

#### SCANNING RANGE

Field of View: 24 cm  
 Scan Thickness: 5.0 mm  
 Interscan Spacing: 1.5 mm  
 Start Location: (I/S) I22.5  
 End Location: (I/S) S22.5  
 No. Of Scan Locations: 8  
 FOV Center:

#### IMAGING PARAMETERS

Image Mode: 2D  
 Pulse Sequence: spin Echo  
 Imaging Option: None  
 Enter PSD Filename:

(L/R): 0  
 (P/A): 0

#### SCAN TIMING

Number of Echoes: 1  
 TE: 30  
 Rep Time (TR): 500

#### ACQUISITION TIME

Acq Matrix: freq 256  
 Ac1 Matrix: phase 128  
 Phase FOV: 24 cm  
 Frequency Direction: A/P  
 Imaging Time: 1 NEX 1:12  
 Contrast: No

#### SCAN SET-UP

Prescan Options:

Auto CF: Autoshim  
 Water  
 Receive bandwidth (+/-)  
 16.00 kHz

## APPENDIX E

### HEAT STRESS INDEX

The focus of this dissertation was to derive a dosimetry method applicable to the human head and the phantom head. One method of dosimetry researched that was applicable only to the human head was Heat Stress Index (HSI). Industrial Hygienists utilize a HSI to monitor a worker's condition. Since the results of RF energy deposition was similar to that of energy deposition resulting from work, a HSI was originally considered as an option for RF dosimetry. This method would provide a qualitative dose reference relying on an individual's own metabolism. Physiological parameters such as heart rate, breathing rate, temperature and perspiration would be the indicators to determine an individual's dose limits. Originally this method seemed plausible, however, reliability would be difficult to ensure for all patients. This appendix is included to provide information about heat stress indicators and demonstrate the reasoning behind their unusability.

The body's temperature-regulating center lies in the hypothalamus. The anterior portion of the hypothalamus responds to its own increase in temperature and to nerve impulses from receptors in the skin. The hypothalamus contains a group of neurons in the anterior portion referred to as the preoptic area. Increased blood temperature increases the rate of neuron impulses while decreased blood

temperature decreases the rate of neuron impulses (Tortora 1981). The blood circulates and temperatures can fluctuate between 35.5 °C to 40 °C with it remaining mostly at 37 °C. During MRI, as RF energy heats local tissue, neuron impulses increase. The hypothalamus responds by triggering increased blood flow to transport heat to the skin and then trigger sweating if needed. The heat transported to the skin and any energy deposition in the skin can be released to the environment through conduction, convection, radiation and evaporation of sweat (Adair 1992).

The most common indicators of heat stress used by Industrial Hygienists are sweat rate, skin temperature, heart rate and core temperature (Patty's 1978). Sweat rate can be an indicator over the entire range of heat stress. Its rise parallels a core temperature rise and an increase in heart rate. Sweat rates are not instantaneous but are a time-weighted average of heat stress. The rate of evaporation is the difference between the vapor pressure of the wetted skin and the partial pressure of water vapor in the ambient air. The vapor pressure of the wetted skin can also be affected by the skin temperature. Increased skin temperature increases vapor pressure and encourages evaporation. The endothermic action of evaporation then reduces skin temperatures. The body's first and most prevalent response in maintaining a thermal balance without a rise in core temperature was to increase the heart rate. This increased blood flow channels more blood past heated tissue and transports the heat to the body surface.



Heart rate has the dual function of responding to increased work of muscles to re-oxygenate them and to remove heat.

During a MRI of the head, there are two areas of concern. First, increased heating to the head may excite the hypothalamus thereby signaling the body to respond to a heat stress that may not be present throughout the entire body. An increase in heart rate could generate an unnecessary increase of heat loss (Polk 1986). Second, RF signals may be of such a frequency and/or intensity as to generate or suppress neuron impulses. This may also affect the hypothalamus into misinterpreting signals. Gradient magnetic fields are known to generate false impulses in the optic nerve manifesting in magnetophosphenes. However, there was no information addressing whether RF signals can generate or suppress the neuron impulses to the hypothalamus.

The HSI combines the heat-exchange components of radiation and convection with the metabolic heat generation of the body. The resultant expression was a function of stress in terms of the required sweat evaporation. The physiological strain of an individual can then be expressed as a percentage of the required sweat evaporation to the maximum evaporation possible by an individual. Stated algebraically:

$$HSI = 100 \left( \frac{\text{metabolic heat} \pm \text{radiation} \pm \text{convection}}{\text{maximum evaporation}} \right)$$

A HSI greater than 100 indicates the body stores heat and a HSI less than 100 indicates the body loses heat.

### Convection

Convection was a function of the difference in temperature between the skin and the surrounding air with an additional effect from the movement of air over the skin surface.

$$C = 1.0 V^{0.6} (T_A - T_S)$$

where  $C$  = convection (kcal/hr)

$V$  = air speed (m/min)

$T_A$  = air temperature ( $^{\circ}\text{C}$ )

$T_S$  = skin surface temperature ( $^{\circ}\text{C}$ )

Convection increased when the air temperature ( $T_A$ ) was greater than the skin surface temperature ( $T_S$ ) and the individual stores heat. The exponent, 0.6, applies to forced convection over vertical cylinders which was empirically derived from a simplistic geometric configuration of a man. The coefficient 1.0 was a function of the surface area for an "average" man ( $1.8 \text{ m}^2$ ). A non-average

individual would adjust this coefficient as a ratio of their estimated skin area to 1.8 m<sup>2</sup>. An exact estimate was not required.

### Radiation

Radiation was a function of the difference in temperature between the skin and the mean radiant temperature (MRT) of the solid in contact with the skin. Tests have shown that radiative heat exchange was a function of the fourth power of absolute temperature (Patty's 1978). Within the small temperature range of the equipment that a patient would be in contact with during an MRI a first-order approximation was sufficiently accurate for estimating radiation.

$$R = 11.3 (MRT - TS)$$

where R = radiation (kcal/hr)

MRT = mean radiant temperature of the solid surroundings (°C)

TS = skin surface temperature (°C)

The coefficient 11.3 was an empirically derived value. From just radiation and convection, the body loses heat wherever air touches the skin and a cooler item touches the skin. Radiation was reduced when the patient was placed on a cushion. The thermal properties of the cushion insulate the body. Additionally,

since the MRI chamber was kept cool, the patient may also be provided a blanket. This prevents convection and, after the inside of the blanket has reached equilibrium with the skin temperature, also prevents radiation. The body's natural heat loss avenues are now restricted to evaporation.

### Evaporation

Evaporation was a function of the difference between the vapor pressure of perspiration on the skin (vapor pressure of water at skin temperature) and the partial pressure of water in the surrounding air. There was an additional effect of air speed over the skin which can reduce the partial pressure of water in the immediate air and increase evaporation. Evaporative heat loss in humid environments was reduced as the capacity of the ambient air to accept additional moisture decreases. In a MRI chamber, humidity was kept low thereby increasing the difference in the vapor pressure of perspiration and the partial pressure of water.

$$E_{\max} = 2 V^{0.6} (VPS - PPA)$$

where  $E_{\max}$  = maximum evaporative capacity (kcal/he)

$V$  = air speed (m/min)

$VPS$  = vapor pressure of water on the skin (mm Hg)

PPA = partial pressure of water in air (mm Hg)

In dryer environments, such as the MRI chamber, the maximum heat exchange from evaporation becomes limited by the amount of perspiration that can be produced by the individual. Maximum sweating was slightly above one liter per hour which was equivalent to an evaporative heat loss of 580 kcal/hr. A MRI patient will not reach this limit since a large portion of skin area was in contact with the cloths and the carriage. These pores are unable to remove heat from the body.

Example information concerning heat loss from patients was not available, but information was available from laborers. For a laborer and under favorable conditions, 25 percent of metabolic heat was lost through convection to cooler air, 50 percent by radiation to cooler surfaces and 25 percent by evaporation. In comparison, a patient undergoing an MRI has a larger portion of their body in contact with the carriage which would account for a large percentage of heat loss through radiation. If the patient were on a cushion there would be a reduced heat loss through radiation. Additionally, the MRI area maintains a relative humidity below 60% which becomes favorable for heat transfer to the environment through convection. As long as the patient has the ability to sweat, heat transfer away from a patient undergoing an MRI examination would be accounted for by a higher heat loss from evaporation.



Body temperatures range from 35.5 to 40 °C and are the result of circadian variation, vigorous exercise, variations in ambient temperature, sequelae of food intake, age factors, cyclical variation in females and emotional factors. In the steady state the body obeys the first law of thermodynamics where the heat produced in the body was balanced by the heat lost to the environment.

Quantitatively, up to 25 kcal/hr of energy deposition may not be noticed by an individual. For reference, greater than 80 kcal/hr represents the usual upper limit from exercise and work. At double this value (160 kcal/hr) there was a 50% risk of collapse and triple this value (240 kcal/hr) becomes intolerable. Evaporation of water can remove 0.58 kcal per gram. The body's maximum sweat rate was approximately 1 liter per hour or 580 kcal per hour. The SAR limit for RF exposure to the head is currently at 3.2 W/kg. This equates to 13.4 kcal/hr. This was below the 25 kcal/hr threshold for an individual to notice the heat, however, the heat may be deposited in a small region such as the vitreous humor.

Measurement of skin temperature, heart rate and core temperature in high magnetic fields was possible. However using HSI for dosimetry would be difficult. A baseline of responses to the deposition of RF energy and subsequent increases in thermal loads would need to be established for each patient. Each individual responds differently as a function of their age and conditioning. Establishing one universal baseline to apply to all patients would vary as a function of the following variables:

1. As heat was deposited within the body, blood flow increases to transport the heat to the skin. This response was a function of an individual's cardiovascular fitness and was unique to each individual. It was this uniqueness that makes developing a uniform standard using heart rate for identifying heat stress difficult. A given heart rate signifies approximately the same level of strain regardless of the degree of an individual's fitness, but a person with high cardiovascular fitness will achieve a given heart rate at a higher level of thermal stress than an unfit person. A corollary to cardiovascular fitness was the effect an illness imposes. An illness weakens autonomic functions. This would prevent developing a baseline thermal stress indicator for an individual and using it for subsequent MRI sessions.
2. Another variable of heat tolerance was obesity. Obese or stocky individuals have a lower surface area to weight ratio. An individual can become acclimatized over time, but in general obese individuals are at a greater risk of succumbing to heat strain. This factor was slightly mitigated by the bore size of the MRI unit. Some obese or stocky individuals are physically limited from access to higher field MRI units.
3. An older individual was at a distinct disadvantage compared with younger individuals. An older individual compensates for increased heat less effectively than do younger individuals, as indicated by higher core temperature and peripheral blood flow. This occurs because there was a delay in the onset of

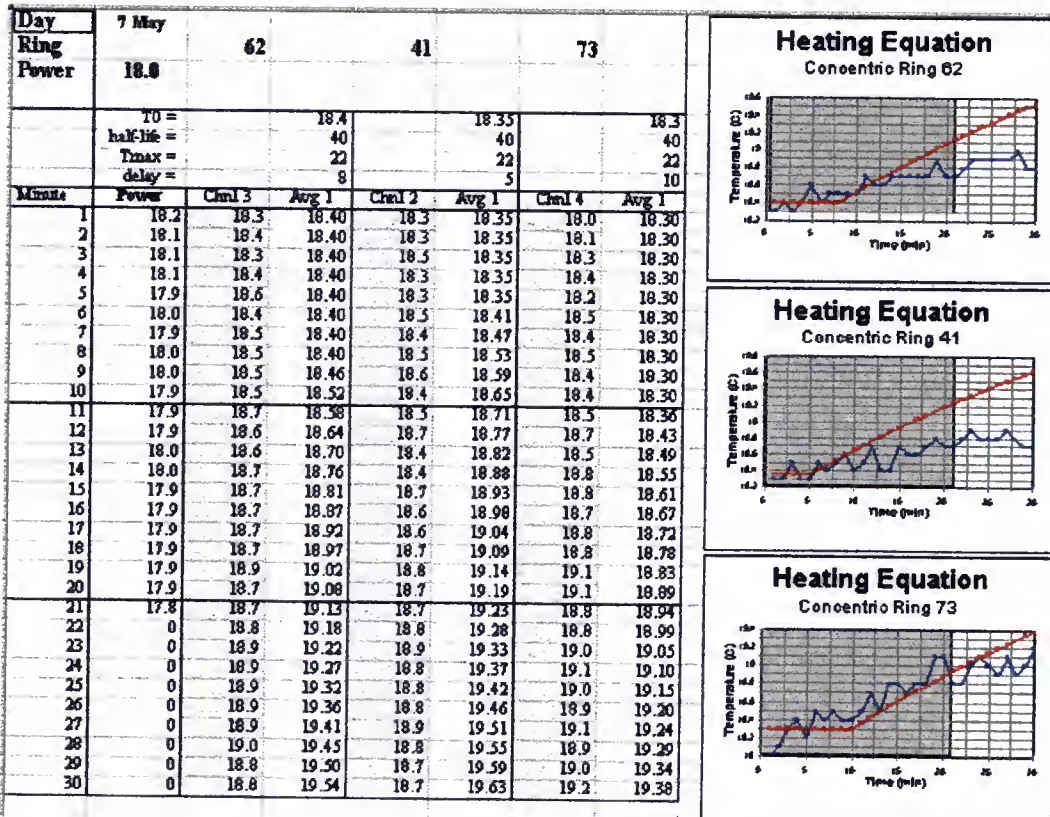
sweating and a lower sweat rate capacity in older individuals resulting in greater heat storage and longer time for heat recovery. Biological effects and hazards are a function of the dose rate and not the total dose. Delays in reacting to a thermal insult would cause the most damage. Acute increases in core temperatures would not trigger heat stress indicators to provide sufficient warnings of danger. Again, illnesses would further alter any established baseline responses.

4. Drugs can adversely affect a patient's tolerance from thermal insults. Dogs have displayed a greater susceptibility to microwave heating after administration of pentobarbital sodium, morphine sulfate or chlorpromazine, indicating that mechanisms of heat loss may be compromised by treatment with certain drugs (Polk 1986). RF exposure produced greater increases in core temperature than occurred in untreated control animals indicating an interference with the body's natural tendency to reduce excess heat. The variety of medications administered to individuals would need to be tested in order to determine their effect on thermoregulation. Again, individual responses to medications would make this difficult.

While the concept of a heat stress index as a MRI dosimeter appears feasible, the practical application makes its effectiveness tentative (Shellock 1992). Without extensive testing on each individual to determine their response to thermal stress, quantifying the amount of energy deposition would not be possible. However, monitoring heart rate and skin temperature could be used to ensure

patients remain comfortable and are not in the early stages of thermal stress. This would become valid at the higher field strength magnets where more energy deposition was expected. While a better, more quantitative method of SAR was required, HSI would still provide a good secondary indicator.

# APPENDIX F EXPERIMENTAL RESULTS

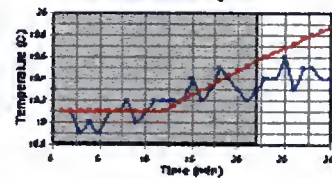




Day	8 May						
Ring		74		40		91	
Power	18.9227						
	T0 =	19.1		19		18.9	
	Half-life =	40		40		40	
	Tmax =	22		22		22	
	delay =	12		6		7	
Minute	Power	Chnl 3	Avg 1	Chnl 2	Avg 1	Chnl 4	Avg 1
1	19.2	19.1	19.10	19.0	19.00	18.9	18.90
2	19.1	19.1	19.10	19.0	19.00	18.9	18.90
3	19.0	18.9	19.10	18.8	19.00	18.8	18.90
4	19.1	19.0	19.10	19.0	19.00	18.9	18.90
5	19.0	18.9	19.10	19.0	19.00	18.9	18.90
6	18.9	19.1	19.10	19.1	19.00	18.8	18.90
7	18.9	19.1	19.10	19.1	19.05	19.0	18.90
8	18.8	19.2	19.10	19.2	19.10	19.1	18.95
9	18.9	19.0	19.10	19.1	19.15	19.0	19.01
10	18.8	19.1	19.10	19.2	19.20	19.1	19.06
11	18.9	19.2	19.10	19.2	19.25	19.2	19.11
12	18.9	19.2	19.10	19.2	19.30	19.1	19.16
13	19.0	19.2	19.15	19.2	19.34	19.3	19.21
14	19.0	19.2	19.20	19.3	19.39	19.2	19.25
15	18.9	19.4	19.25	19.2	19.43	19.4	19.30
16	18.9	19.2	19.29	19.4	19.48	19.6	19.35
17	18.8	19.3	19.34	19.3	19.52	19.3	19.39
18	18.8	19.5	19.39	19.4	19.56	19.4	19.44
19	18.9	19.4	19.43	19.4	19.60	19.3	19.48
20	18.8	19.3	19.48	19.2	19.65	19.4	19.53
21	18.8	19.2	19.52	19.1	19.69	19.4	19.57
22	18.9	19.3	19.56	19.4	19.73	19.5	19.61
23	0	19.4	19.60	19.4	19.77	19.3	19.65
24	0	19.4	19.64	19.5	19.80	19.6	19.69
25	0	19.6	19.68	19.5	19.84	19.6	19.73
26	0	19.3	19.72	19.5	19.88	19.4	19.77
27	0	19.5	19.76	19.3	19.91	19.4	19.81
28	0	19.5	19.80	19.5	19.95	19.6	19.85
29	0	19.4	19.84	19.4	19.99	19.5	19.88
30	0	19.4	19.88	19.4	20.02	19.6	19.92

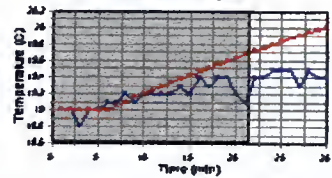
### Heating Equation

Concentric Ring 74



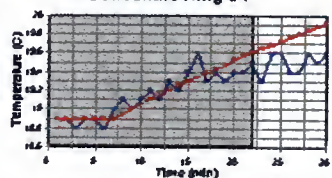
### Heating Equation

Concentric Ring 40



### Heating Equation

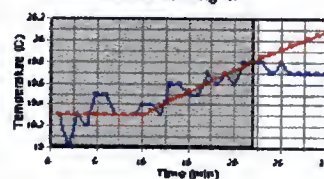
Concentric Ring 01



Day	9 May	47	38	57			
Ring							
Power	18.0						
	10 =	19.3	19.2	18.6			
	half life =	40	40	40			
	Tmax =	22	22	22			
	delay =	10	8	0			
Minute	Power	Chnl 3	Avg 1	Chnl 2	Avg 1	Chnl 4	Avg 1
1	18.4	19.3	19.30	19.2	19.20	18.8	18.66
2	18.3	19.0	19.30	19.0	19.20	18.7	18.72
3	18.2	19.3	19.30	19.2	19.20	18.9	18.77
4	18.2	19.2	19.30	19.2	19.20	19.1	18.83
5	18.0	19.5	19.30	19.3	19.20	19.0	18.88
6	17.9	19.5	19.30	19.3	19.20	19.1	18.94
7	18.0	19.3	19.30	19.2	19.20	19.1	18.99
8	18.0	19.3	19.30	19.2	19.20	19.2	19.04
9	18.0	19.3	19.30	19.3	19.25	19.2	19.09
10	18.1	19.4	19.30	19.2	19.30	19.2	19.14
11	18.0	19.4	19.35	19.4	19.34	18.9	19.19
12	17.9	19.3	19.39	19.3	19.39	19.3	19.24
13	18.0	19.6	19.44	19.4	19.43	19.3	19.29
14	18.0	19.6	19.48	19.4	19.48	19.4	19.33
15	18.0	19.5	19.52	19.5	19.52	19.3	19.38
16	17.9	19.5	19.57	19.5	19.56	19.5	19.42
17	17.9	19.7	19.61	19.6	19.60	19.5	19.47
18	17.9	19.6	19.65	19.4	19.65	19.3	19.51
19	18.0	19.7	19.69	19.5	19.69	19.4	19.55
20	18.0	19.6	19.73	19.3	19.73	19.5	19.60
21	17.9	19.8	19.77	19.5	19.76	19.5	19.64
22	17.9	19.8	19.81	19.6	19.80	19.6	19.68
23	0	19.8	19.84	19.6	19.84	19.7	19.72
24	0	19.7	19.88	19.7	19.88	19.7	19.76
25	0	19.8	19.92	19.5	19.91	19.6	19.80
26	0	19.7	19.95	19.6	19.95	19.5	19.83
27	0	19.7	19.99	19.7	19.99	19.6	19.87
28	0	19.7	20.02	19.5	20.02	19.4	19.91
29	0	19.7	20.06	19.7	20.05	19.7	19.94
30	0	19.7	20.09	19.7	20.09	19.6	19.98

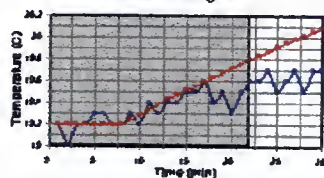
### Heating Equation

Concentric Ring 47



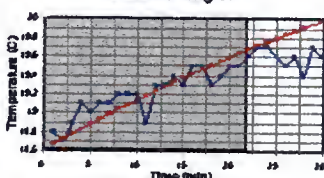
### Heating Equation

Concentric Ring 38



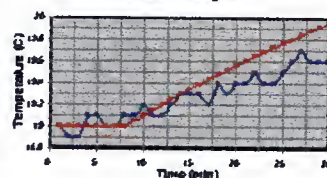
### Heating Equation

Concentric Ring 57

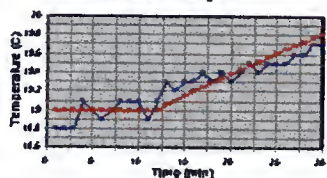


Day Ring Power	10 May	46	30	64			
	16.8483						
	T0 =	19	19	19			
	half-life =	40	40	40			
	Tmax =	22	22	22			
	delay =	8	12	12			
Minute	Power	Chnl 3	Avg 1	Chnl 2	Avg 1	Chnl 4	Avg 1
1	0	19.0	19.00	18.8	19.00	18.8	19.00
2	17.2	18.9	19.00	18.8	19.00	19.0	19.00
3	17.1	18.9	19.00	18.8	19.00	18.9	19.00
4	16.9	19.1	19.00	19.1	19.00	19.0	19.00
5	16.8	19.1	19.00	19.0	19.00	19.0	19.00
6	16.8	19.0	19.00	18.9	19.00	19.0	19.00
7	16.9	19.0	19.00	19.0	19.00	19.1	19.00
8	16.9	19.1	19.00	19.1	19.00	19.2	19.00
9	16.8	19.1	19.05	19.1	19.00	19.1	19.00
10	16.8	19.2	19.10	19.1	19.00	19.1	19.00
11	16.9	19.1	19.15	18.9	19.00	19.2	19.00
12	16.9	19.1	19.20	19.1	19.00	19.1	19.00
13	16.8	19.2	19.25	19.3	19.05	19.4	19.05
14	16.8	19.3	19.30	19.2	19.10	19.4	19.10
15	16.8	19.3	19.34	19.3	19.15	19.3	19.15
16	16.9	19.3	19.39	19.3	19.20	19.5	19.20
17	16.9	19.2	19.43	19.4	19.25	19.5	19.25
18	16.9	19.4	19.48	19.3	19.30	19.5	19.30
19	16.8	19.3	19.52	19.4	19.34	19.5	19.34
20	16.7	19.4	19.56	19.3	19.39	19.5	19.39
21	16.9	19.4	19.60	19.4	19.43	19.7	19.43
22	16.7	19.5	19.65	19.5	19.48	19.7	19.48
23	16.8	19.4	19.69	19.4	19.52	19.5	19.52
24	16.8	19.4	19.73	19.5	19.56	19.6	19.56
25	16.8	19.5	19.77	19.5	19.60	19.7	19.60
26	16.7	19.6	19.80	19.5	19.65	19.9	19.65
27	16.8	19.7	19.84	19.6	19.69	19.8	19.69
28	16.8	19.6	19.88	19.6	19.73	19.8	19.73
29	16.8	19.6	19.91	19.7	19.77	19.8	19.77
30	16.9	19.6	19.95	19.7	19.80	19.8	19.80

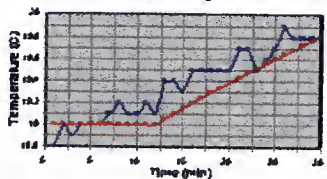
**Heating Equation**  
Concentric Ring 46



**Heating Equation**  
Concentric Ring 30



**Heating Equation**  
Concentric Ring 64

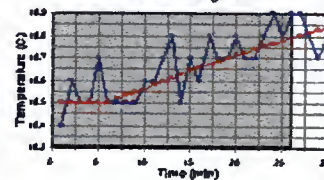




Day Ring Power	12 May 17.3	28	51	53			
	T0 =	18.5	18.6	18.7			
	half life =	40	40	40			
	Tmax =	19.5	22	21			
	delay =	6	10	0			
Minute	Power	Chn2	Avg 1	Chn3	Avg 1	Chn4	Avg 1
1	17.5	18.4	18.50	18.6	18.60	18.7	18.74
2	17.5	18.6	18.50	18.5	18.60	18.7	18.78
3	17.299999	18.5	18.50	18.5	18.60	18.8	18.82
4	17.299999	18.5	18.50	18.6	18.60	18.9	18.85
5	17.299999	18.7	18.50	18.6	18.60	18.9	18.89
6	17.299999	18.5	18.50	18.6	18.60	18.9	18.93
7	17.299999	18.5	18.52	18.6	18.60	19.0	18.96
8	17.200001	18.5	18.53	18.8	18.60	19.1	19.00
9	17.299999	18.5	18.55	18.6	18.60	19.0	19.03
10	17.299999	18.6	18.57	18.8	18.60	19.0	19.07
11	17.299999	18.6	18.58	18.7	18.66	19.2	19.10
12	17.299999	18.7	18.60	18.8	18.72	19.3	19.13
13	17.299999	18.8	18.61	18.9	18.77	19.2	19.16
14	17.4	18.5	18.63	18.6	18.83	19.1	19.20
15	17.299999	18.7	18.64	18.8	18.88	19.2	19.23
16	17.299999	18.6	18.66	18.8	18.94	19.3	19.26
17	17.299999	18.8	18.67	18.9	18.99	19.3	19.29
18	17.200001	18.7	18.69	18.9	19.04	19.3	19.32
19	17.299999	18.7	18.70	19.0	19.09	19.3	19.35
20	17.200001	18.8	18.72	19.0	19.14	19.3	19.37
21	17.299999	18.7	18.73	19.0	19.19	19.7	19.40
22	17.200001	18.7	18.74	19.0	19.24	19.5	19.43
23	17.299999	18.8	18.76	19.1	19.29	19.5	19.46
24	17.299999	18.9	18.77	19.0	19.33	19.6	19.48
25	17.200001	18.8	18.78	19.1	19.38	19.6	19.51
26	17.299999	18.9	18.79	19.0	19.42	19.7	19.53
27	0	18.9	18.80	19.2	19.47	19.7	19.56
28	0	18.8	18.82	19.1	19.51	19.7	19.58
29	0	18.7	18.83	19.1	19.55	19.6	19.61
30	0	18.8	18.84	19.0	19.60	19.7	19.63

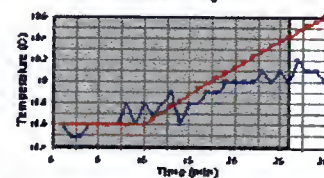
### Heating Equation

Concentric Ring 28



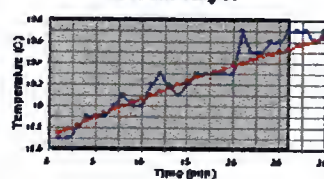
### Heating Equation

Concentric Ring 51



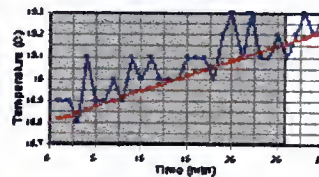
### Heating Equation

Concentric Ring 53

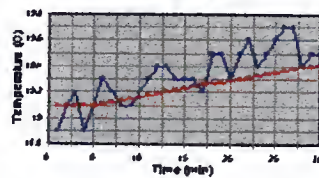


Day	13 May	25	43	42			
Ring							
Power	10.10333						
	T0 =	18.8	19.1	19.3			
	half-life =	150	150	150			
	Tmax =	22	22	22			
	delay =	0	5	5			
Minute	Power	Chnl2	Avg 1	Chnl3	Avg 1	Chnl4	Avg 1
1	10.3	18.9	18.81	18.9	19.10	19.2	19.30
2	10.3	18.9	18.83	19.1	19.10	19.4	19.30
3	10.2	18.8	18.84	19.2	19.10	19.4	19.30
4	10.1	19.1	18.86	18.9	19.10	19.3	19.30
5	10.2	18.9	18.87	19.1	19.10	19.3	19.30
6	10.1	18.9	18.89	19.3	19.11	19.4	19.31
7	10.1	19.0	18.90	19.2	19.13	19.6	19.32
8	10.2	18.9	18.92	19.1	19.14	19.5	19.34
9	10.2	19.1	18.93	19.1	19.15	19.5	19.35
10	10.1	19.0	18.94	19.2	19.17	19.6	19.36
11	10.1	19.1	18.96	19.3	19.18	19.6	19.37
12	10.2	19.0	18.97	19.4	19.19	19.7	19.39
13	10.2	19.0	18.99	19.4	19.21	19.8	19.40
14	10.2	19.0	19.00	19.3	19.22	19.7	19.41
15	10.1	19.1	19.01	19.3	19.23	19.5	19.42
16	10.2	19.1	19.03	19.3	19.24	19.8	19.43
17	10.2	19.1	19.04	19.2	19.26	19.8	19.45
18	10.2	19.0	19.06	19.5	19.27	19.8	19.46
19	10.2	19.2	19.07	19.5	19.28	19.9	19.47
20	10.2	19.3	19.08	19.3	19.29	19.7	19.48
21	10.2	19.1	19.10	19.5	19.31	19.8	19.49
22	10.2	19.3	19.11	19.6	19.32	20.0	19.50
23	10.2	19.1	19.12	19.4	19.33	19.9	19.52
24	10.2	19.1	19.14	19.5	19.34	20.0	19.53
25	10.2	19.2	19.15	19.6	19.36	19.9	19.54
26	10.2	19.1	19.16	19.7	19.37	20.0	19.55
27	10.2	19.2	19.18	19.7	19.38	19.9	19.56
28	10.2	19.3	19.19	19.4	19.39	19.9	19.57
29	10.1	19.2	19.20	19.5	19.40	19.9	19.58
30	10.2	19.3	19.21	19.5	19.42	19.9	19.59

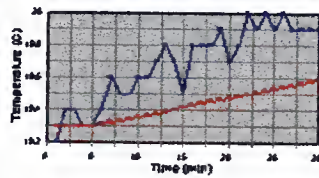
**Heating Equation**  
Concentric Ring 25



**Heating Equation**  
Concentric Ring 43



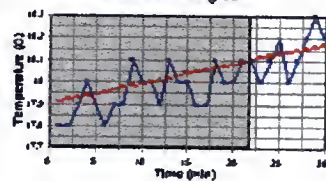
**Heating Equation**  
Concentric Ring 42



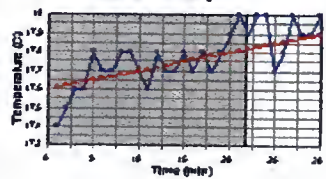


Day	16 May						
Ring		30		24	8		
Power	6.2						
	T0 =	17.9		17.6	17.3		
	half-life =	300		300	300		
	Tmax =	22		22	22		
	delay =	0		0	0		
Mikans	Power	Chnl2	Aug 1	Chnl3	Aug 1	Chnl4	Aug 1
1	6.3	17.8	17.91	17.4	17.61	17.2	17.31
2	6.4	17.8	17.92	17.5	17.62	17.3	17.32
3	6.2	17.9	17.93	17.6	17.63	17.3	17.33
4	6.2	18.0	17.94	17.6	17.64	17.3	17.34
5	6.2	17.9	17.95	17.8	17.65	17.4	17.35
6	6.0	17.8	17.96	17.7	17.66	17.4	17.36
7	6.1	17.9	17.97	17.7	17.67	17.4	17.38
8	6.1	17.9	17.98	17.8	17.68	17.4	17.39
9	6.1	18.1	17.98	17.8	17.69	17.4	17.40
10	6.2	18.0	17.99	17.7	17.70	17.5	17.41
11	6.2	18.0	18.00	17.6	17.71	17.5	17.42
12	6.1	17.9	18.01	17.8	17.72	17.6	17.43
13	6.0	18.1	18.02	17.7	17.73	17.5	17.44
14	6.2	18.0	18.03	17.7	17.74	17.5	17.45
15	6.2	18.0	18.04	17.8	17.75	17.6	17.46
16	6.0	17.9	18.05	17.7	17.76	17.5	17.47
17	6.3	17.9	18.06	17.8	17.77	17.6	17.48
18	6.1	18.1	18.07	17.7	17.78	17.5	17.49
19	6.3	18.0	18.08	17.8	17.79	17.5	17.50
20	6.1	18.0	18.09	17.9	17.80	17.5	17.51
21	6.1	18.1	18.09	18.0	17.81	17.7	17.52
22	6.1	18.1	18.10	17.9	17.82	17.5	17.53
23	0	18.0	18.11	18.0	17.83	17.5	17.54
24	0	18.1	18.12	18.0	17.84	17.6	17.55
25	0	18.2	18.13	17.7	17.85	17.6	17.56
26	0	18.0	18.14	17.8	17.86	17.6	17.57
27	0	18.1	18.15	18.0	17.87	17.7	17.58
28	0	18.2	18.16	17.9	17.88	17.6	17.59
29	0	18.3	18.17	17.9	17.89	17.5	17.60
30	0	18.2	18.17	18.0	17.89	17.6	17.61

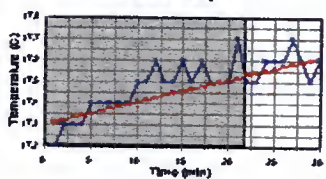
**Heating Equation**  
Concentric Ring 30



**Heating Equation**  
Concentric Ring 24

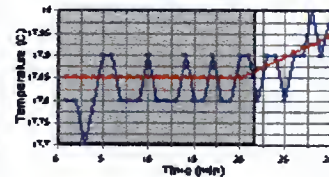


**Heating Equation**  
Concentric Ring 8

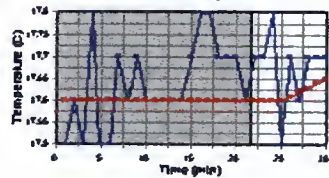


Day	17 May						
Ring		25		66		80	
Power	5.6						
			17.85		17.6		17.55
			300		300		300
			22		22		22
			20		25		20
Minute	Power	Chnl2	Avg 1	Chnl3	Avg 1	Chnl4	Avg 1
1	5.7	17.8	17.85	17.5	17.60	17.3	17.55
2	5.7	17.8	17.85	17.6	17.60	17.3	17.55
3	5.8	17.7	17.85	17.5	17.60	17.3	17.55
4	5.5	17.8	17.85	17.8	17.60	17.4	17.55
5	5.5	17.9	17.85	17.5	17.60	17.6	17.55
6	5.5	17.9	17.85	17.5	17.60	17.2	17.55
7	5.7	17.8	17.85	17.7	17.60	17.6	17.55
8	5.7	17.8	17.85	17.6	17.60	17.5	17.55
9	5.6	17.8	17.85	17.7	17.60	17.5	17.55
10	5.6	17.9	17.85	17.6	17.60	17.5	17.55
11	5.7	17.8	17.85	17.6	17.60	17.6	17.55
12	5.6	17.8	17.85	17.6	17.60	17.5	17.55
13	5.7	17.8	17.85	17.6	17.60	17.5	17.55
14	5.4	17.9	17.85	17.6	17.60	17.5	17.55
15	5.6	17.8	17.85	17.7	17.60	17.6	17.55
16	5.6	17.8	17.85	17.8	17.60	17.4	17.55
17	5.7	17.9	17.85	17.8	17.60	17.5	17.55
18	5.5	17.8	17.85	17.7	17.60	17.6	17.55
19	5.5	17.8	17.85	17.7	17.60	17.6	17.55
20	5.5	17.9	17.85	17.7	17.60	17.7	17.55
21	5.5	17.9	17.86	17.6	17.60	17.7	17.56
22	5.5	17.8	17.87	17.7	17.60	17.6	17.57
23	0	17.9	17.88	17.7	17.60	17.5	17.58
24		17.9	17.89	17.8	17.60	17.7	17.59
25		17.8	17.90	17.5	17.60	17.6	17.60
26		17.9	17.91	17.7	17.61	17.7	17.61
27		17.9	17.92	17.6	17.62	17.6	17.62
28		18.0	17.93	17.7	17.63	17.8	17.63
29		17.9	17.94	17.7	17.64	17.6	17.64
30		18.0	17.94	17.7	17.65	17.8	17.65

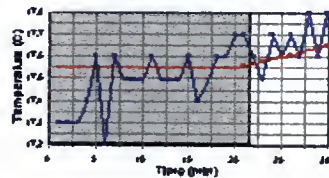
**Heating Equation**  
Concentric Ring 25

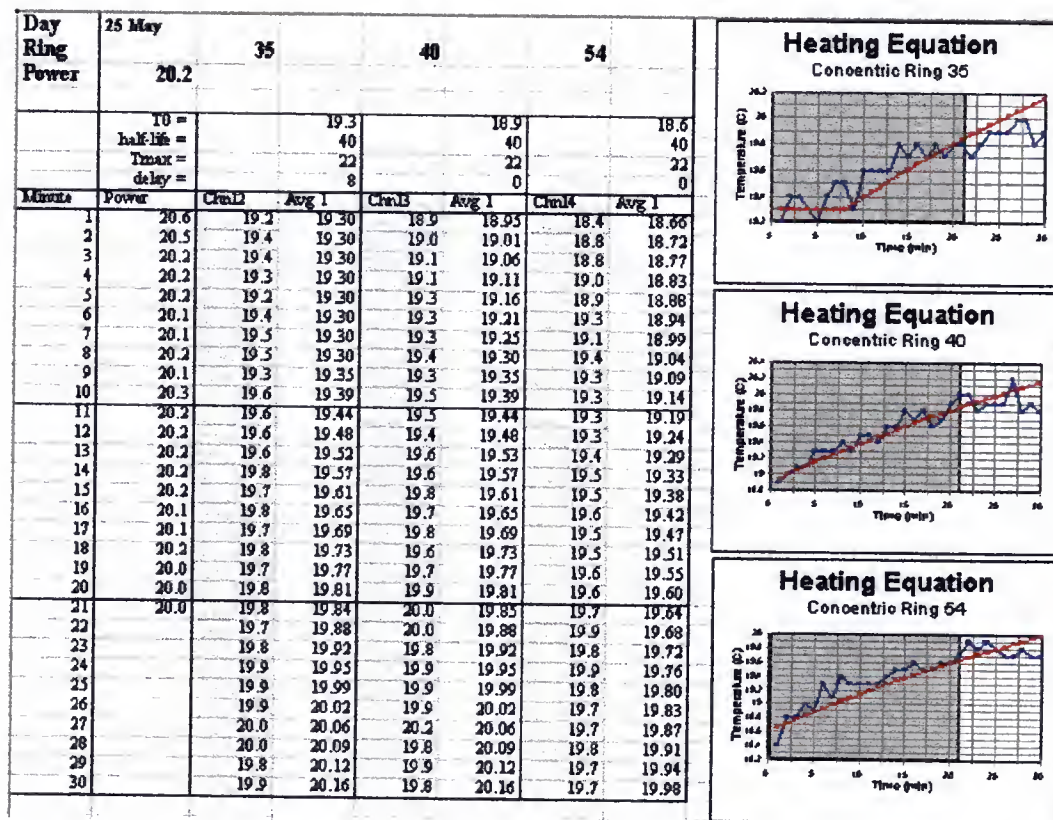


**Heating Equation**  
Concentric Ring 66



**Heating Equation**  
Concentric Ring 80





## APPENDIX G ARTIFACT TUNING

### Ghost Tuning.

5. Log onto the InstaScan Computer.
6. Remove Ghost images.
  - a. Go to the ANMR console.
    1. Select a **New Exam**.
    2. Select **Site Protocol List**.
    3. Select Protocol **16. Clinical Heads**.
    4. Select **View Protocols**.
    5. Select **Next**.
    6. Select **4. Series EPI Sequences**.
    7. Select **Scan 1: HEAD,Axial,2D,Research,ismemp,None**.
    8. Select **Scan Ops**.
    9. Select **Auto Prescan**.

NOTE: There is a possibility of getting a message “Auto Prescan incomplete ....” In this case, select **Manual Prescan**. Once an image is seen on the display screen, select **Backup**.
  - b. Go to the InstaScan computer.
    1. Select **Open Database** and select desired database or create a new database.
    2. Select **Options | Save Raw Data**.
    3. Select **Scan Setup**.

NOTE: The InstaScan computer will direct the operator to begin the scan on the ANMR console.
  - c. Go to the ANMR console.
    1. Select **Scan**.

NOTE: The EPI technique creates a single image in less than a second. The image will be displayed on the InstaScan computer.
  - d. Go to the InstaScan computer.
    1. Select **Utility | Autotuning**
    2. Tag one of the square boxes and move it over a ghost image. Do not place the box on an actual (desired) image.
    3. Repeat with the second box.



4. Repeat step 2.d.2. through 2.d.4. as needed to remove the ghost images.  
NOTE: If the desired diffusion technique is applicable to only a single slice direction then removing ghosts from the other two perpendicular directions is not required. Proceed to step 3, otherwise continue.
- e. Go to the ANMR console.
  1. Select **CANCEL**.
  2. Select **RxAhd Exam**.
  3. Select **CANCEL**.
  4. Select **RxAhd Series**.  
NOTE: This methods retains the positioning information of the phantom head. If this is not used then the phantom head will require a new landmark position.
  5. Select **Acq. Time**.
  6. Change **Frequency Direction** to **R/L**.
  7. Select **Scan Ops**.
  8. Select **Auto Prescan**.  
NOTE: There is a possibility of getting a message "Auto Prescan incomplete ...." In this case, select **Manual Prescan**. Once an image is seen on the display screen, select **Backup**.
- f. Repeat 2.b.2. through 2.d.5.
- g. Go to the ANMR console.
  1. Select **Patient Position**.
  2. Select **Scan Plane = Sagital**.
  3. Select **Scanning Range**.
  4. Enter for **Start (L/R): L0**.
  5. Enter for **End (L/R): R0**.
  6. Select **Scan Ops**.
  7. Select **Auto Prescan**.  
NOTE: There is a possibility of getting a message "Auto Prescan incomplete ...." In this case, select **Manual Prescan**. Once an image is seen on the display screen, select **Backup**.
- h. Repeat 2.b.2. through 2.d.5.



## APPENDIX H

### DIFFUSION IMAGING

8. Go to the ANMR console.
  - i. If ghost tuning has just been performed, do the following.
    1. Select **CANCEL**.
    2. Select **RxAhd Exam**.
    3. Select **CANCEL**.
    4. Select **RxAhd Series**.

NOTE: This methods retains the positioning information of the phantom head. If this is not used then the phantom head will require a new landmark position.
  - j. Select the diffusion technique.
    1. Select **List/Sel Protocol**.
    2. Select **Protocol 45**.
    3. Select **View Protocol**.
    4. Select **Series 1**.
    5. Select **Scan Ops**.
    6. Select **Auto Prescan**.
  - k. Go to the InstaScan computer.
    1. Select **Scan Setup**.

NOTE: The InstaScan computer will direct the operator to begin the scan on the ANMR console.
  - l. Go to the ANMR console.
    1. Select **Scan**.

NOTE: The diffusion technique creates seven images within 44 seconds. The image will be displayed on the InstaScan computer.

# APPENDIX I DIFFUSION IMAGING PROTOCOL

## Protocol 45: GEORGE HARDER TEST

1. Series: Head,Axial,2D,Spin Echo,None

Scan 1: HEAD,Axial,2D,Research,isdiff3T,None

### **PATIENT POSITION**

Patient Entry: Head First

Patient Position: Supine

Axial/Sag Landmark:

Coil Type: Head

Scan Plane: Axial

### **SCAN SET-UP**

Auto CF: Water

### **SCANNING RANGE**

Field of View: 40 cm

Scan Thickness: 5 mm

Interscan Spacing: 5 mm

Start Location: (I/S) 0

End Location: (I/S) 0

No. Of Scan Locations: 1

FOV Center: (L/R): 0

(P/A): 0

### **IMAGING PARAMETERS**

Image Mode: 2D

Pulse Sequence: Spin Echo

Imaging Option: None

Enter PSD Filename: isdiff3T

### **USER CV**

Image/Slice 1.000000

Enhance 1.000000

# of Shots 1.000000

Catch and Hold 0.000000

# of diffusion steps 2.000000

diffusion weight (s/mm2) 900.000000

### **ACQUISITION TIME**

Acq Matrix: freq

256

Ac1 Matrix: phase

128

Phase FOV: ½ 20

cm

Frequency Direction: A/P

Imaging Time: 1 NEX

0:44

Contrast: No

### **SCAN TIMING**

TE: Minimum

Full

Rep Time (TR): Other 4000

## APPENDIX J IMAGE TRANSFER

2. Go to the UF3T Sun workstation.
  - m. Log onto the UF3T system.
  - n. Change directory to the desired location for placing the images.  
Use the Unix command **CD {path}**.
  - o. Enter **xferx** at the prompt. This program allows transfer of images from the ANMR to a temporary directory for further processing.
  - p. Under **List Exa** select the desired exam from the ANMR system.
  - q. Under **List Ser** select the desired series from the selected exam.
  - r. Under **List Ima** select the desired images from the select series.
  - s. Hit **Get From Remote** to transfer the images.
  - t. Hit **Quit** to exit the xferx program.
  - u. Enter **signa2unc {path only}** at the prompt. Ensure that the entire path and only the path is entered after the signa2unc command.  
This program converts the images to a format that can be recognized by the Unix computer.
  - v. Repeat the above until all the images have been converted.
  - w. Enter **xidbmaint** at the prompt. This is the only acceptable method for deleting images retrieved from the ANMR system.
  - x. Select **connect**.
  - y. For **SYS**: select **VA3**.
  - z. For **PAT**: select **patient**.
  - aa. Delete images
  - bb. Quit xidbmaint.
  - cc. Enter **XV** at the prompt. This program displays the images and provides a method of transferring the images from a Unix workstation to a PC.
  - dd. Select the desired image.
  - ee. Save the image in **\*.PGM (ASCII)** format.
  - ff. Repeat the conversion for all images.
  - gg. Select **Quit**.
  - hh. The images, in a **\*.PGM (portable gray map)** format can now be transferred to disc.
  - ii. Log off the UF3T system.
3. Go to PC system.

- a. Access an image using a drawing program, such as Paint Shop Pro, by JASC, Inc.
- b. Save the image in a \*.BMP (bitmap) format.

## APPENDIX K

### DIFFUSION IMAGE CONVERSION PROGRAM

```
Begin Program.
Private Declare Function GetFocus Lib "user32" () As Long
Private Declare Function GetPixel Lib "gdi32" (ByVal hdc As Long, ByVal X As
    Long, ByVal Y As Long) As Long
Private Declare Function SetPixel Lib "gdi32" (ByVal hdc As Long, ByVal X As
    Long, ByVal Y As Long, ByVal crColor As Long) As Long
Private Declare Function GetBkColor Lib "gdi32" (ByVal hdc As Long) As Long
Private Declare Function GetColorSpace Lib "gdi32" (ByVal hdc As Long) As
    Long
Private Declare Function LoadBitmap Lib "user32" Alias "LoadBitmapA" (ByVal
    hInstance As Long, ByVal lpBitmapName As String) As Long
Private Declare Function GetDC Lib "user32" (ByVal hwnd As Long) As Long
Private Declare Function EmptyClipboard Lib "user32" () As Long
Private Declare Function CloseClipboard Lib "user32" () As Long
Private Declare Function OpenClipboard Lib "user32" (ByVal hwnd As Long) As
    Long
Private Declare Function SetClipboardData Lib "user32" Alias
    "SetClipboardDataA" (ByVal wFormat As Long, ByVal hMem As Long)
    As Long
Private Declare Function SetClipboardViewer Lib "user32" (ByVal hwnd As
    Long) As Long
Private Declare Function SelectObject Lib "user32" (ByVal hdc As Long, ByVal
    hObject As Long) As Long
Private Declare Function CreateCompatibleBitmap Lib "gdi32" (ByVal hdc As
    Long, ByVal nWidth As Long, ByVal nHeight As Long) As Long
Private Declare Function CreateCompatibleDC Lib "gdi32" (ByVal hdc As Long)
    As Long

Dim Myhwd As Long
Dim MyDb As Database
Dim MySet As Recordset
Dim MySetA As Recordset
Dim MySetB As Recordset
Dim MyRay
```



```

Dim WhichImage As Integer
Private Const CF_BITMAP = 2
Private Const CF_DIB = 8
Private Const CF_DIF = 5
Private Const CF_DSPBITMAP = &H82
Private Const CF_DSPMETAFILEPICT = &H83

```

```

Private Sub Form_Load()
    Set MyDb = OpenDatabase(App.Path + "\diff.mdb")
    For i = 0 To 27
        Pic1(i).Visible = True
        Pic1(i).Scale (210, 0)-(550, 385)
    Next
End Sub

```

```

Public Sub LoadImage()
    MousePointer = 11
    MySet.MoveFirst
    Do While Not MySet.EOF
        Pic2.PSet (MySet("X"), MySet("Y")), MySet("dwColor")
        MySet.MoveNext
    Loop
    Pic2.AutoRedraw = False
    MousePointer = 0
End Sub

```

```

Public Sub DecipherImage(ByRef TableName As String)
    MousePointer = 11 'hourglass
    Set MySet = MyDb.OpenRecordset(TableName)
    Label6 = TableName
    Pic1(0).SetFocus
    hwd2& = GetFocus()
    Myhwd = GetDC(hwd2&)
    For i = 0 To 385
        Label1 = i
        Gauge1.Value = i
        For j = 210 To 550
            dwColor& = GetPixel(Myhwd, j, i)
            MySet.AddNew
            MySet("X") = j
            MySet("Y") = i
            MySet("dwColor") = dwColor&

```

```
        MySet.Update
        DoEvents
    Next
Next
LoadImage
MySet.Close
Duration = Timer + 3
Do While Timer < Duration
    DoEvents
Loop
MousePointer = 0
End Sub

Private Sub Menu21_Click()
    On Error Resume Next
    MySet.Close
    Set MySet = MyDb.OpenRecordset("002 Image 1")
    On Error GoTo 0
    LoadImage
End Sub

Private Sub Menu22_Click()
    On Error Resume Next
    MySet.Close
    Set MySet = MyDb.OpenRecordset("002 Image 2")
    On Error GoTo 0
    LoadImage
End Sub

Private Sub Menu23_Click()
    On Error Resume Next
    MySet.Close
    Set MySet = MyDb.OpenRecordset("002 Image 3")
    On Error GoTo 0
    LoadImage
End Sub

Private Sub Menu24_Click()
    On Error Resume Next
    MySet.Close
```

```
Set MySet = MyDb.OpenRecordset("002 Image 4")
On Error GoTo 0
LoadImage
End Sub
```

```
Private Sub Menu25_Click()
    On Error Resume Next
    MySet.Close
    Set MySet = MyDb.OpenRecordset("002 Image 5")
    On Error GoTo 0
    LoadImage
End Sub
```

```
Private Sub Menu26_Click()
    On Error Resume Next
    MySet.Close
    Set MySet = MyDb.OpenRecordset("002 Image 6")
    On Error GoTo 0
    LoadImage
End Sub
```

```
Private Sub Menu27_Click()
    On Error Resume Next
    MySet.Close
    Set MySet = MyDb.OpenRecordset("002 Image 7")
    On Error GoTo 0
    LoadImage
End Sub
```

```
Private Sub Menu41_Click()
    On Error Resume Next
    MySet.Close
    Set MySet = MyDb.OpenRecordset("004 Image 1")
    On Error GoTo 0
    LoadImage
End Sub
```

```
Private Sub Menu42_Click()
```

```
On Error Resume Next
MySet.Close
Set MySet = MyDb.OpenRecordset("004 Image 2")
On Error GoTo 0
LoadImage
End Sub
```

```
Private Sub Menu43_Click()
On Error Resume Next
MySet.Close
Set MySet = MyDb.OpenRecordset("004 Image 3")
On Error GoTo 0
LoadImage
End Sub
```

```
Private Sub Menu44_Click()
On Error Resume Next
MySet.Close
Set MySet = MyDb.OpenRecordset("004 Image 4")
On Error GoTo 0
LoadImage
End Sub
```

```
Private Sub Menu45_Click()
On Error Resume Next
MySet.Close
Set MySet = MyDb.OpenRecordset("004 Image 5")
On Error GoTo 0
LoadImage
End Sub
```

```
Private Sub Menu46_Click()
On Error Resume Next
MySet.Close
Set MySet = MyDb.OpenRecordset("004 Image 6")
On Error GoTo 0
LoadImage
End Sub
```

```
Private Sub Menu47_Click()  
    On Error Resume Next  
    MySet.Close  
    Set MySet = MyDb.OpenRecordset("004 Image 7")  
    On Error GoTo 0  
    LoadImage  
End Sub
```

```
Private Sub Menu51_Click()  
    On Error Resume Next  
    MySet.Close  
    Set MySet = MyDb.OpenRecordset("005 Image 1")  
    On Error GoTo 0  
    LoadImage  
End Sub
```

```
Private Sub Menu52_Click()  
    On Error Resume Next  
    MySet.Close  
    Set MySet = MyDb.OpenRecordset("005 Image 2")  
    On Error GoTo 0  
    LoadImage  
End Sub
```

```
Private Sub Menu53_Click()  
    On Error Resume Next  
    MySet.Close  
    Set MySet = MyDb.OpenRecordset("005 Image 3")  
    On Error GoTo 0  
    LoadImage  
End Sub
```

```
Private Sub Menu54_Click()  
    On Error Resume Next  
    MySet.Close  
    Set MySet = MyDb.OpenRecordset("005 Image 4")  
    On Error GoTo 0  
    LoadImage  
End Sub
```



```

Private Sub Menu55_Click()
    On Error Resume Next
    MySet.Close
    Set MySet = MyDb.OpenRecordset("005 Image 5")
    On Error GoTo 0
    LoadImage
End Sub

```

```

Private Sub Menu56_Click()
    On Error Resume Next
    MySet.Close
    Set MySet = MyDb.OpenRecordset("005 Image 6")
    On Error GoTo 0
    LoadImage
End Sub

```

```

Private Sub Menu57_Click()
    On Error Resume Next
    MySet.Close
    Set MySet = MyDb.OpenRecordset("005 Image 7")
    On Error GoTo 0
    LoadImage
End Sub

```

```

Private Sub MenuQuit_Click()
    End
End Sub

```

```

Private Sub MenuShowAll_Click()
    On Error Resume Next
    Label1.Visible = False
    Label2.Visible = False
    Label4.Visible = False
    Label5.Visible = False
    Label6.Visible = False
    Gauge1.Visible = False
    'use red to contrast images
    For k = 14 To 27

```

```

Label3 = "Contrast box " & Format(k, "#")
Pic1(k).Cls
Pic1(k).AutoRedraw = True
For i = 210 To 550
    For j = 0 To 385
        Pic1(k).PSet (i, j), RGB(255, 0, 0)
    Next
Next
Pic1(k).AutoRedraw = False
Next
'display images
For i = 0 To 27
    Select Case i
        Case 0: TableName = "002 Image 1"
        Case 1: TableName = "002 Image 2"
        Case 2: TableName = "002 Image 3"
        Case 3: TableName = "002 Image 4"
        Case 4: TableName = "002 Image 5"
        Case 5: TableName = "002 Image 6"
        Case 6: TableName = "002 Image 7"
        Case 7: TableName = "004 Image 1"
        Case 8: TableName = "004 Image 2"
        Case 9: TableName = "004 Image 3"
        Case 10: TableName = "004 Image 4"
        Case 11: TableName = "004 Image 5"
        Case 12: TableName = "004 Image 6"
        Case 13: TableName = "004 Image 7"
        Case 14: TableName = "Image 1"
        Case 15: TableName = "Image 2"
        Case 16: TableName = "Image 3"
        Case 17: TableName = "Image 4"
        Case 18: TableName = "Image 5"
        Case 19: TableName = "Image 6"
        Case 20: TableName = "Image 7"
        Case 21: TableName = "Image 1-45"
        Case 22: TableName = "Image 2-45"
        Case 23: TableName = "Image 3-45"
        Case 24: TableName = "Image 4-45"
        Case 25: TableName = "Image 5-45"
        Case 26: TableName = "Image 6-45"
        Case 27: TableName = "Image 7-45"
    End Select
    Label3 = "Drawing " + TableName

```

```

DoEvents
MySet.Close
Set MySet = MyDb.OpenRecordset(TableName)
MousePointer = 11
Pic1(i).Visible = True
Pic1(i).Cls
Pic1(i).AutoRedraw = True
MySet.MoveFirst
Do While Not MySet.EOF
    Pic1(i).PSet (MySet("X"), MySet("Y")), Abs(MySet("dwColor"))
    MySet.MoveNext
Loop
Pic1(i).AutoRedraw = False
MousePointer = 0
DoEvents
Next
Label3.Visible = False
On Error GoTo 0
End Sub

```

```

Private Sub MenuStart_Click()

```

```

    Pic1(0).Cls
    Pic1(0).AutoRedraw = True
    Pic2.Scale (235, 0)-(600, 301)
    For ImageNr = 12 To 21
        Select Case ImageNr
            Case 1: PictureName = "T002_1.bmp"
                TableName = "002 Image 1"
            Case 2: PictureName = "T002_2.bmp"
                TableName = "002 Image 2"
            Case 3: PictureName = "T002_3.bmp"
                TableName = "002 Image 3"
            Case 4: PictureName = "T002_4.bmp"
                TableName = "002 Image 4"
            Case 5: PictureName = "T002_5.bmp"
                TableName = "002 Image 5"
            Case 6: PictureName = "T002_6.bmp"
                TableName = "002 Image 6"
            Case 7: PictureName = "T002_7.bmp"
                TableName = "002 Image 7"
            Case 8: PictureName = "T004_1.bmp"
                TableName = "004 Image 1"

```

```

Case 9: PictureName = "T004_2.bmp"
      TableName = "004 Image 2"
Case 10: PictureName = "T004_3.bmp"
      TableName = "004 Image 3"
Case 11: PictureName = "T004_4.bmp"
      TableName = "004 Image 4"
Case 12: PictureName = "T004_5.bmp"
      TableName = "004 Image 5"
Case 13: PictureName = "T004_6.bmp"
      TableName = "004 Image 6"
Case 14: PictureName = "T004_7.bmp"
      TableName = "004 Image 7"
Case 15: PictureName = "T005_1.bmp"
      TableName = "005 Image 1"
Case 16: PictureName = "T005_2.bmp"
      TableName = "005 Image 2"
Case 17: PictureName = "T005_3.bmp"
      TableName = "005 Image 3"
Case 18: PictureName = "T005_4.bmp"
      TableName = "005 Image 4"
Case 19: PictureName = "T005_5.bmp"
      TableName = "005 Image 5"
Case 20: PictureName = "T005_6.bmp"
      TableName = "005 Image 6"
Case 21: PictureName = "T005_7.bmp"
      TableName = "005 Image 7"
End Select
If ImageNr = 1 Or ImageNr = 2 Or ImageNr = 11 Or ImageNr = 12 Or
ImageNr = 13 Or ImageNr = 15 Or ImageNr = 19 Or ImageNr = 20 Or ImageNr
= 21 Then
    Label3 = PictureName
    Pic1(0).Picture = LoadPicture(App.Path + "\" + PictureName)
    Pic2.Cls
    DecipherImage (TableName)
End If
Next
'Analyze Image Sets
ReDim MyRay(210 To 550, 0 To 385, 0 To 2)
On Error Resume Next
MySet.Close
For m = 2 To 7
    WhichImage = m
    Select Case m

```

```

Case 1: Set MySetA = MyDb.OpenRecordset("005 Image 1")
      Set MySetB = MyDb.OpenRecordset("004 Image 1")
      Set MySet = MyDb.OpenRecordset("Image 1-45")
Case 2: Set MySetA = MyDb.OpenRecordset("005 Image 2")
      Set MySetB = MyDb.OpenRecordset("004 Image 2")
      Set MySet = MyDb.OpenRecordset("Image 2-45")
Case 3: Set MySetA = MyDb.OpenRecordset("005 Image 3")
      Set MySetB = MyDb.OpenRecordset("004 Image 3")
      Set MySet = MyDb.OpenRecordset("Image 3-45")
Case 4: Set MySetA = MyDb.OpenRecordset("005 Image 4")
      Set MySetB = MyDb.OpenRecordset("004 Image 4")
      Set MySet = MyDb.OpenRecordset("Image 4-45")
Case 5: Set MySetA = MyDb.OpenRecordset("005 Image 5")
      Set MySetB = MyDb.OpenRecordset("004 Image 5")
      Set MySet = MyDb.OpenRecordset("Image 5-45")
Case 6: Set MySetA = MyDb.OpenRecordset("005 Image 6")
      Set MySetB = MyDb.OpenRecordset("004 Image 6")
      Set MySet = MyDb.OpenRecordset("Image 6-45")
Case 7: Set MySetA = MyDb.OpenRecordset("005 Image 7")
      Set MySetB = MyDb.OpenRecordset("004 Image 7")
      Set MySet = MyDb.OpenRecordset("Image 7-45")
End Select
AnalyzeImage
MySet.Close
Next
MyDb.Close
End Sub

```

```

Private Sub Pic1_GotFocus(Index As Integer)
  Select Case Index
    Case 0: TableName = "002 Image 1"
    Case 1: TableName = "002 Image 2"
    Case 2: TableName = "002 Image 3"
    Case 3: TableName = "002 Image 4"
    Case 4: TableName = "002 Image 5"
    Case 5: TableName = "002 Image 6"
    Case 6: TableName = "002 Image 7"
    Case 7: TableName = "004 Image 1"
    Case 8: TableName = "004 Image 2"
    Case 9: TableName = "004 Image 3"
    Case 10: TableName = "004 Image 4"
    Case 11: TableName = "004 Image 5"
  End Select

```



```

Case 12: TableName = "004 Image 6"
Case 13: TableName = "004 Image 7"
Case 14: TableName = "005 Image 1"
Case 15: TableName = "005 Image 2"
Case 16: TableName = "005 Image 3"
Case 17: TableName = "005 Image 4"
Case 18: TableName = "005 Image 5"
Case 19: TableName = "005 Image 6"
Case 20: TableName = "005 Image 7"

```

```
End Select
```

```
Label6 = TableName
```

```
End Sub
```

```
Private Sub Pic1_MouseMove(Index As Integer, Button As Integer, Shift As Integer, X As Single, Y As Single)
```

```
Label4 = Format(X, "###")
```

```
Label5 = Format(Y, "###")
```

```
End Sub
```

```
Public Sub AnalyzeImage()
```

```
MousePointer = 11
```

```
'load a set of images into the array
```

```
MySetA.MoveFirst
```

```
Label3 = "Loading A - " & Format(WhichImage, "#")
```

```
DoEvents
```

```
Do While Not MySetA.EOF
```

```
MyRay(MySetA("X"), MySetA("Y"), 0) = MySetA("dwColor")
```

```
MySetA.MoveNext
```

```
Loop
```

```
MySetA.Close
```

```
MySetB.MoveFirst
```

```
Label3 = "Loading B - " & Format(WhichImage, "#")
```

```
DoEvents
```

```
Do While Not MySetB.EOF
```

```
MyRay(MySetB("X"), MySetB("Y"), 1) = MySetB("dwColor")
```

```
MySetB.MoveNext
```

```
Loop
```

```
MySetB.Close
```

```
DoEvents
```

```
Label3 = "Subtracting Images"
```

```
Gauge1.Min = 210
Gauge1.Max = 550
DoEvents
Label6 = MySet.Name
For nx = 210 To 550
    Gauge1.Value = nx
    DoEvents
    For ny = 0 To 385
        MySet.AddNew
        MySet("X") = nx
        MySet("Y") = ny
        MySet("dwColor") = MyRay(nx, ny, 0) - MyRay(nx, ny, 1)
        MySet.Update
    Next
Next
Next
MousePointer = 0
DoEvents
End Sub
```

## LIST OF REFERENCES

- Adair 1992                      Adair, Eleanor R., Berglund, Larry G., Annals New York Academy of Sciences, 649, 188-200, (1992).
- Boesiger 1992                      Boesiger, Peter, Buchli, Reto; Saner, Martin; Meier, Dieter, Annals New York Academy of Sciences, 649, 160-165, (1992).
- Bottomley 1981                      Bottomley, Paul A., Edelstein, William A., Medical Physics, 8 (4), 510-512, (1981).
- Bottomley 1985                      Bottomley, Paul A., Redington, Rowland W.; Edelstein, William A.; Schenck, John F., Magnetic Resonance in Medicine, 2, 336-349, (1985).
- Budinger 1992                      Budinger, Thomas F., Annals New York Academy of Sciences, 649, 1-17 (1992).
- Chou 1984                              Chou, C.K., Bioelectromagnetics, 5(4), 435-441, (1984).
- DePoorter 1994                      De Poorter, J., De Wagter, C.; De Deene, Y.; Thomsen, C.; Stahlberg, F.; Achten, E., Journal of Magnetic Resonance, Series B, 103, 234-241, (1994).
- Deichmann 1992                      Deichmann, R., Haase, A., Journal of Magnetic Resonance, 96, 608-612, (1992).
- Delannoy 1991                      Delannoy, J., Chen' Ching-Nien; Turner, R.; Levin, R.L.; Le Bihan, D., Magnetic Resonance in Medicine, 19, 333-339, (1991).
- Gordon 1992                              Gordon, Christopher J., Annals New York Academy of Sciences, 649, 273-284 (1992).

- Gore 1982 Gore, J.C., McDonnell, M.J.; Pennock, J.M.; Phil, M.; Stanbrook, H.S., Magnetic Resonance Imaging, 1, 4, 191-195 (1982).
- Hall 1990 Hall, Alistair S., Prior, Michael V.; Hand, Jeffrey W.; Young, Ian R.; Dickinson, Robert J., Journal of Computer Assisted Tomography, 14 (3), 430-436, (1990).
- INIRC-IRPA 1991 International Non-Ionizing Radiation Committee of the IRPA (INIEC-IRPA), Health Physics, 61 (6), 923-928 (1991).
- Ishihara 1995 Ishihara, Yasutoshi, Calderon, Arturo; Watanabe, Hidehiro; Okamoto, Kazuya; Suzuki, Yoshinori; Kuroda, Kagayaki; Suzuki, Magnetic Resonance in Medicine, 34, 6, 814-823, (1995).
- Knuttel 1986 Knuttel, B., Juretschke, H.P., Recent Results in Cancer Research, 101, 109-118, (1986).
- LeBihan 1988 Le Bihan, Denis, Breton, Eric; Lallemand, Denis; Aubin, Marie-louise; Vignaud, Jacqueline; Laval-Jeantet, Maurice, Radiology, 168, 2, 497-505, (1988).
- LeBihan 1989 Le Bihan, Denis, Delannoy, Jose; Levin, Ronald L., Radiology, 171, 3, 853-857, (1989).
- Leonard 1984 Leonard, Jonathan B., Foster, Kenneth R.; Athey, T. Whit, IEEE Trans. BioMedical Engineering, 31, 7, 533-536, (1984).
- Mahoney 1995 Mahony, Clare, Forbes, Larry K.; Crozier, Stuart; Doddrell, David M., Journal of Magnetic Resonance, 107, 145-151, (1995).
- McCain 1995 McCain, Douglas C., McCain, Douglas C., Journal of Magnetic Resonance, 109, 209-212, (1995).
- Mischler 1995 Mischler, E., Humbert, F.; Canet, D., Journal of Magnetic Resonance, 109, 121-125, (1995).

- Nekolla 1992      Nekolla, Stephan, Gneiting, Thomas; Syha, Jutta; Deichmann, Ralf; Haase, Axel, Journal of Computer Assisted Tomography, 16, 2, 327-332, (1992).
- Nelson 1987      Nelson, T.R., Tung, S.M., Magnetic Resonance Imaging, 5, 3, 189-199, (1987).
- Parker 1983      Parker, Dennis L., Smith, Vernon; Sheldon, Philip; Crooks, Lawrence E.; Fussel, Lauren, Medical Physics, 10, 3, 321-325, (1983).
- Roschmann 1987      Roschmann, P., Medical Physics, 14, 6, 922-931, (1987).
- Schwarzbauer 1995      Schwarzbauer, C., Zange, J.; Adolg, H.; Deichmann, R.; Noth, U.; Haase, A., Journal of Magnetic Resonance, Series B, 106, 178-180, (1995).
- Shellock 1992      Shellock, Frank G., Annals New York Academy of Sciences, 649, 260-272, (1992).
- Stehling 1991      Stehling, Michael K., Turner, Robert; Mansfield, Peter, Science, 254, 43-50, (1991).
- Stuchley 1985      Stuchley, Maria A., Draszewski, Andrzej; Stuchly, Stanislaw S., IEEE Transactions on Medical Engineering, 32, 8, 609-616, (1985).
- Turner 1990      Turner, Robert, Le Bihan, Densi; Maier, Joseph; Vavrek, Robert; Hedges, L. Kyle; Pekar, James, Radiology, 177, 2, 407-414, (1990).
- Werner 1993      Werner, J, Webb, P, The Annals of Physiological Anthropology, 12, 123-134, (1993).



## LIST OF SUPPLEMENTAL REFERENCES

- |                  |  |
|------------------|--|
| Abbound 1996     | Abbound, Shimon, Rosenfeld, Moshe; Luzon, Jacob, <u>IEEE Transactions of Biomedical Engineering</u> , <b>43</b> , 7, 690-696 (1996).                 |
| Adair 1986       | Adair, Eleanor R., Berglund, Larry G., <u>Magnetic Resonance Imaging</u> , <b>4</b> , 321-333 (1986).  |
| Athey 1989       | Athey, T. Whit, <u>Magnetic Resonance in Medicine</u> , <b>9</b> , 177-184 (1989).   |
| Barnes 1992      | Barnes, Frank S., <u>Annals New York Academy of Sciences</u> , <b>649</b> , 69-73 (1992).  |
| Cavagnetto 1993  | Cavagnetto, F., Prati, P.; Ariola, V.; Corvisiero, P.; Marinelli, M.; Pilot, A.; Taccini, G., <u>Health Physics</u> , <b>65</b> , 2, 172-177 (1993). |
| Chung 1984       | Chung-Kwang Chou, Gang-Wu Chen, Arthur W. Guy, Kenneth H.Luk, <u>Bioelectromagnetics</u> , <b>5</b> , 435-441 (1984).                                |
| Cwikiel 1993     | Cwikiel, W., Stridbeck, H.; Stenram, U., <u>Acta Radiologica</u> , <b>34</b> , 258-262 (1993).   |
| DeCertaines 1992 | De Certaines, J.D., <u>Annals New York Academy of Sciences</u> , <b>649</b> , 35-43 (1992).  |
| Doran 1995       | Doran, Simon J., Decorps, Michel, <u>Journal of Magnetic Resonance</u> , <b>117</b> , 311-316 (1995).  |
| Durney 1992      | Durney, Carl H., <u>Annals New York Academy of Sciences</u> , <b>649</b> , 19-34 (1992).   |
| Fidanza 1953     | Fidanza, Flamino, Keys, Ancel; Anderson, Joseph T., <u>Journal of Applied Physiology</u> , <b>6</b> , 252-256 (1953).                                |

- Fischell 1994 Fischell, Tim A., Kharm, Bassam K.; Fischell, David R.; Loges, Peter G.; Coffey II, Charles W.; Duggan, Dennis M.; Naftilan, 2956-2963 (1994).
- Garn 1995 Garn, Heinrich, Gabriel, Camelia, Health Physics, 68, 2, 147-156 (1995).
- Haase 1990 Haase, A., Magnetic Resonance in Medicine, 13, 77-89 (1990).
- Henry 1993 Henry-Feugeas, M.C., Edy-Peretti, I.; Blanchet, B.; Hassine, D.; Zannoli, G.; Schouman-Claeys, E., Magnetic Resonance Imaging, 11, 8, 1107-1118 (1993).
- Hendee 1994 Hendee, William R., Boteler, John C., Health Physics, 66, 2, 127-136 (1994).
- Hua 1995 Hua, Jianmin, Hurst, Gregory C., Journal of Magnetic Resonance Imaging, 5, 1, 113-120 (1995).
- Kanal 1990 Kanal, Emanuel, Shellock, Frank G.; Talagala, Lalith, Radiology, 176, 3, 593-606 (1990).
- LeBihan 1986 Le Bihan, Denis, Breton, Eric; Lallemand, Denis; Grenier, Philippe; Cabanis, Emmanuel; Laval-Jeantet, Maurice, Radiology, 161, 2, 401-407 (1986).
- Liu 1993 Liu, J.C., Mao, Stan; McCall, R.C.; Donahue, R., Health Physics, 64, 1, 59-63 (1993).
- Lorenz 1991 Lorenz, Christine H., Pickens III, David R.; Puffer, Donald B.; Price, Ronald R., Magnetic Resonance in Medicine, 19, 254-260 (1991).
- MacFall 1996 MacFall, James R., Prescott, Deborah M.; Charles, H. Cecil; Samulski, Thaddeus V., Medical Physics, 23, 10, 1775-1782 (1996).
- Maier 1994 Maier, Stephan E., Hardy, Christopher J.; Jolesz, Ferenc A., Radiology, 193, 2, 477-483 (1994).
- Majumdar 1989 Majumdar, S., Zoghbi, S.; Pope, C.F.; Gore, J.C., Magnetic Resonance in Medicine, 9, 185-202 (1989).

- McRobbie 1993      McRobbie, D.W., Medical Physics, 20, 5, 1555-1560 (1993).
- Mendez 1960      Mendez, Jose, Keys, Ancel, Journal of Applied Physiology, 9, 2, 184-188 (1960).
- Nekolla 1992      Nekolla, Stephan, Gneiting, Thomas; Syha, Jutta; Deichmann, Ralf; Haase, Axel, Journal of Computer Assisted Tomography, 16, 2, 327-332 (1992).
- Noll 1995      Noll, Douglas C, Cohen, Jonathan D.; Meyer, Craig H.; Schneider, Walter, Journal of Magnetic Resonance Imaging, 5, 1, 49-56 (1995).
- Nordell 1988      Nordell, B., Stahlberg, F.; Ericsson, A.; Ranta, C., Magnetic Resonance Imaging, 6, 695-705 (1988).
- Olsen 1992      Olsen, Richard G., Annals New York Academy of Sciences, 649, 237-241 (1992).
- Orcutt 1988      Orcutt, Niel, Gandhi, Om P., IEEE Transactions on Biomedical Engineering, 35, 8, 577-583 (1988).
- Pavlicek 1983      Pavlicek, William, Geisinger, Michael; Castle, Lon; Borkowski, Gregory P.; Meaney, Thomas F.; Bream, Bruce L.; Gallagher, Joe H., Radiology, 147, 1, 149-153 (1983).
- Pollak 1993      Pollak, V.A., Ferbert, A.; Schulze-Clewing, J., Medical & Biological Engineering & Computing, 0, 388-391 (1993).
- Prasad 1990      Prasad, Naresh, Wright, David A.; Ford, Joseph J.; Thornby, John I., Radiology, 174, 1, 251-253 (1990).
- Reilly 1989      Reilly, J.P., Medical & Biological Engineering & Computing, 0, 101-110 (1989).
- Rohan 1992      Rohan, Michael L., Rzedzian, Richard R., Annals New York Academy of Sciences, 649, 118-129 (1992).
- Santyr 1995      Santyr, Giles E., Mulkern, Robert V., Journal of Magnetic Resonance Imaging, 5, 1, 121-124 (1995).

- Schepps 1980      Schepps, Jonathan L., Foster, Kenneth R., Phys. Med. Biol., 25, 6, 1149-1159 (1980).
- Schaefer 1992      Schaefer, Daniel J., Annals New York Academy of Sciences, 649, 225-235 (1992).
- Schenck 1992      Schenck, J.F., Dumoulin, C.L.; Redington, R.W., Med. Phys., 19, 4, 1089-1098 (1992).
- Scott 1995      Scott, G.C., Joy, M.L.G.; Armstrong, R.L.; Henkelman, R.M., IEEE Transactions on Medical Imaging, 14, 3, 515-524 (1995).
- Shellock 1991      Shellock, Frank G., Kanal, Emanuel, Journal of Magnetic Resonance Imaging, 1, 1, 97-101 (1991).
- Shellock 1992      Shellock, Frank G., Annals New York Academy of Sciences, 649, 260-272 (1992).
- Simunic 1996      Simunic, Dina, Wach, Paul; Renhart, Werner; Stollberger, Rudolf, IEEE Trans. Biomedical Engineering, 43, 1, 88-94 (1996).
- Srebro 1996      Srebro, Richard, IEEE Transactions on Medical Engineering, 43, 6, 650-653 (1996).
- Steen 1994      Steen, R. Grant, Gronemeyer, Suzanne A., Journal of Magnetic Resonance Imaging, 5, 1, 43-48 (1994).
- Tofani 1995      Tofani, S., Ossola, P.; d'Amore, G.; Gandhi, O.P., Health Physics, 68, 1, 71-78 (1995).
- van Heteren 1987      van Heteren, John G., Henkelman, R. Mark; Bronskill, Michael J., Magnetic Resonance Imaging, 5, 2, 93-99 (1987).
- Wevers 1995      Wevers, Ron A., Engelke, Udo; Wendel, Udo; deJong, Jan G.N.; Gabreels, Fons J.M.; Heerschap, Arend, Clinical Chemistry, 41, 5, 744-751 (1995).
- Wieringa 1993      Wieringa, H.J., Peters, M.J., Medical & Biological Engineering & Computing, 0, 600-606 (1993).

Young 1994

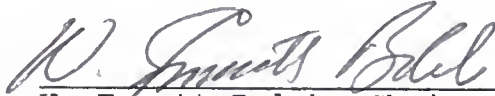
Young, I.R., Hand, J.W.; Oatridge, A.; Prior, M.V.; Forse, G.R., Magnetic Resonance in Medicine, 31, 342-345 (1994).



## BIOGRAPHICAL SKETCH

George Harder is a native Floridian of German descent. After High School he went into the Navy for five years serving in Greece, Newfoundland and the Persian Gulf. Upon his honorable discharge from the Navy, he used the G.I. Bill to receive a Bachelor of Science in Electrical Engineering from the University of Florida. George worked for the Department of Defense for six years working with inertial navigation systems onboard submarines and eventually in non-ionizing radiation from surface combatant ships. He pursued this course of studies by returning to the University of Florida's Department of Environmental Engineering Sciences. In 1995 he received a Master of Engineering in environmental engineering and was accepted for the doctoral program. George currently works at the Gainesville office of Perma-Fix Environmental Services, Inc., as a Senior Health Physicist.

I certify that I have read this study and that in my opinion it conforms to acceptable standards of scholarly presentation and is fully adequate, in scope and quality, as a dissertation for the degree of Doctor of Philosophy.



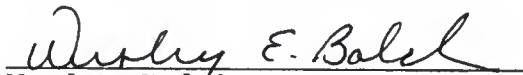
W. Emmett Bolch, Chair  
Professor of Environmental  
Engineering Sciences

I certify that I have read this study and that in my opinion it conforms to acceptable standards of scholarly presentation and is fully adequate, in scope and quality, as a dissertation for the degree of Doctor of Philosophy.



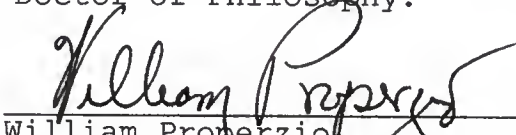
Jeff Fitzsimmons  
Professor of Nuclear and  
Radiological Engineering

I certify that I have read this study and that in my opinion it conforms to acceptable standards of scholarly presentation and is fully adequate, in scope and quality, as a dissertation for the degree of Doctor of Philosophy.



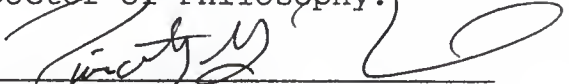
Wesley Bolch  
Associate Professor of  
Nuclear and Radiological  
Engineering

I certify that I have read this study and that in my opinion it conforms to acceptable standards of scholarly presentation and is fully adequate, in scope and quality, as a dissertation for the degree of Doctor of Philosophy.



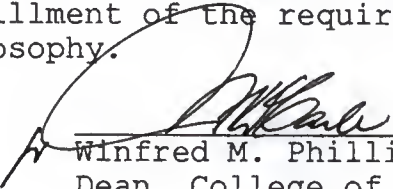
William Properzio  
Professor of Environmental  
Engineering and Sciences

I certify that I have read this study and that in my opinion it conforms to acceptable standards of scholarly presentation and is fully adequate, in scope and quality, as a dissertation for the degree of Doctor of Philosophy.

  
\_\_\_\_\_  
Timothy Townsend  
Assistant Professor of  
Environmental Engineering  
Sciences

This dissertation was submitted to the Graduate Faculty of the College of Engineering and to the Graduate School and was accepted as partial fulfillment of the requirements for the degree of Doctor of Philosophy.

August, 1998

  
\_\_\_\_\_  
Winfred M. Phillips  
Dean, College of  
Engineering

\_\_\_\_\_  
Karen A. Holbrook  
Dean, Graduate School

LD 1780 1772

.H259

UNIVERSITY OF FLORIDA



3 1262 08554 5746